GULF GENERAL ATOMIC

GA-10509

THE PHYSICS DESIGN OF THE GAS-COOLED FAST BREEDER REACTOR DEMONSTRATION PLANT

by

Bruno Pellaud

Prepared under
Contract AT(04-3)-167
Project Agreement No. 23
for the
San Francisco Operations Office
U.S. Atomic Energy Commission

Date Published: August 29, 1971

GULF GENERAL ATOMIC COMPANY
P.O. BOX 608, SAN DIEGO, CALIFORNIA 92112

GULF GENERAL ATOMIC

GA-10509

THE PHYSICS DESIGN OF THE GAS-COOLED FAST BREEDER REACTOR DEMONSTRATION PLANT

by

Bruno Pellaud

Prepared under
Contract AT(04-3)-167
Project Agreement No. 23
for the
San Francisco Operations Office
U.S. Atomic Energy Commission

Gulf General Atomic Project 393

Date Published: August 29, 1971

GULF GENERAL ATOMIC COMPANY
P O BOX 608, SAN DIEGO, CALIFORNIA 92112

ABSTRACT

This report summarizes the reactor physics work related to the Gas Cooled Fast Reactor Demonstration Plant. Special attention is devoted to control rods, fuel management, and blanket design. A complete description of studies related to static and burnup behavior, reactivity coefficients, and reactor kinetics is supplied.

A major section on basic data gives special attention to the cross section of Pu-239, Pu-240, and U-238. Methods for calculating neutron spectra and streaming effects are described.

CONTENTS

TABLES

FIGURES

1. INTRODUCTION

Investigation of gas-cooling for fast reactors began in the early 1960's at Gulf General Atomic Europe in Zurich, Switzerland, and was continued in the United States at Gulf General Atomic (GGA) and Oak Ridge National Laboratory (ORNL) under the sponsorship of the U.S. Atomic Energy Commission and under a privately supported program by GGA and a group of utility companies. The studies confirmed that cooling with pressurized gas (70 to 120 atm) and with surface-roughened fuel rods was feasible and economical for fast breeder reactors.

Gas cooling is particularly attractive from the reactor physics viewpoint. Helium, the preferred gas coolant, has a negligible absorption cross section and a small scattering cross section. Reactor safety is thereby enhanced since total voiding has a minor influence on reactivity. Moreover, with no phase change, local voiding becomes impossible.

Another feature of the Gas-Cooled Fast Breeder Reactor (GCFR) is that the performance of the GCFR benefits from the hard neutron spectrum, which is harder than that of other fast breeder types. A hard spectrum allows concurrent high breeding and internal conversion ratios, which lead not only to low fuel cycle costs but also to design flexibility. In this latter respect, a GCFR can operate economically with either a batch refueling scheme, in which the internal conversion ratio is near unity, the reactivity is constant, and the specific power is relatively low, or with a partial refueling scheme, in which the internal conversion ratio is less than unity, the reactivity decreases with time, and the specific power is high.

Prior work related to the physics design of the GCFR has been documented in a series of reports dealing with large commercial GCFR plants or with the demonstration plant (Refs. 1-6). In this report the physics aspects of the GCFR demonstration plant are reviewed in the light of the improved data and

methods that have become available in recent years. The physics studies presented are primarily on the 300-MW(e) GCFR demonstration plant, which has been the focus of GGA's work on the GCFR program during the last two years. In some instances, the discussion also covers the larger commercial-size GCFR.

The GCFR demonstration plant primary system is briefly described in Section 2, and the details of the core arrangement, along with a discussion of the general design philosophy, are given in Section 3. In Section 4 the status of basic cross sections for the nuclides of importance in fast-reactor physics is reviewed in the light of the most recent measurements. The remaining sections of the report deal with computational methods and with fundamental results, including the impact of cross-section uncertainties on GCFR performance.

2. PLANT AND PRIMARY SYSTEM DESCRIPTION

The 300-MW(e) GCFR demonstration plant and the characteristics of its primary system are described in this section.

The GCFR demonstration plant is housed in a reactor building and a turbine building. The reactor building (see Fig. 2.1) contains the prestressed concrete reactor vessel (PCRV) that encloses the reactor, the primary coolant system, and the steam generators. This building also functions as a secondary containment structure and includes the fuel-handling area and the reactor plant process and service systems. The fuel storage pool is adjacent to the reactor building and is connected to it through a loading port. The configuration of the reactor and its associated primary circuit components within the PCRV are shown in Fig. 2.2. The PCRV is similar to the twenty PCRVs that have already been built or are under construction around the world for thermal gas-cooled reactors. It is reinforced with steel rods and is prestressed after completion of concrete construction by a system of longitudinal and circumferential steel tendons. The PCRV is made gas-tight by means of an inner steel liner supplemented by the substantially impervious thick concrete walls. The closures for the PCRV cavities and penetrations are also steel lined and are provided with flow-limiting devices to limit the rate of depressurization in the case of a penetration failure. The liner is insulated by a thermal barrier, and cooling of the liner and penetrations is provided by cooling tubes on the exterior surface of the steel liner. The number of redundant tension members (steel tendons and reinforcing bars) in this typical PCRV design renders a gross failure of the pressure vessel incredible. Secondary containment is provided and is designed to ensure a minimum coolant pressure of 2 atm (the equilibrium pressure) following a complete primary depressurization.

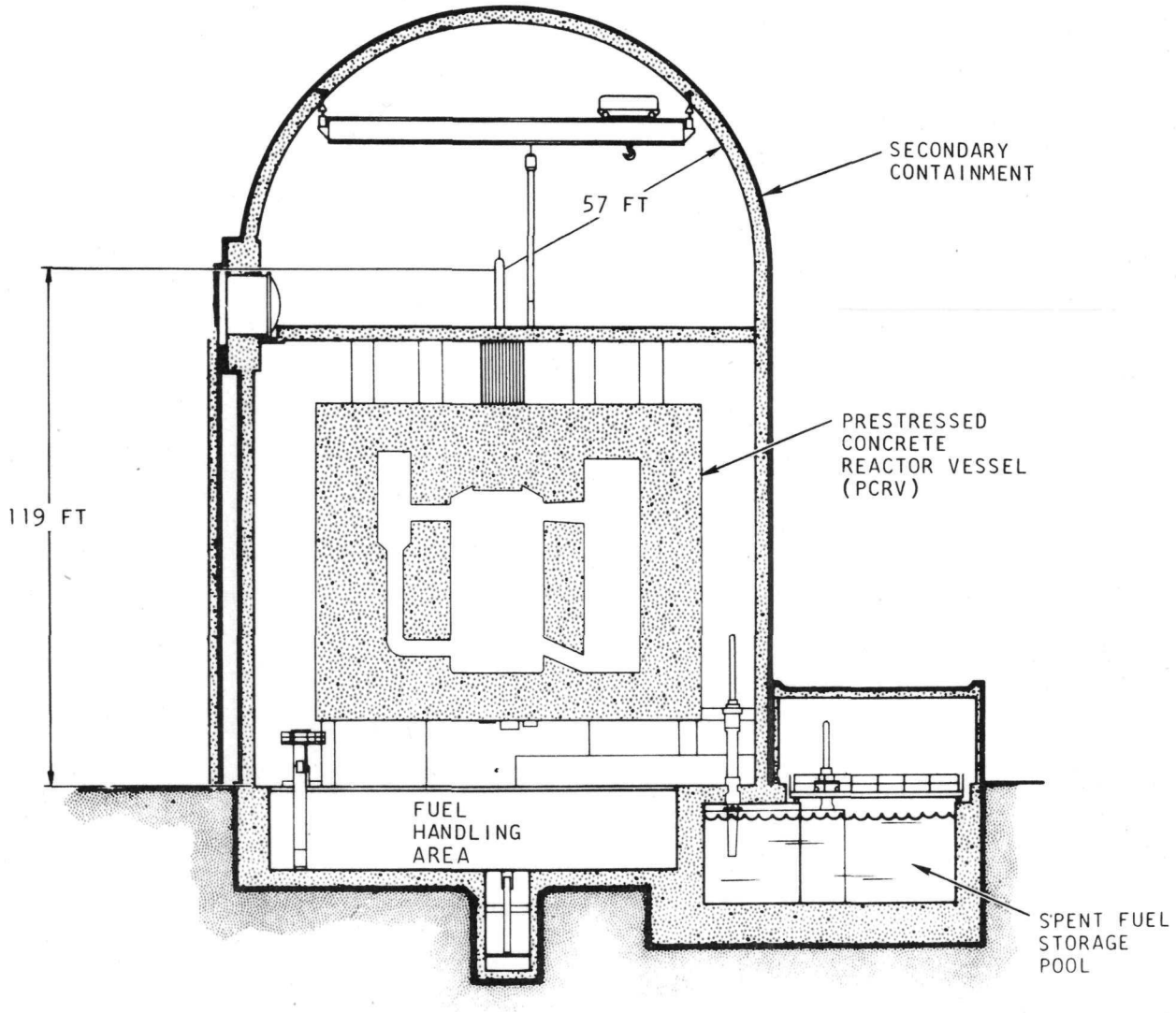

Fig. 2.1. Reactor building

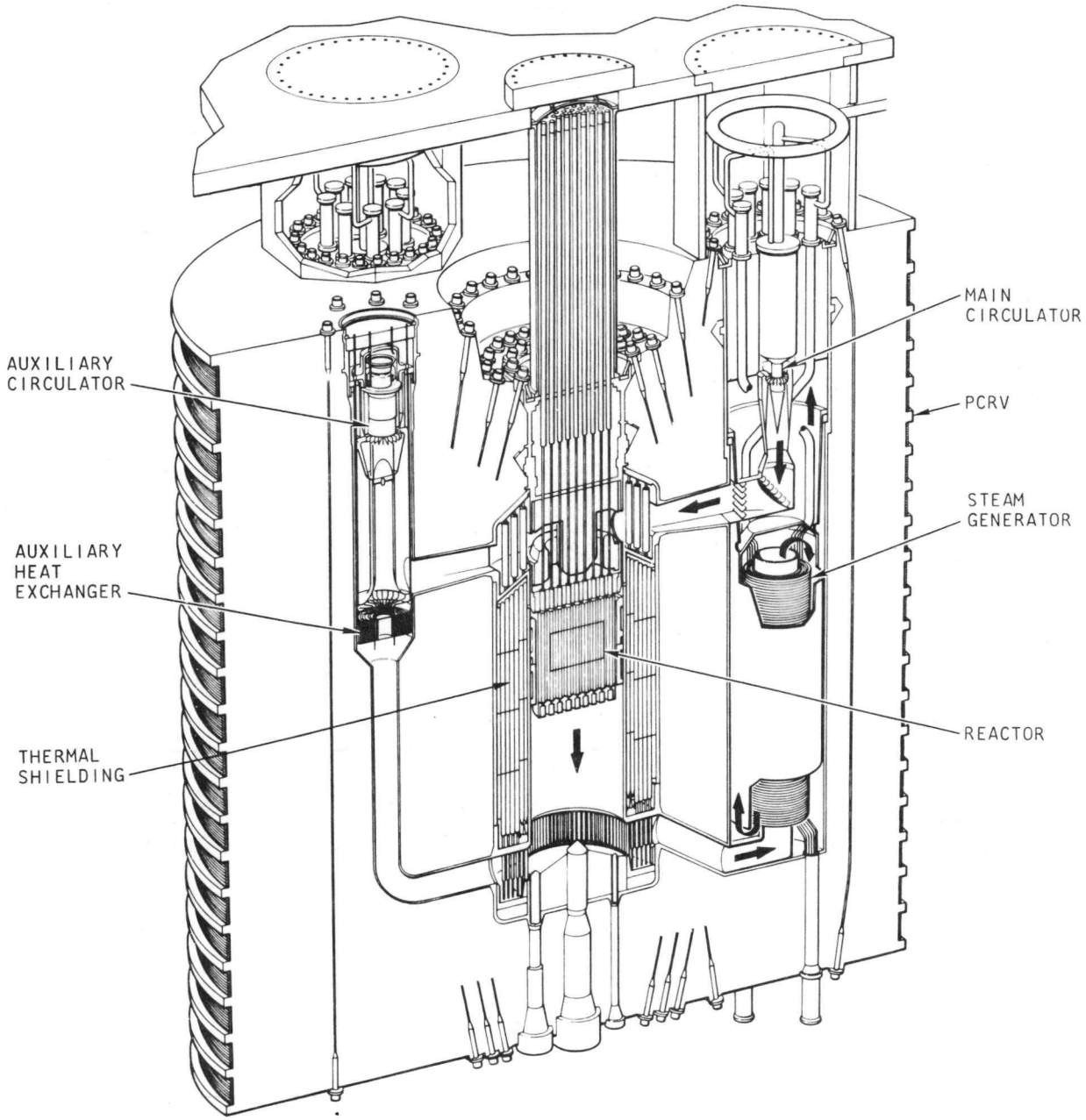

Fig. 2.2. Cutaway view of GCFR demonstration plant

The closures for the main cavities in the PCRV are concrete lined with steel and are secured so that thrust loads are taken primarily by top compression struts, backed up by an independent lock acting through appropriate anchors within the vessel structure. These cavity closures would not normally be removed, so they are joined to the PCRV liner by seal welds.

The primary coolant system for the demonstration plant contains three main loops, each with independent steam generators and circulators (on the right in Fig. 2.2), and three auxiliary loops (on the left in Fig. 2.2), each with its own circulator and heat-removal system. The auxiliary loops are used for long-term shutdown cooling and as backup for the main loops. The steam generators and their associated circulators are housed in vertical cavities in the PCRV walls that surround the reactor core. The helium coolant, at a pressure of about 85 atm, flows downward through the core, where it is heated to a temperature of 542°C. The flow is also downward across the tube banks of the helically coiled, once-through steam generators to accommodate use of upflow boiling in the generators. The appropriate flow reversals of the gas path are obtained by directing the core exit gas up through a central hole in the boiler, down over the tube bundles, up again around the boiler shells, and then to top-mounted circulators, from which the gas is discharged to the reactor top plenum at a temperature of 312°C.

The reactor core (illustrated in Fig. 2.3) is comprised of 211 hexagonal fuel and radial blanket elements containing the fuel and blanket rods. The elements, which are 3 meters in total length and each about 16.5 cm across flats, are supported from a top-mounted single grid plate to which each element is rigidly attached, and thus they are clamped to the grid plate solely at their cold ends. The fuel elements are initially spaced some 6.4 mm apart over their entire length to accommodate the effects of radiation-induced swelling. Bowing of elements due to this cause will be reduced to amounts that can be accommodated by rotating elements around their own axes during fuel reloading at approximately annual intervals. The

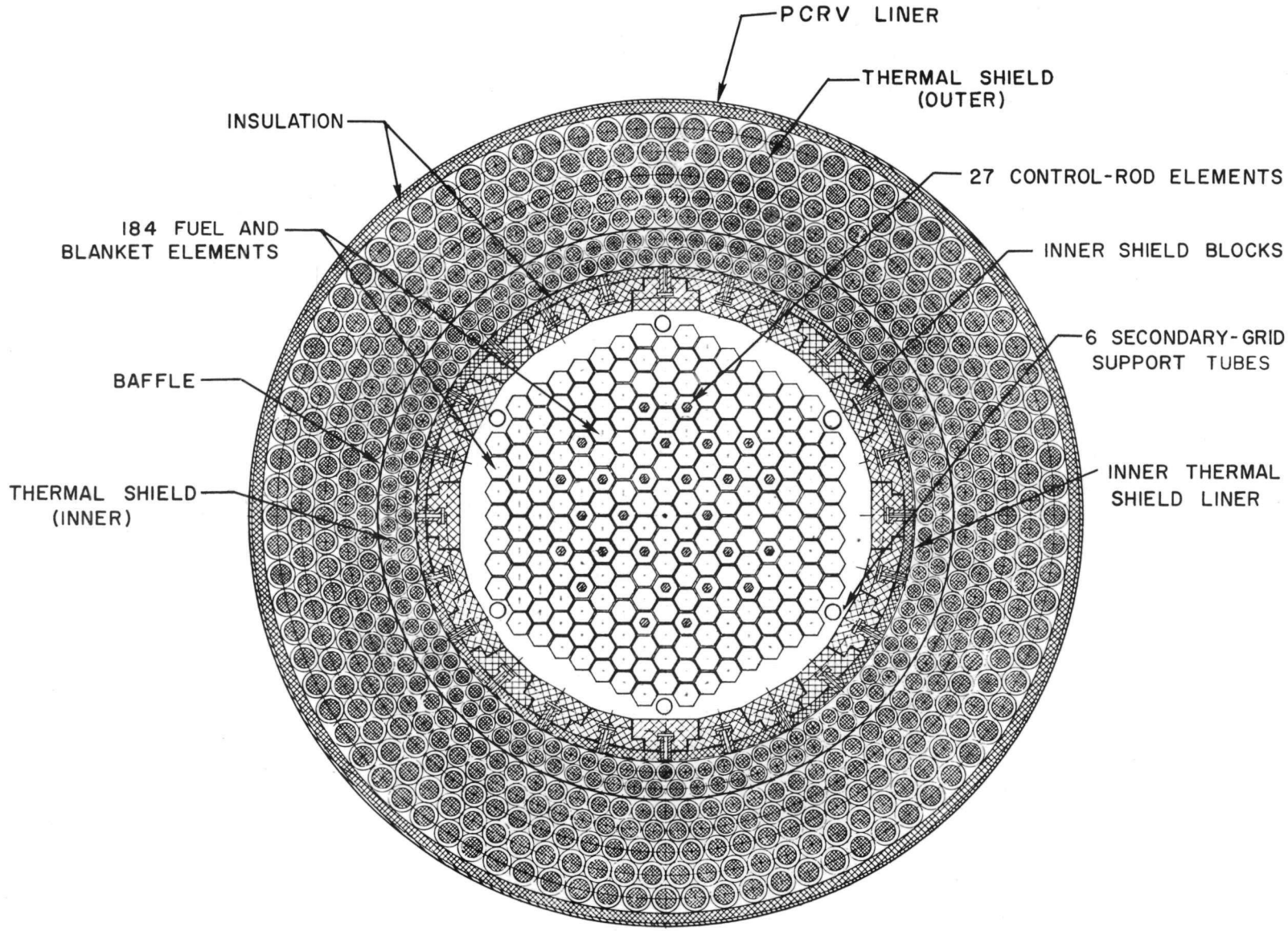

Fig. 2.3. Horizontal section through reactor cavity

grid plate, which consists essentially of a solid 3.3-m-diam, 61-cm-thick disc with closely spaced 15-cm holes to accommodate circular extensions to the fuel elements, is itself supported by a surrounding cylinder connected to the top of the liner of the vessel top penetration. The central PCRV top closure allows the entire grid plate to be replaced if necessary. The clamping of the fuel elements to the grid plate, as well as the means for operating variable orifices within each fuel element, is facilitated by providing individual small penetrations in the top access plug above each element.

Each standard fuel element contains 271 fuel rods; the control fuel elements contain 234 rods. The fuel rods are similar to Liquid Metal Fast Breeder Reactor (LMFBR) fuel rods except for the cladding surface roughening that is used to improve the surface heat transfer, as is done in British Advanced Gas-Cooled Reactors (AGRs). The fuel rods consist of annular PuO_2-UO_2 pellets contained within a 316 stainless steel cladding that is 1/2 mm thick. Pressure equalization of the fuel rods with the primary coolant is achieved by collective venting of the fission gases through a manifold and then to the helium purification system. This system relieves the cladding from mechanical stresses due to external gas coolant pressure and also from internal fission-product gas pressure. In addition, this system provides a basis for leaky rod detection.

Upper and lower axial blankets are contained in the ends of the fuel rods and consist of depleted UO_2 pellets. The two rows of radial blanket elements have the same external dimensions as the fuel elements. The blanket elements contain 127 rods of relatively large diameter that contain depleted UO_2 pellets. The flow in each element is orificed so that the same hot-spot cladding temperature is reached in each element. On-line adjustment of all orifices is provided.

Core loading (requiring shutdown and depressurization) is effected by inserting a fuel-transfer machine through the bottom of the PCRV. This machine lowers and traverses fuel in the vacant space below the core to a single exit port leading to a transporting cask beneath the vessel structure.

Reactivity control is by 27 rods in the control fuel elements, which have a central space to accommodate the rods. The control-rod drives are located above the reactor.

Protection of the PCRV liner and ducts from neutron irradiation is provided by thick shielding. Around the core, this shielding takes the form of a removable inner layer of steel blocks surrounded by an annular region of steel cylinders containing graphite, as shown in Fig. 2.3. Above the grid plate, an annular duct through the shield protects both the reactor cavity plug and the radial intake ducts. Cooling of the radial shielding is by a small bypass from the entry helium, which is arranged to stimulate internal circulation by injector action.

A major design criterion applied to all penetrations is that flow restriction means be provided to limit the depressurization rate in the event of primary barrier failure to a value that does not jeopardize core cooling.

The principal design data for the demonstration plant reactor are summarized in Table 2.1.

TABLE 2.1

GENERAL REACTOR CHARACTERISTICS

Reactor thermal power	826 MW(t)
Net electrical power	311 MW(e)
Plant efficiency	37.6%
Reactor outlet temperature	542°C
Reactor inlet temperature	312°C
Average fuel temperature	1030°C
Hot-spot cladding temperature, mid-clad	700°C
Total helium coolant flow rate	689 kg/sec
Average power density	235 kW(t)/liter of core
Helium pressure	85 atm
Helium inventory (all loops)	3950 kg
Primary system volume (all loops)	595 m^3
Maximum linear rating	453 (13.8) W/cm (kW/ft)
System pressure loss	4.1 atm

3. REACTOR CHARACTERISTICS

3.1. NUCLEAR DESIGN SUMMARY

The nuclear design of the GCFR demonstration plant is based on the uranium-plutonium cycle, with the fuel in the form of mixed uranium and plutonium dioxide pellets enclosed in stainless steel tubes extending the length of the core and both axial blankets. The pellets in the axial blankets and in the radial blanket rods are made of depleted uranium. Rods are clustered in an hexagonal array to form elements, each contained in a hexagonal stainless steel box.

The reactor core is composed of 118 elements, 27 of which are special fuel elements from which a sufficient number of fuel rods have been removed to allow the insertion of a boron-carbide control rod. The core is surrounded by 93 radial blanket elements, whose boxes have the same dimensions as core element boxes.

The core closely approximates the shape of a right circular cylinder, 1 meter in radius and 1 meter in height. Its volume is thus slightly less than 3200 liters. At the beginning of the equilibrium cycle, the fissile inventory is 1320 kg. About 28% of the core volume is occupied by fuel (whose average fissile content is 18%) and 45% by the helium coolant, with the remainder being taken up by structural materials and gaps.

In order to provide a flattened radial power profile, the core is divided into four enrichment zones. Approximately one-third of the elements in each zone are replaced at the end of an annual reload interval [of 250 full power days (FPD)]. It follows that a fuel segment stays in the core for a period of three reload cycles, a residence time that corresponds to 750 FPD, a maximum burnup of 100,000 MWd/Te, and a maximum fast fluence ($E > 0.1$ MeV) of 2×10^{23} nvt.

A negative Doppler temperature coefficient (-2.6×10^{-6} $\delta k/\delta T$ at operating fuel temperature), coupled with a negative axial expansion coefficient (-4.2×10^{-6} $\delta k/\delta T$), ensures safe and stable operation of the reactor. Reactor control is achieved by two independent systems. The first, called the control system, includes 21 rods with an individual worth of \$0.85. It provides normal control requirements encountered in reactor operation, including shutdown capability for planned shutdowns or scrams. The second, called the shutdown system, includes six rods with an individual worth of \$1.60. It acts as a backup if the control system fails to respond to a scram signal and also provides a large negative reactivity during shutdown and refueling conditions.

The basic physics characteristics of the GCFR demonstration plant are summarized in Table 3.1.

3.2. CORE ENRICHMENT AND ZONING

The average core enrichment determines the internal conversion ratio, which in turn fixes the reactivity loss that accompanies fuel burnup. The selected average enrichment (18% of fissile plutonium) leads to a reactivity loss between refuelings that results in acceptable control requirements. A simple method for the evaluation of the core average enrichment on the basis of reactivity loss, average burnup, and number of refueling cycles is presented in Appendix A.

The size, shape, and fuel volume fraction are derived from overall thermodynamics, heat transfer, and economic requirements. On the basis of fuel enrichment and criticality constraint, basic core and fuel pin dimensions are determined from such factors as surface temperature limitations, gas temperatures, pressure, and pumping powers. The core parameters shown in Table 3.1 not only allow good economic performance of the plant, but they also result in fuel performances that are suitable for the demonstration of the GCFR concept for large commercial plants.

TABLE 3.1

CORE PHYSICS CHARACTERISTICS

Reactor thermal output	826 MW(t)
Active core height	100.5 cm
Equivalent active core diameter	200.9 cm
Core volume	3,200 liters
Core length-to-diameter ratio	0.5
Axial blanket thickness	45 cm
Radial blanket thickness	33 cm
Number of standard elements in core	91
Number of control elements in core	27
Number of blanket elements	93
Fuel lifetime	750 full power days
Refueling cycle	1 yr
Average power density	235 kW(t)/liter of core
Reactor power fractions at midcycle	
Core	91%
Axial blankets	4.55%
Radial blankets	4.45%
Core volume fractions	
Fuel (excluding central hole and gap)	27.7%
Helium coolant	44.6%
Cladding	9.7%
Structure	6.3%
Gaps (box interspace, control-rod channel, fuel)	11.7%
Core fissile enrichment, average	18 atom-%
Fissile masses (Pu-239 and Pu-241) at midcycle	
Core	1,280 kg
Axial blanket	84 kg
Radial blanket	253 kg
Core fissile loading at beginning of cycle	1,320 kg

TABLE 3.1 (Continued)

Loading (Pu plus U) at beginning of cycle	
Core	7,340 kg
Axial blanket	7,480 kg
Radial blanket	15,300 kg
Average breeding ratio	1.33
Maximum fuel burnup	100,000 MWd/Te heavy metal
Doppler constant	-0.0034 Tdk/kdT (T in °K)
Total helium reactivity worth	$0.38
Average fast neutron flux (E > 0.1 MeV)	2.2×10^{15} n/cm^2-sec
Reactor rating	0.625 MW(t)/kg fissile
Reactivity control requirements	
Cold-to-hot operating	-$3.00
Reactivity swing over equilibrium cycle	-$9.00
Compensation for He and Np-239	-$1.00
Shutdown margin (minimum + extra)	-4.85
Total control capability (control system only)	-17.85
Absorber material	B_4C
Cladding material	316 SS
Average rod worth	
Control	$0.85
Shutdown	$1.60
Effective delayed neutron fraction	0.00351
Prompt neutron lifetime	4.3×10^{-7} sec
Isothermal temperature coefficient at 20°C	-6.2×10^{-6} Δk/k/°C
Isothermal temperature coefficient at 312°C	-7.6×10^{-6} Δk/k/°C
Steady state power coefficient	-3.2×10^{-6} Δk/k/MWt
Coolant reactivity coefficient	$+2.0 \times 10^{-6}$ Δk/k/°C
Axial expansion coefficient	-4.2×10^{-6} Δk/k/°C, clad temp

Power flattening is achieved by a radial subdivision of the core into a set of enrichment zones. The range of practical number of enrichment zones is from two to five. A small number reduces fabrication and handling costs and simplifies fuel management. However, the smaller the number of zones, the higher the peak-to-average power ratio and hence the larger the pumping losses associated with orificing. Since it is desirable to keep pumping losses at a minimum in order to enhance reactor performance, more than two zones are necessary to achieve a low peak-to-average power ratio. It was found that four enrichment zones represent an acceptable compromise.

Once a particular number of enrichment zones has been selected, a specific enrichment and specific elements of the hexagonal array must be assigned to each zone. Such a selection is performed automatically by a special version of the two-dimensional, hexagonal diffusion code GAUGEF (see Appendix B). In a first pass, the code determines by iteration the enrichment required by each element (and its symmetric counterparts) for obtaining a perfectly flat radial power profile. Then, on the basis of such an ideal zoning pattern, a systematic search is performed on all the possible combinations of four enrichments and element locations, with a least-squares criterion on the peak element power to core average ratio. The zones would normally appear as concentric rings of fuel elements. However, because of the gross nature of the hexagonal grid, the outer zones may be discontinuous and intermingled, depending on the degree of symmetry, size, and total number of fuel elements. For the current reactor design of the GCFR demonstration plant, the optimum zoning pattern is that shown in Fig. 3.1. The corresponding zone characteristics are given in Table 3.2.

Although the relative enrichments shown in Table 3.2 are derived from multigroup, space-dependent calculations, it is of interest that they can be found with a fair accuracy from the simple, one-group method discussed in Appendix A, provided that the zone fractional volumes are already known.

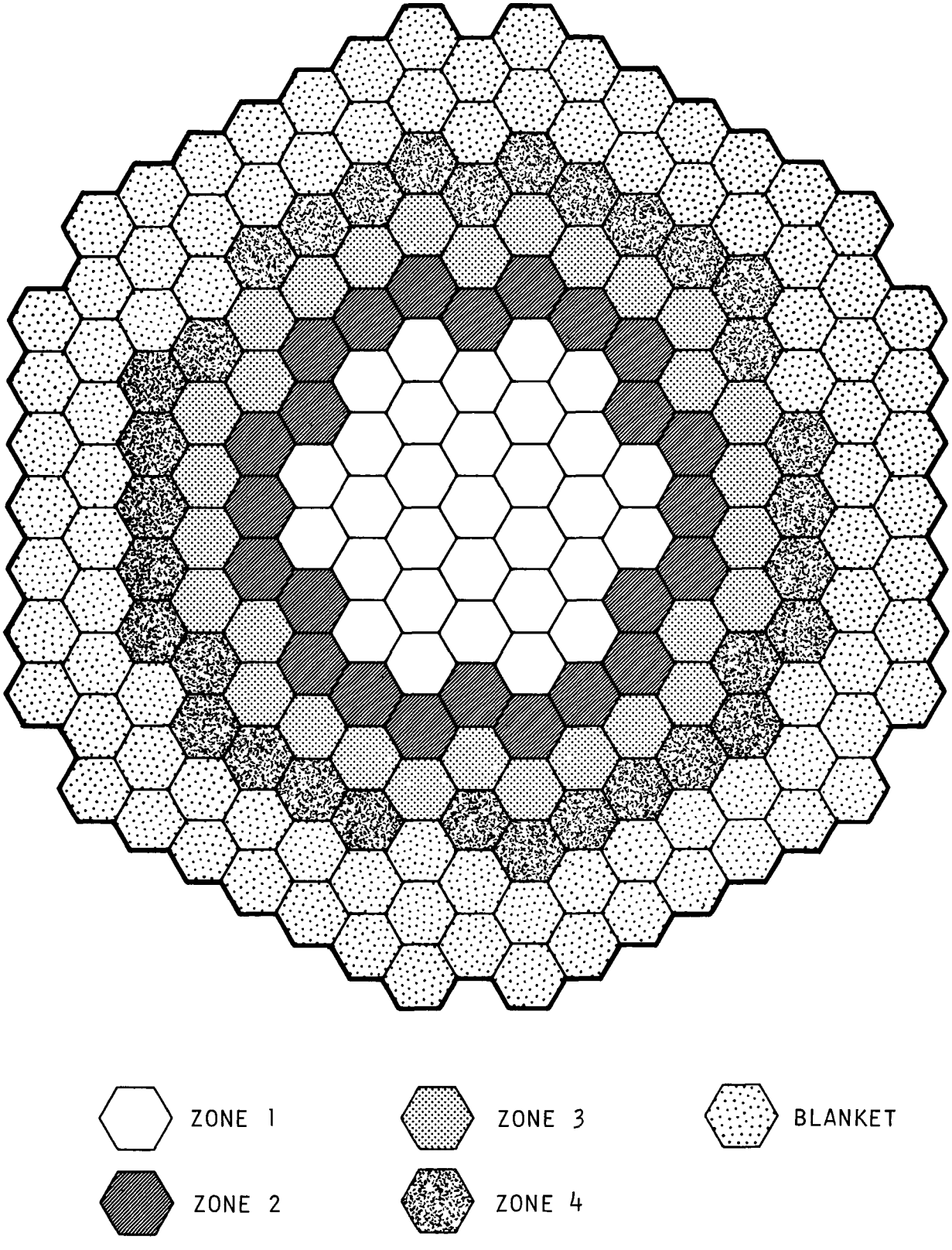

Fig. 3.1. Core zoning scheme

TABLE 3.2

ZONE DESCRIPTION

	Zone 1	Zone 2	Zone 3	Zone 4
Number of elements	31	24	30	33
Number of control elements	6	9	12	0
Fuel volume fraction	0.279	0.271	0.271	0.286
Equivalent radius, cm	51.49	68.54	85.26	100.46
Volume, liters	837	648	809	890
U/Pu (feed)	4.62	3.80	3.33	2.73
Fissile enrichment (feed), %	14.7	17.2	19.0	22.1
Rod fissile density (feed), g/cm^3	1.24	1.46	1.61	1.87

It should be emphasized that the selection of an optimum zoning scheme is based on the element peak power, and not on the element average power. Power flattening therefore refers to the maximum rod power of each zone. With this method, a limited, but considerable number of rods in every zone will operate close to the maximum temperature conditions.

3.3. BLANKET DESIGN

The blanket design is determined by the economics of fuel breeding and the capital costs associated with the size of the reactor cavity. The fertile density in the blanket, its thickness, and the frequency and mode of reloading represent the main parameters that have to be selected. The blanket fertile density, which is proportional to the fuel volume fraction and the oxide density, is determined mainly by heat transfer requirements, while the thickness and reloading scheme depend exclusively on economic factors.

Since the design of the reactor hardware does not distinguish between core and blanket elements, the element pitch is the same through the reactor, and the radial blanket thickness may thus be characterized by its number of

rows. More rows mean more bred plutonium (but with a diminishing return) and a larger reactor vessel, but also less shielding. The same holds for the axial blanket thickness. Whereas the axial blanket is replaced according to the core fuel management, the radial blanket may be reloaded with its own frequency and scheme. The study of optimum blanket management (Ref. 7) considered two schemes: a fixed blanket, in which a blanket element remains at the same position until discharged, and a shuffled blanket, in which outer blanket elements are first moved to the inner row before being discharged.

With regard to the axial blanket, the optimum thickness lies between 45 and 70 cm, depending on the choice of economic parameters, with the lower limit corresponding to pessimistic assumptions concerning the value of plutonium, fabrication, and reprocessing costs.

When the economics of breeding and PCRV capital costs are taken into account, it turns out that two rows of blanket elements are optimum for the GCFR demonstration plant, regardless of the assumptions made for the economic parameters just mentioned. Although a shuffled blanket would be more advantageous than a fixed blanket, the gain offered by the shuffling scheme is not large enough to justify the additional operational complexity. The optimum management of such a fixed blanket involves the replacement of the inner row every 3 or 4 yr and the replacement of the outer row every 6 to 9 yr.

3.4. STANDARD, CONTROL, AND BLANKET ELEMENTS

The core contains a total of 118 fuel elements, 91 standard elements and 27 control elements. There are 93 radial blanket elements. The location and the geometry of these three types of elements are shown in Fig. 3.2. They all have the same box wall dimensions and pitch.

A standard fuel element contains 271 fuel rods, with a 7.2-mm o.d. The rods have a 0.5-mm stainless steel cladding and, before irradiation, a

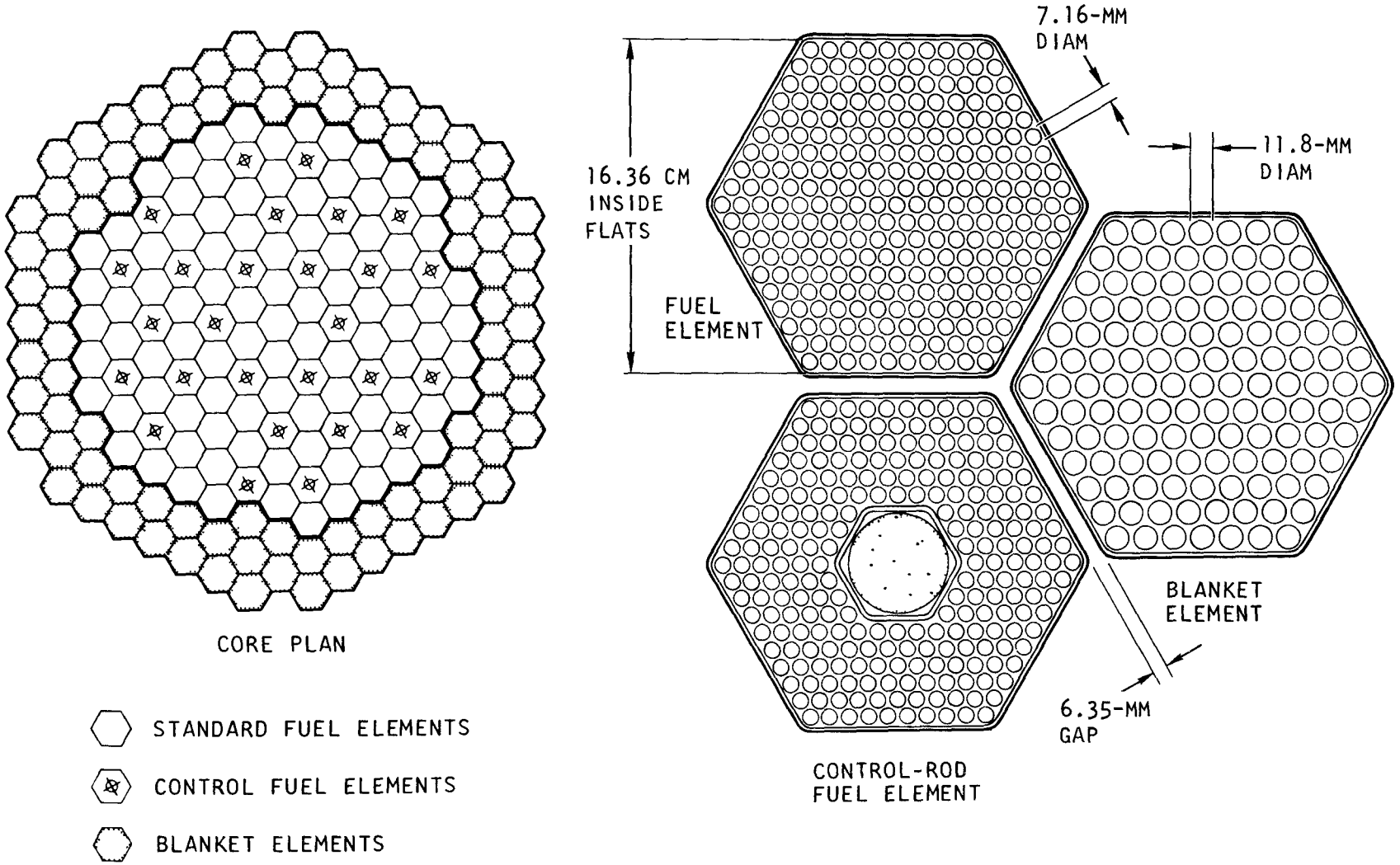

Fig. 3.2. Core and fuel-element plan for demonstration plant

0.07-mm gap between fuel and cladding. The enclosed fuel pellets have a central hole whose diameter is 20% of the pellet diameter. This hole reduces center-line temperature and provides a path for gaseous fission products to move toward the fission product venting system which attaches at the upper end of the element. The dimensions of fuel rods and standard elements are shown in Table 3.3 and the element volume fractions in Table 3.4.

A control element corresponds simply to a standard element whose central 37 rods have been removed to accommodate a hexagonal guide wall for a 5-cm-diam control rod. Otherwise the element and rod geometry are the same as for the standard element. Volume fractions are shown in Table 3.4.

Blanket elements experience a lower burnup and a lower power density than core elements. The blanket rods can therefore be larger than core rods, and no central hole is required to facilitate fission product escape. The geometry of blanket elements is described in Table 3.3, and the resulting volume fractions are shown in Table 3.4.

3.5. REACTOR VOLUME FRACTIONS AND COMPOSITION

The volume fractions for the four core zones and the radial blanket are shown in Table 3.5. These values are based on the number and location of control rods shown in Table 3.2 and Fig. 3.2.

The fuel consists of a homogeneous mixture of uranium and plutonium oxides. The volume fraction α of UO_2 in the fuel pellet is given by

$$\frac{1}{\alpha} = 1 + 0.004022 \frac{A_{Pu}}{\beta} .$$

Here A_{Pu} is the average plutonium atomic mass (i.e., $239\ \gamma_9 + 240\ \gamma_o + 241\ \gamma_1 + 242\ \gamma_2$, where γ_i is the isotopic fraction of the various plutonium isotopes), β is the U/Pu atomic ratio (itself related to the enrichment e by $\beta = (\gamma_9 + \gamma_1)/(e - 1)$, and 0.004022 is equal to the ratio of UO_2 to PuO_2 theoretical densities divided by 238. The volume fraction of PuO_2 in solid fuel is then $1 - \alpha$.

TABLE 3.3

ELEMENT GEOMETRY

Standard Fuel Element		
Element pitch	17.51	cm
Gap between elements	0.635	cm
Box wall thickness	0.254	cm
Flat-to-flat inside dimension	16.36	cm
Number of core fuel rods	271	
Control Fuel Element		
Same as standard element, except for:		
Flat-to-flat inside guide wall dimension	5.33	cm
Guide wall thickness	0.191	cm
Radial clearance, rod to guide	0.251	cm
Control rod outside diameter	4.83	cm
Number of core fuel rods	234	
Blanket Fuel Element		
Same as standard element, except for:		
Number of blanket fuel rods	127	
Core Fuel Rod		
Fuel rod pitch (triangular)	9.80	mm
Rod diameter	7.16	mm
Cladding wall thickness	0.47	mm
Cladding o.d./i.d. ratio	1.15	
Gap between fuel pellet and cladding	0.066	mm
Fuel pellet outside diameter	6.10	mm
Central hole diameter	1.22	mm
Blanket Fuel Rod		
Fuel rod pitch (triangular)	14.35	mm
Rod diameter	11.80	mm
Cladding wall thickness	0.54	mm
Cladding o.d./i.d. ratio	1.10	
Gap between fuel pellet and cladding	0.04	mm
Fuel pellet outside diameter	10.64	mm

TABLE 3.4

ELEMENT VOLUME FRACTIONS[a]

	Standard Element	Control Element	Blanket Element
Fuel hole	0.0119	0.0103	---
Fuel	0.2861	0.2470	0.4257
Gap (cladding-fuel)	0.0130	0.0113	0.0057
Cladding	0.1004	0.0867	0.0906
Coolant	0.4573	0.4071	0.3497
Box wall	0.0551	0.0551	0.0551
Gap between boxes	0.0712	0.0712	0.0712
Spacers	0.0050	0.0050	0.0020
Guide wall	---	0.0137	---
Gap (control rod-guide)	---	0.0237	---
Control rod	---	0.0689	---

(a) Based on the element volume, including the corresponding portion of interbox gaps

TABLE 3.5

CORE AND BLANKET VOLUME FRACTIONS

	Zone 1	Zone 2	Zone 3	Zone 4	Core	Blanket
Fuel (PuO_2-UO_2)	0.2785	0.2714	0.2705	0.2861	0.2771	0.4257
Coolant (helium)	0.4475	0.4385	0.4372	0.4573	0.4458	0.3497
Clad (316 SS)	0.0977	0.0953	0.0949	0.1004	0.0973	0.0906
Structure (316 SS)	0.0627	0.0652	0.0656	0.0601	0.0632	0.0571
Gaps (helium)	0.1001	0.1038	0.1043	0.0961	0.1008	0.0769
Control (B_4C+C)	0.0134	0.0258	0.0276	----	0.0158	----

Both UO_2 and PuO_2 have a fraction of theoretical density equal to 0.87 in the core and 0.912 in the blanket (theoretical densities being 10.97 g/cm^3 for UO_2 and 11.46 g/cm^3 for PuO_2); these fractions refer to solid fuel in the pellets.

The full density of helium at a pressure of P atmospheres and T degrees Kelvin amounts to 48 P/T g/liter in the pressure and temperature range of interest in GCFR design. The full atomic density is then given by 0.00723 P/T atom/(barn·cm).

Cladding and structural components (such as box walls and spacers) are made of type 316 stainless steel for which the following composition has been assumed: 17.5% chromium, 67.5% iron, 12.4% nickel, and 2.6% molybdenum.

3.6. FUEL MANAGEMENT

The GCFR demonstration plant fuel cycle involves a partial reloading scheme wherein about one-third of the core is replaced at each reload interval. A fuel segment stays in the core for a period of three reload cycles. This residence time corresponds to 750 FPD, a maximum burnup of 100,000 MWd/Te (U plus Pu), and a maximum fast fluence (E > 0.1 MeV) of 2×10^{23} nvt.

Because of the nature of the hexagonal grid, it is not possible to reload exactly one-third of every zone each time. For this reason, there is no single equilibrium cycle, but rather three phases in a longer cycle, one phase corresponding to each reload. Positioning of fresh elements is dictated by the requirement that no two adjacent elements be of the same age. This criterion reduces the clearance needed between elements to allow for irradiation-induced swelling and bowing. Table 3.6 shows the heavy metal loadings for the beginning and end of a typical phase of the equilibrium cycle.

The plutonium isotopic composition of the feed material is taken to be 80% Pu-239, 15.5% Pu-240, 2.5% Pu-241, and 2% Pu-242. The fissile enrichments (Pu-239 and Pu-241) correspond to feed material for equilibrium operation. During the approach to equilibrium, appropriate adjustments will be made to reduce the excess reactivity that would result from loading the first core with equilibrium feed enrichments. Lower reactivity can be achieved by various techniques, such as (1) lower fissile enrichment, (2) fuel poisoning, and (3) zone redistribution with nominal feed enrichments.

Fuel management during the approach to equilibrium is dictated not only by economic considerations, but also by the purpose of the demonstration plant, which is to provide experiences in fuel technology and component performance. Therefore, it is expected that during the approach to equilibrium, the demonstration plant would be refueled more frequently in order to yield operating data for fuel segments of increasing burnup. A possible plan for the approach to equilibrium is outlined in Table 3.7. The approach to equilibrium spans the first 3.5 yr of the plant lifetime. During this period, component and fuel testing, as well as semiannual refuelings, entail a lower load factor. In order to obtain more useful irradiation data, the number of core reload sets is increased from three to five during the initial period. In this particular example, a reduction of the initial excess reactivity is accomplished by a 5% lower fissile content of the two reload segments that are first unloaded.

TABLE 3.6

MASS BALANCE

(mass in kg)

Nuclide	Core	Axial Blanket	Radial Blanket	Total
Beginning of Cycle				
U^{235}	12	17	34	63
U^{238}	5,701	7,408	15,065	28,174
Pu^{239}	1,272	56	213	1,541
Pu^{240}	274	1	3	278
Pu^{241}	43	---	---	43
Pu^{242}	33	---	---	33
Fissile Pu	1,315	56	213	1,584
Fertile	5,975	7,409	15,068	28,452
Total	7,335	7,482	15,315	30,132
End of Cycle				
U^{235}	10	16	32	58
U^{238}	5,575	7,343	14,967	27,885
Pu^{239}	1,200	112	292	1,604
Pu^{240}	284	2	6	292
Pu^{241}	43	---	---	43
Pu^{242}	32	---	---	32
Fissile Pu	1,243	112	292	1,647
Fertile	5,859	7,345	14,973	28,177
Total	7,144	7,473	15,297	29,914
Kilograms fissioned	191	9	18	218

TABLE 3.7

PROPOSED APPROACH TO EQUILIBRIUM FOR THE GCFR DEMONSTRATION PLANT

No.of Cycle	Operational Status	Amount of Core Replaced at End of Cycle	Max.Burnup of Discharged Fuel (MWd/Te)	Full Power Days	Cumulative Full Power Days	Load Factor	Cumulative Calendar Days	Max. Clad Temp (°C)	Thermal Power (MW)
1	Component testing	1/6	33,000	294	294	0.5	588	650	702
2	Fuel element testing	1/6	50,000	147	441	0.65	814	650	702
3	Fuel element testing	1/6	66,000	147	588	0.65	1040	650	702
4	Fuel element testing	1/6	83,000	147	735	0.65	1266	650	702
5	Fuel element testing	1/3	100,000	147	882	0.65	1492	650	702
6	Quasi-equilibrium	1/3	100,000	250	1132	0.8	1804	700	826
7	Quasi-equilibrium	1/3	100,000	250	1382	0.8	2116	700	826
8	Equilibrium	1/3	100,000	250	1632	0.8	2428	700	826

Concurrently with reactor reloading, some fuel elements that stay in the core are rotated 180° around their own axis. As shown in Fig. 5.4, large flux tilts occur in elements located in the outer part of the core and the blanket. The resulting temperature and swelling differences induce fuel element bowing and, moreover, the necessary overcooling reduces thermal efficiency. Periodic rotation of such fuel elements alleviates these performance losses. A multigroup study in hexagonal geometry has shown that rotation of the elements adjacent to the core-blanket interface completely flattens fast fluences and burnup at the end of the third cycle, when the element is unloaded. The maximum values of fast fluences are reduced by 13% in the core and 28% in the blanket, while the maximum burnup decreases by 12% in the core and 39% in the blanket. In addition, flux tilts are decreased somewhat. The main benefit of rotation lies in the prevention of excessive bowing by flattening of average fluences and temperature.

3.7. EXCESS REACTIVITY

The core fuel loading provides sufficient excess reactivity to accommodate reactivity losses arising from (1) the temperature defect from the cold shutdown to hot operating condition, (2) the depletion of fissile material, (3) the buildup of fission products, (4) the core expansion due to box swelling, (5) the buildup of Np-239, which because of its 2.35-day half-life delays the buildup of Pu-239, and (6) the pressurization of the helium coolant.

The magnitude of the various components of the excess reactivity requirement is given in Table 3.8. Together with the Doppler effect, expansion effects reduce core reactivity when the temperature increases from the cold shutdown to hot operating condition. In particular, the grid plate expands radially and the fuel, along with the cladding, expands axially. As shown, those expansion effects exceed in total magnitude the Doppler effect.

TABLE 3.8

REACTIVITY REQUIREMENTS FOR THE CONTROL ROD SYSTEM

(reactivity in dollars: $1 = 0.00351 Δk)

	$
Cold-to-Hot Operation	
Doppler effect	-1.30
Grid plate expansion and distortion	-1.05
Fuel-length expansion	-0.60
Radial distortion (thermal bowing)	-0.05
Subtotal (temperature defect)	-3.00
Loss during Cycle	
Burnup[(a)]	-8.20
Axial swelling	-0.25
Radial swelling and distortion	-0.55
Subtotal	-9.00
Other Allowances	
Compensate removal of He	-0.40
Compensate Np^{239} decay	-0.60
Subtotal	-1.00
Minimum Shutdown Margin	
(one stuck rod + standard 0.01 Δk margin)	-3.85
Total Control Requirements	-16.85
Total control capability (control system only)	-17.85
Extra shutdown margin (to cover some uncertainties)	-1.00

(a) Conservative allowance

The dominant long-term reactivity effect is due to fuel burnup. The remaining contribution comes from cladding and fuel-box swelling. Cladding swelling leads to axial expansion of the fuel, and uneven swelling of the fuel box in the radial flux-temperature gradient spreads the fuel elements apart in the lower region of the core.

Other reactivity allowances cover the loss associated with helium pressurization and delay in the decay of Np-239 into Pu-239.

The excess reactivity requirements shown in Table 3.8 are based on the phase of the equilibrium cycle with the largest drop in burnup reactivity. The excess reactivity requirements of the first core (approach to equilibrium) will be equal to or smaller than those shown in Table 3.8.

The reactor reactivity balance for various stages of reactor operation and shutdown and various combinations of control rod availability are presented in Table 3.9.

3.8. REACTOR CONTROL

Reactivity control is provided by 27 neutron-absorbing rods grouped in two independent systems: the control rod system and the shutdown rod system. They are independent with regard to both instrumentation and operation.

The control rod system has 21 rods with a total worth of $17.85 or 0.0627 Δk. Since the worth of a single rod amounts to $0.85, or less than $1.00, the reactor could not become prompt critical with the accidental removal of a single rod. Under normal operating conditions, 10 or fewer rods are required for reactor control. Control rod insertion is varied as necessary during a reload interval to compensate for the changes in the components of the excess reactivity described in Section 3.7. As shown in Table 3.9, the control rod system provides adequate control margin for all operating conditions. In fact, during normal power operation, the control rod system is the only one used.

TABLE 3.9

REACTIVITY STATUS AT BEGINNING OF CYCLE FOR VARIOUS CONDITIONS

(Reactivity in $)

Control-rod set (C) total worth = $17.85 (each rod $0.85)
Shutdown-rod set (S) total worth = $9.60 (each rod $1.60)

Core Status	Core Excess Reactivity[a]	Assumed Mode of Control	Availability of Control and Shutdown Rods	Inserted Worth of Control Set		Inserted Worth of Shutdown Set	Total Worth Inserted	Excess Control in the Core	Excess Control Out of the Core
				Assigned to Burnup Reactivity	Other Rods in Control Set				
Cold Shutdown									
1. Cold, depressurized, Np^{239} decayed, subcritical	13	C + S	All available	9	8.85	9.60	27.45	14.45	0
Startup (after long shutdown)[b]									
1. Cold, depressurized, Np^{239} decayed, subcritical	13	C	All available	9	8.85	0	17.85	4.85	9.60
2. Cold, pressurized, Np^{239} decayed, critical	12.60	C	All available	9	3.60	0	12.60	0	14.85
Hot Standby									
1. Warm (at inlet temperature), pressurized, with Np^{239}, subcritical	10.90[c]	C + S	All available	9	8.85	9.60	27.45	16.55	0
2. Same as 1	10.90	C - 1	1 stuck control	9	8	0	17	6.10	9.60
3. Same as 1	10.90	S - 1	1 stuck shutdown	9	0	8	17	6.10	8.85
4. Same as 1, critical	10.90	C	All available	9	1.90	0	10.90	0	16.55
Power Operation									
1. Hot, full power	9	C	All available	9	0	0	9	0	18.45

[a] With respect to hot, full power, end of cycle.

[b] For a startup after a short shutdown, the core reactivity is smaller by up to $0.60 ($Np^{239}$ not completely decayed).

[c] The temperature defect "cold-to-inlet temperature" amounts to $1.10.

The shutdown rod system provides an independent shutdown capability. The system serves two functions. Normally, it provides a substantial negative reactivity while the reactor is in the shutdown condition, especially during refueling. In addition, since it is always withdrawn prior to approach to criticality, in the event of failure of the control system, the shutdown system can scram the reactor independently. Note that neither of these functions requires anything other than that the rods in the shutdown system be either fully in or fully out. Partial insertion or single rod functioning is not required. Hence, the system can be made up of a few, relatively high-worth rods, in this case six with a total worth of $9.60 or 0.0337 Δk. This total worth is smaller than that of the control rod system because, as a scram backup, the shutdown system must cover only the excess reactivity not compensated by already inserted control rods.

Control and shutdown rods, including specifications, effects on power distribution, and control rod burnup, are discussed in more detail in Section 5.3.

4. BASIC PHYSICS DATA AND METHODS

The validity of reactor physics calculations depends on the availability of reliable computational methods and accurate cross-section data. The intensive research work that has been expended in the development of computational methods for the physics design of thermal and fast reactors has brought to the reactor physicist a full array of computer codes that offer him flexibility and accuracy for most calculations. By contrast, the basic nuclear data available for fast-reactor analysis still contain gaps or insufficiently accurate values that severely limit the precision achievable in the calculation of fundamental reactor parameters such as critical mass and breeding ratio. The LMFBR program plan (Ref. 8) indicates a resulting uncertainty of ±3% in k (equivalent to about ±5% in critical mass for the GCFR) and an uncertainty of ±0.2 in breeding ratio.

Many difficulties with basic nuclear data lie in the poor status of certain cross sections in the resonance range between 0.5 and 50 keV. The experimental difficulties encountered in the measurement of cross sections at such energies lead to a lack of completely reliable data, even for such important nuclides as Pu-239 and U-238. Since many fast-reactor characteristics are strongly influenced by the reaction rates in that energy range, the data uncertainty leads to uncertainties in reactor characteristics. In this respect it should be noted that the GCFR is less sensitive to resonance-cross-section uncertainties than LMFBRs because of the inherently harder spectrum; i.e., there is less flux in the resonance region. For example, the ±0.2 uncertainty in breeding ratio quoted in Ref. 8 for the LMFBR is probably excessive in the case of the GCFR; less than ±0.1 would be more appropriate. As a matter of fact, the hard spectrum of the GCFR leads not only to a higher breeding ratio than for other breeder types, but also to a greater certitude that the breeding ratio will indeed be high.

4.1. CROSS SECTIONS

Most of the cross-section data used in GCFR physics have been evaluated at Gulf General Atomic on the basis of available experimental results and accepted nuclear theories. Through active participation in the Cross Section Evaluation Working Group, which is responsible for the updating of the ENDF/B cross-section file, Gulf General Atomic has access to the latest cross-section information. ENDF/B data tapes can be immediately converted into the standard GGA file format with the help of the interfacing codes GFE-II and GAND (see Appendix A).

The three nuclides of particular importance in fast-reactor physics are Pu-239, Pu-240, and U-238. All three are important for criticality calculations, and U-238 determines the Doppler coefficient.

4.1.1. Plutonium-239

Until recently, the well known uncertainty in Pu-239 capture to fission cross-section ratios (α values) below 20 keV has represented the most important cross-section uncertainty for plutonium-fueled reactors. Several measurements, in particular those performed at Oak Ridge National Laboratory by Gwin and his co-workers (Ref. 9), have apparently settled the matter. Gwin's results are shown in Fig. 4.1, with those of Lottin (Oak Ridge Van de Graff measurements, Ref. 10), Czirr (Ref. 11), and some preliminary results (Ref. 12).

Earlier measurements by Schomberg, et al. (Ref. 13), Patrick, et al. (Ref. 14), James and Patrick (Ref. 15), and Michaudon (Ref. 16) showed the presence of a peak (to about 1.3) in the α curve in the vicinity of 6 keV, a peak that has not been found in the measurement displayed in Fig. 4.1. This area represents possibly the last significant uncertainty in plutonium α.

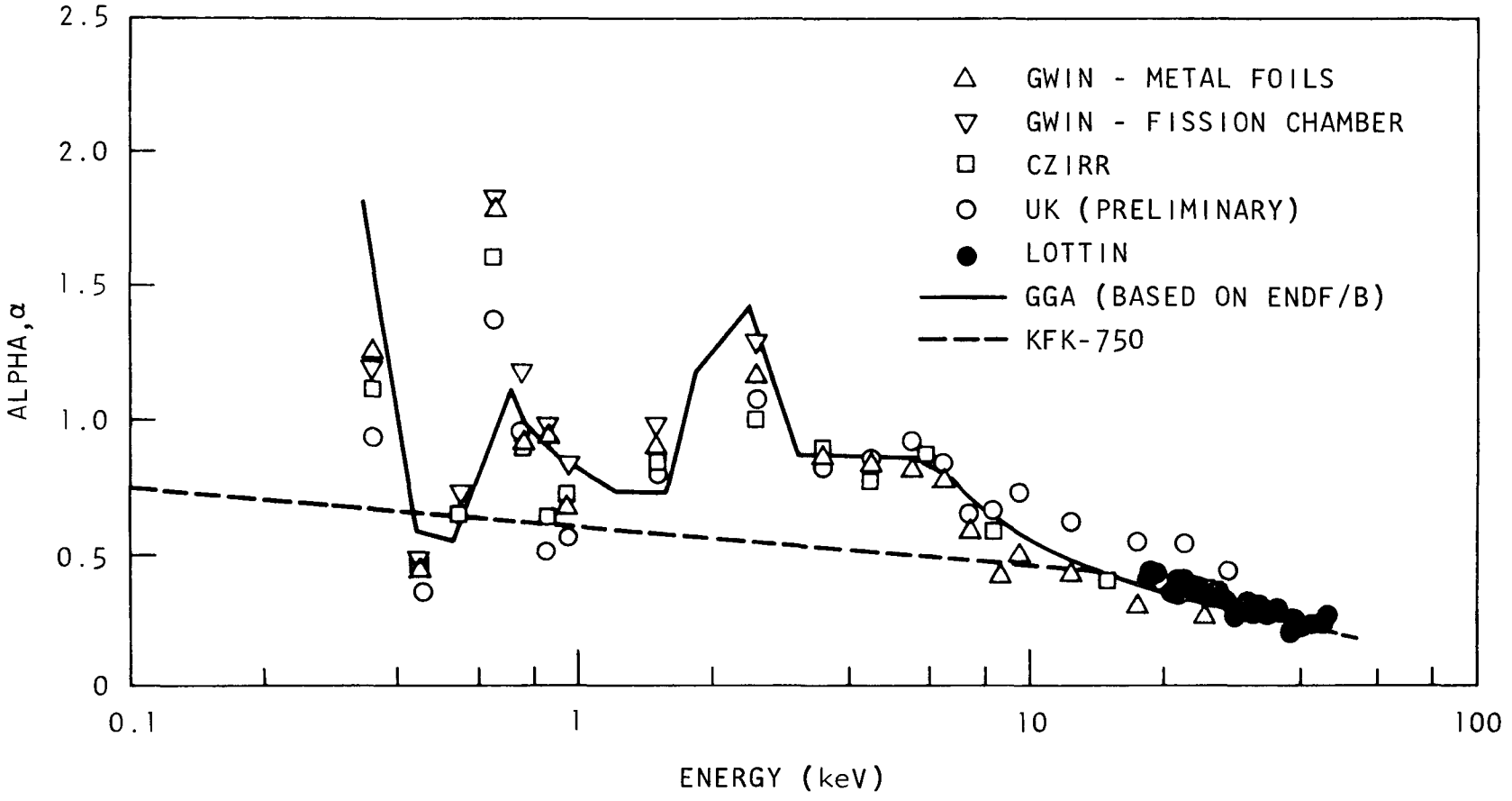

Fig. 4.1. Plutonium-239 capture-to-fission ratio

Most of the calculations reported here were based on Pu-239 cross sections assembled by Schmidt and co-workers in KFK-750 (Ref. 17). The fission and capture cross sections are shown in Fig. 4.2. The fission cross curve follows Smith and co-workers (Ref. 18) above 3 MeV, Smirenkin and co-workers (Ref. 19) between 0.5 and 3 MeV, White, et al. (Ref. 20), and Perkins, et al. (Ref. 21), between 50 and 500 keV, and Coté et al. (Ref. 22), between 1 and 50 keV. The capture cross section is based on the α values of Hopkins and Diven (Ref. 23). The corresponding α values between 0.1 and 50 keV are shown in Fig. 4.1. (These are basically the old KAPL values (Ref. 24).)

The standard KFK-750 data must be corrected in the range 0.3 to 30 keV on the basis of previously mentioned measurements by Gwin. New unresolved resonance parameters have therefore been prepared for use with the GANDY option of GGC-5 (Ref. 25). These parameters were obtained from those developed by Hitchcock and Hutchins (Ref. 12) for ENDF/B, Version II. The new unresolved parameters are listed in Table 4.1 for 18 GAM fine groups along with the resulting cross sections. As seen in Figs. 4.1 and 4.3, these cross sections agree well with experimental measurements, including those of Shunk (Ref. 26) and James (Ref. 27). The differences in broad-group cross section in the GCFR spectrum for the standard KFK-750 data and the revised Gwin-KFK data are shown in Table 4.2.

Unless otherwise noted, all calculations reported here were performed with the standard KFK-750 data in the whole energy range.

4.1.2. Plutonium-240

There is still a significant degree of uncertainty in the cross-section data of Pu-240. The disagreement between various evaluations of the capture cross section exceeds a factor of 2 in the whole energy range up to 1 MeV. In the case of the GCFR, where 15.5% of the plutonium is Pu-240, such a discrepancy is equivalent to about 1% in multiplication factor.

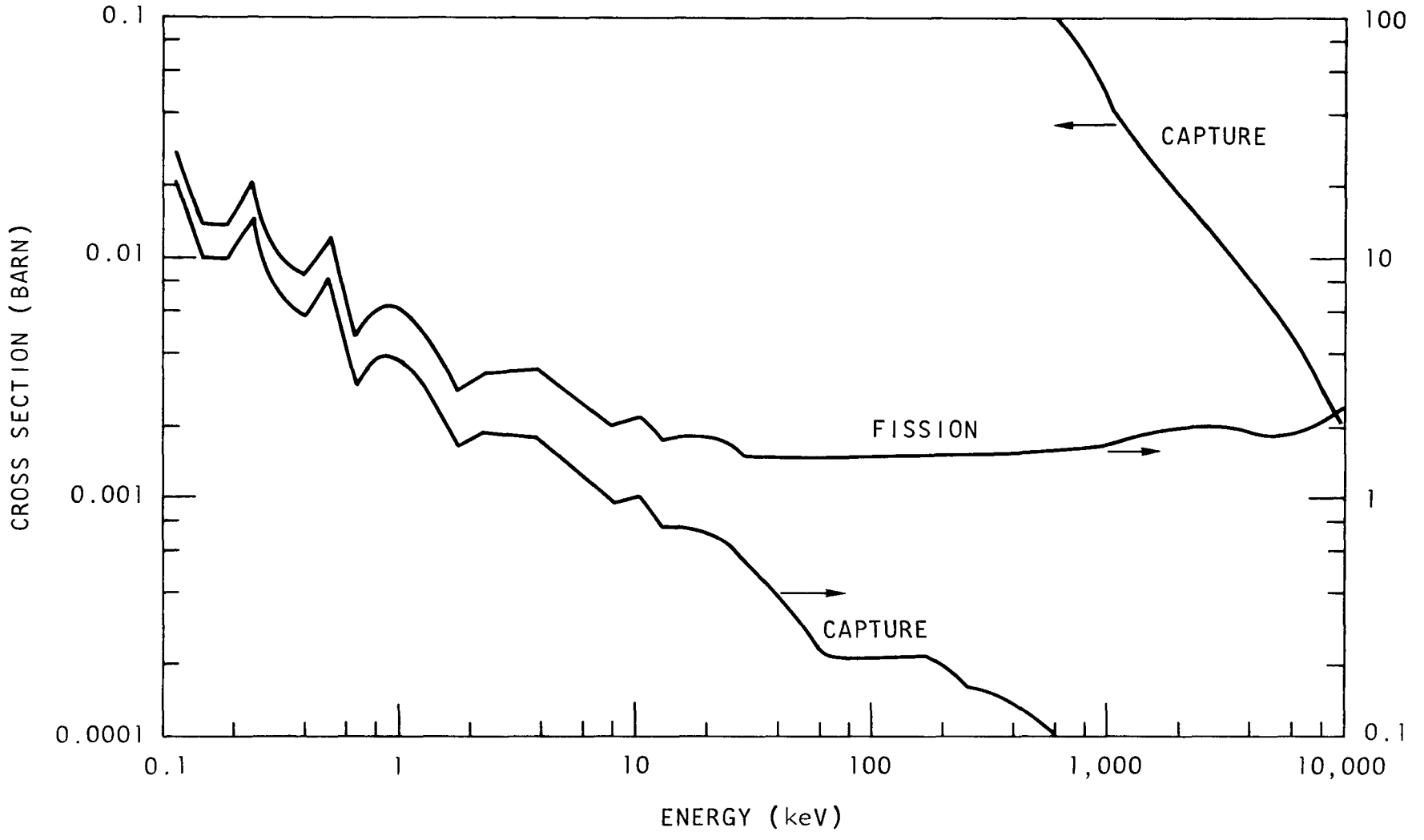

Fig. 4.2. Fission and capture cross sections of Pu-239 (from KFK-750)

TABLE 4.1

UNRESOLVED RESONANCE PARAMETERS FOR Pu-239

(for Gwin data, based on Ref. 12)

Fine Group No.	Midpoint Energy (keV)	s-Wave Strength Function $(eV)^{-1/2}$	s-Wave J-1 Fission Width (eV)	Derived Cross Sections (barns)				
				σ_f	σ_c	α	σ_n	σ_{tot}
56	22.05	0.988×10^{-4}	0.0841	1.813	0.617	0.340	11.13	13.56
57	17.17	0.995×10^{-4}	0.0684	1.848	0.737	0.399	11.30	13.89
58	13.37	1.002×10^{-4}	0.0552	1.912	0.880	0.460	11.48	14.27
59	10.41	1.021×10^{-4}	0.0525	2.046	1.057	0.516	11.70	14.80
60	8.11	1.091×10^{-4}	0.0368	2.143	1.342	0.626	12.08	15.56
61	6.32	1.099×10^{-4}	0.0244	2.182	1.670	0.765	12.38	16.23
62	4.92	1.095×10^{-4}	0.0206	2.324	2.009	0.864	12.61	16.94
63	3.83	1.090×10^{-4}	0.0224	2.701	2.323	0.860	12.74	17.70
64	2.98	1.064×10^{-4}	0.0345	3.034	2.663	0.878	12.84	18.50
65	2.32	1.068×10^{-4}	0.0049	2.548	3.623	1.422	13.33	19.54
66	1.81	1.043×10^{-4}	0.0124	3.343	3.866	1.156	13.20	20.40
67	1.41	0.984×10^{-4}	0.0598	5.006	3.611	0.721	12.73	21.35
68	1.10	1.037×10^{-4}	0.0563	5.834	4.251	0.729	12.95	23.08
69	0.855	0.951×10^{-4}	0.0434	5.722	5.121	0.895	12.88	23.72
70	0.666	0.882×10^{-4}	0.0129	6.188	6.477	1.047	13.23	26.10
71	0.518	1.297×10^{-4}	0.1230	11.86	6.490	0.547	13.74	31.81
72	0.404	0.823×10^{-4}	0.1166	9.643	5.590	0.580	12.39	28.01
73	0.314	1.221×10^{-4}	0.0067	8.075	14.79	1.832	16.17	38.55

NOTES:

$A = 236.999$

$R = 9.05 \times 10^{-13}$ cm

$I = 1/2$

$$D = \begin{cases} 8.78 \text{ eV for } J = 0 \\ 3.12 \text{ eV for } J = 1 \\ 2.123 \text{ eV for } J = 2 \end{cases}$$

$$S^{\ell=1} = 1.5 \times 10^{-4} \ (eV)^{-1.2}$$

$$\left\langle \Gamma_\gamma \right\rangle^{\ell=0} = \left\langle \Gamma_\gamma \right\rangle^{\ell=1} = 0.0416 \text{ eV}$$

$$\left\langle \Gamma_f \right\rangle^{\ell=0} = 1.5 \text{ eV for } J = 0$$

$$\left\langle \Gamma_f \right\rangle^{\ell=1} = \begin{cases} 0.0 \text{ for } J = 0 \\ 1.0 \text{ for } J = 1 \text{ and } 2 \end{cases}$$

$$NDFF^{\ell=0} \begin{cases} 2.0 \text{ for } J = 0 \\ 1.0 \text{ for } J = 1 \end{cases}$$

$$NDFF^{\ell=1} \begin{cases} 2.0 \text{ for } J = 1 \\ 3.0 \text{ for } J = 2 \end{cases}$$

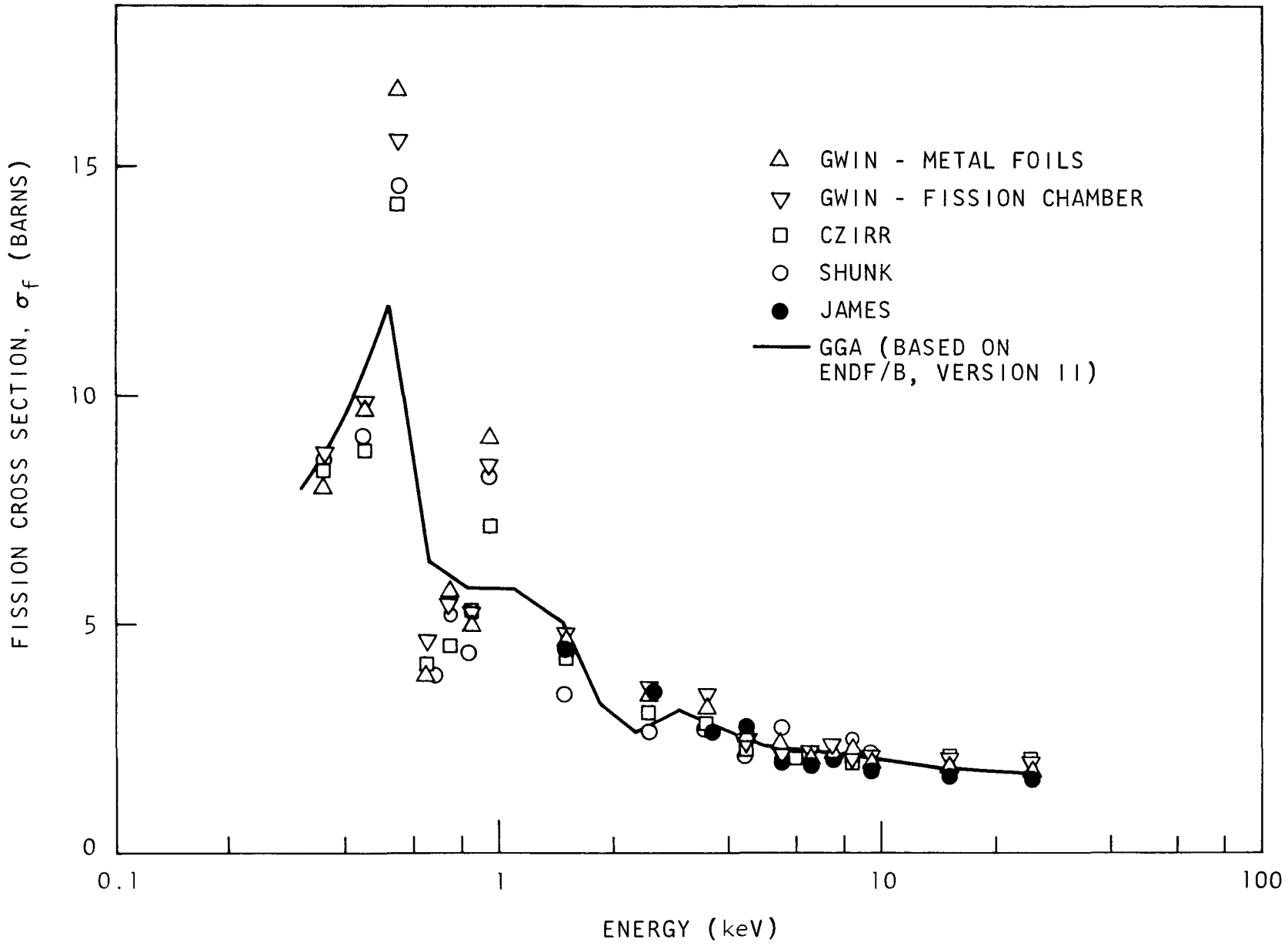

Fig. 4.3. Comparison of Pu-239 σ_f in ENDF/B, Version II, with experimental data

TABLE 4.2

Pu-239 CROSS SECTIONS[a]

Energy		Capture		Fission		Alpha = σ_c/σ_f	
Group	Lower Limit (keV)	Gwin-KFK (new)	KFK (old)	Gwin-KFK (new)	KFK (old)	Gwin-KFK (new)	KFK (old)
1	3679	0.0066	0.0066	1.914	1.914	0.003	0.003
2	1353	0.0186	0.0187	1.943	1.942	0.010	0.010
3	497.9	0.0791	0.0791	1.641	1.641	0.048	0.048
4	183.2	0.1625	0.1626	1.552	1.552	0.105	0.105
5	67.38	0.2151	0.2151	1.501	1.502	0.143	0.143
6	24.79	0.3765	0.3908	1.473	1.529	0.256	0.256
7	9.119	0.7932	0.7871	1.893	1.881	0.419	0.418
8	3.355	1.7784	1.2906	2.300	2.568	0.773	0.503
9	0.454	3.5413	2.6980	3.721	4.124	0.952	0.654
10	0.414 eV	7.5922	7.7764	10.49	9.172	0.724	0.848

[a] Comparison between old data used in GCFR physics (taken from KFK-750, Ref. 17) and new data (KFK-750 data, plus Gwin's values (Ref. 9) between 0.3 and 30 keV)

Up to now, the data of Drake and Dyos (Ref. 28) have been used in GCFR physics work. As shown in Fig. 4.4, their recommended capture cross section curve follows closely the later evaluation of Yiftah (Ref. 29) up to 600 keV, but is much higher than all recent evaluations in the neighborhood of 1 MeV. On the other hand, the fission cross section does not reflect the recently understood phenomenon of a subthreshold fission and drops rapidly below 40 keV (Ref. 30).

The ENDF/B, Version II, data are also shown in Fig. 4.4. Experimental evidence indicates that these latter data should be quite accurate. For example, Schmidt (Ref. 31) reports that the Pitterle evaluation (Ref. 32) (a modified form of ENDF/B, Version I, shown in Fig. 4.4) yields excellent predictions of reactivity differences due to Pu-240 in two SNEAK assemblies and that the result for the assembly with the softer spectrum could be improved by a somewhat higher capture cross section in the keV range, as is indeed the case with the ENDF/B, Version II, capture.

Table 4.3 shows the unresolved resonance parameters for use in GANDY, which correspond to the ENDF/B, Version II, infinite dilution cross sections. The broad-group capture cross sections of Pu-240 in the GCFR spectrum are shown in Table 4.4 for both the previously used Drake data and the new ENDF/B, Version II, data.

4.1.3. Uranium-238

Uranium-238 has now replaced Pu-239 as the nuclide whose cross-section uncertainties have the most important bearing on fast-reactor performances. This is true particularly for the capture cross section, which is uncertain up to 20% over a wide range of the fast spectrum.

Figure 4.5 shows various measurements of the capture cross section between 1 keV and 1 MeV. For the sake of the discussion, it is convenient to consider three energy ranges.

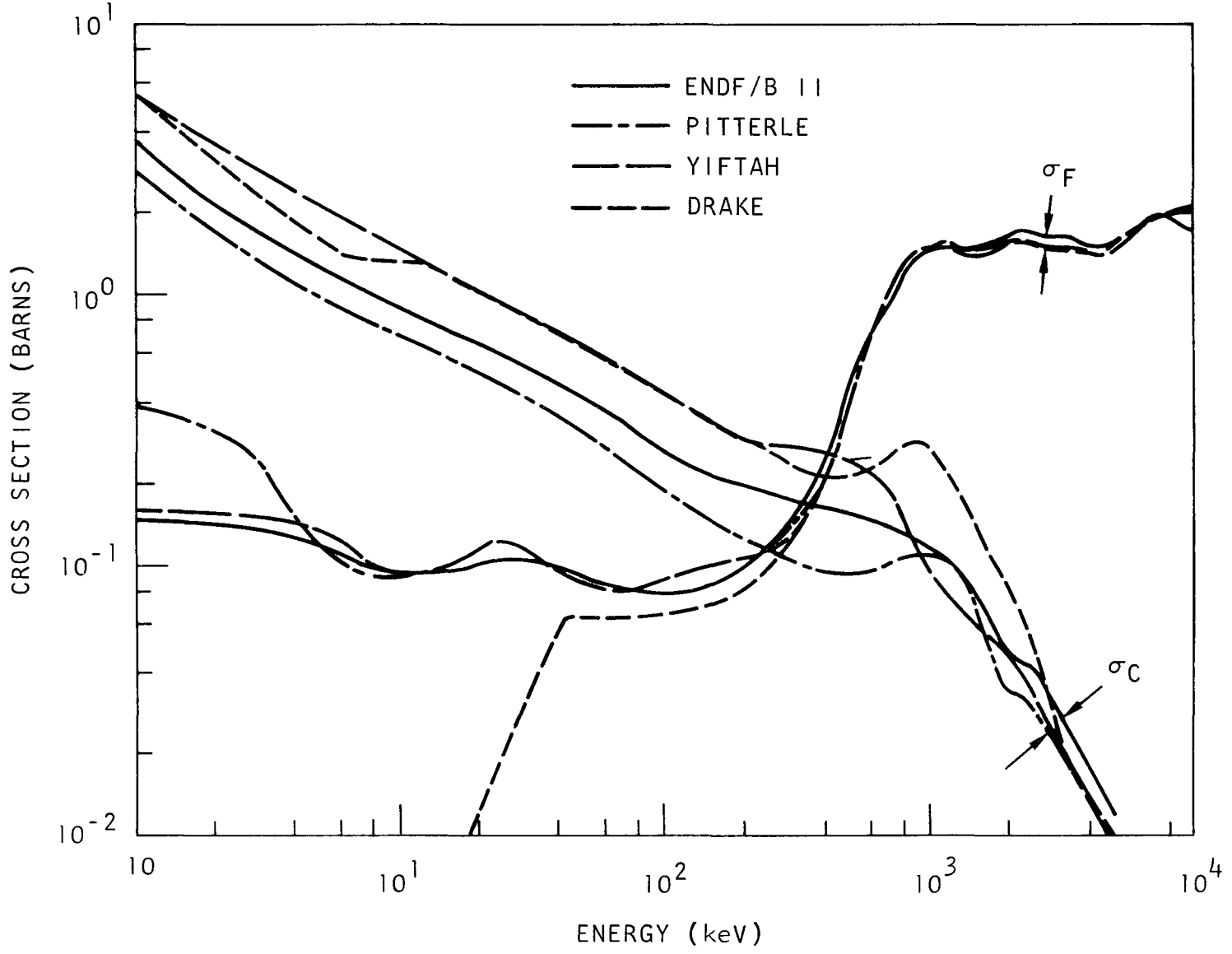

Fig. 4.4. Comparison of fission and capture evaluations for Pu-240

TABLE 4.3

Pu-240 UNRESOLVED RESONANCE PARAMETERS

Average Level Spacing

D = 16 eV for J = 1/2

D = 9.65 eV for J = 3/2

Strength Function

s-wave $1.06\ 10^{-4}\ eV^{-1/2}$

p-wave $1.75\ 10^{-4}\ eV^{-1/2}$

Chi-Square Distributions

Degree of freedom: 1 for all states

Average Radiation Width

$\langle \Gamma_\gamma \rangle$ = 0.030 eV for all J

GAM Group	Mid-energy (keV)	Average Fission Width (eV)		
		ℓ=0	ℓ=1, J=1/2	ℓ=1, J=3/2
54	36.35	1.9×10^{-4}	1.395×10^{-2}	8.43×10^{-3}
55	28.31	1.9×10^{-4}	1.313×10^{-2}	7.93×10^{-3}
56	22.05	1.9×10^{-4}	1.235×10^{-2}	7.44×10^{-3}
57	17.17	1.9×10^{-4}	1.177×10^{-2}	7.10×10^{-3}
58	13.37	1.9×10^{-4}	1.133×10^{-2}	6.86×10^{-3}
59	10.41	1.9×10^{-4}	1.104×10^{-2}	6.68×10^{-3}
60	8.11	1.9×10^{-4}	1.094×10^{-2}	6.60×10^{-3}
61	6.32	1.9×10^{-4}	1.069×10^{-2}	6.43×10^{-3}
62	4.92	1.9×10^{-4}	1.051×10^{-2}	6.34×10^{-3}
63	3.83	1.9×10^{-4}	1.037×10^{-2}	6.26×10^{-3}
64	2.98	1.9×10^{-4}	1.029×10^{-2}	6.22×10^{-3}
65	2.32	1.9×10^{-4}	1.022×10^{-2}	6.18×10^{-3}
66	1.81	1.9×10^{-4}	1.017×10^{-2}	6.12×10^{-3}
67	1.41	1.9×10^{-4}	1.009×10^{-2}	6.09×10^{-3}
68	1.10	1.9×10^{-4}	1.003×10^{-2}	6.05×10^{-3}
69	0.854	1.9×10^{-4}	1.000×10^{-2}	6.03×10^{-3}

TABLE 4.4

Pu-240 CAPTURE BROAD-GROUP CROSS SECTIONS

Group	Lower Energy (keV)	ENDF/B (Version II)	Ref. 28
1	3679	0.0138	0.0235
2	1353	0.0511	0.0810
3	497.9	0.1314	0.2497
4	183.2	0.1760	0.2468
5	67.38	0.2520	0.4226
6	24.79	0.4363	0.7608
7	9.119	0.7312	1.045
8	3.355	1.163	1.297
9	0.454	2.290	2.309
10	0.414 eV	7.890	7.908

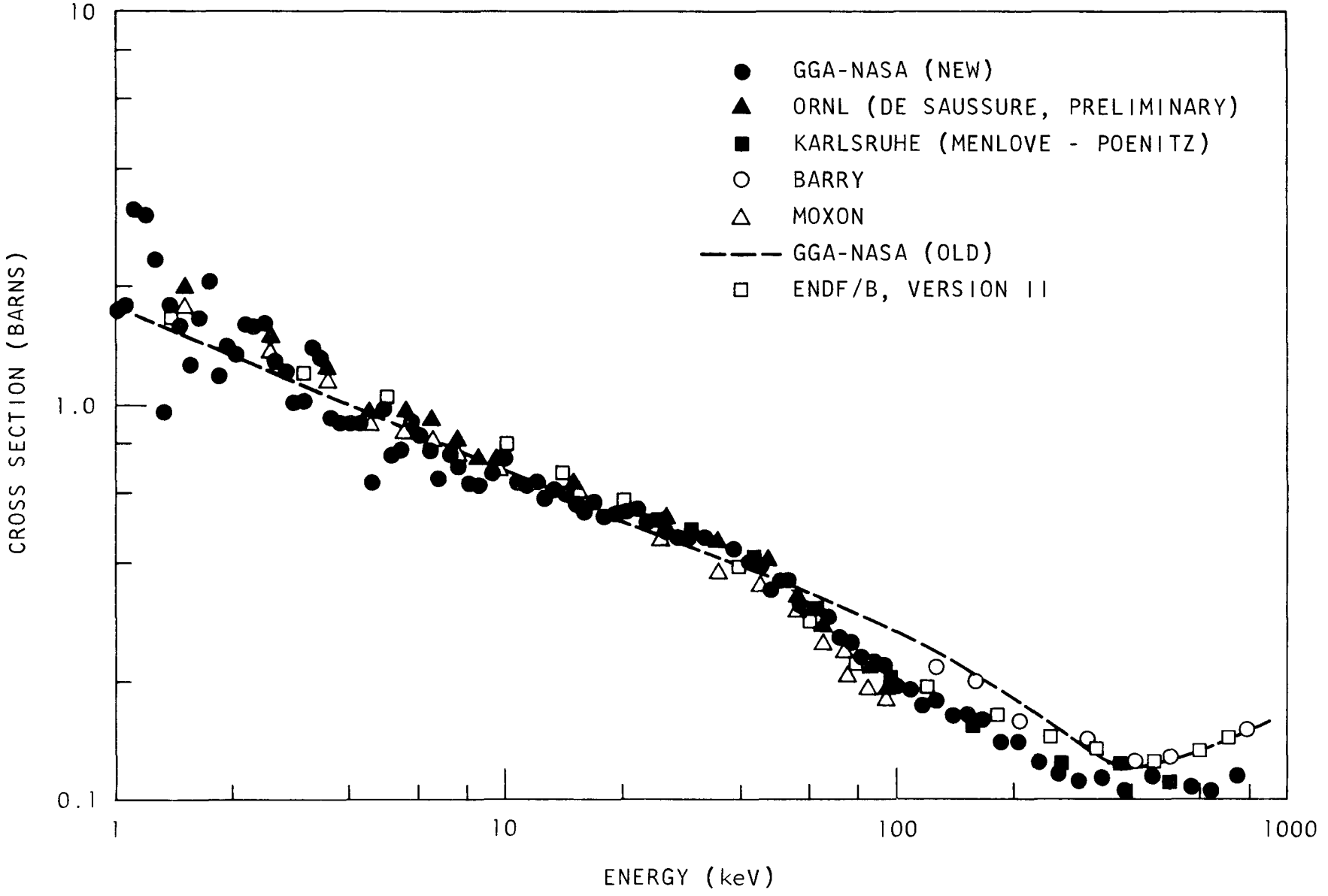

Fig. 4.5. U-238 capture cross section

Between 1 and 20 keV, there is considerable scatter between experiments but the agreement between experimental data and values derived from predicted statistical resonance parameters is reasonable.

Between 20 and 100 keV, the data can be separated into two sets, about 15% apart in the value of the capture cross section. The first set includes the recent measurements performed for NASA by the GGA LINAC group (Refs. 33, 34), preliminary results from Oak Ridge National Laboratory (Ref. 35), and the Karlsruhe measurements of Menlove and Poenitz (Ref. 36). The three measurements in this first set are all within a 5% band. The second set includes the measurements of Moxon (Ref. 37). Contrary to Schmidt's suggestion (Ref. 31) to use Moxon's data, Davey (Ref. 38) rejected them and recommended a curve that follows very closely Menlove and Poenitz. The additional evidence provided by the latest GGA and ORNL results gives further confirmation of the Menlove and Poenitz data. The use of GGA detailed data between 20 and 100 keV thus seems to be justified.

The situation is somewhat more difficult above 100 keV. As stated by Davey (Ref. 38), the measurements of Barry, et al. (Ref. 39), occupy a preeminent place in that energy range. Yet the GGA and Karlsruhe measurements lead to a capture cross section that is up to 20% lower than the Barry results. If the Barry results are considered to be correct, there is then some arbitrariness in the matching of curves at 100 keV. The old GGA-NASA set (Ref. 40) was based mainly on Barry's data, and it therefore disagrees with recent measurements between 60 and 100 keV. Davey decided to drop the two lowest energy points of Barry (at 127 and 160 keV) and to join smoothly the Karlsruhe value at 97.3 keV and the Barry value at 207 keV, thereby rejecting Karlsruhe values above 100 keV. Such a rejection is not supported by the latest measurements. The new GGA-NASA data confirm Karlsruhe results above 100 keV; furthermore, Moxon's results and the preliminary ORNL results up to 100 keV also tend to confirm them.

In summary, the new GGA-NASA data are a good representation of the most recent "low-capture" measurements for U-238, and it appears that these

data should be used in all GCFR physics calculations, together with Barry values above 1 MeV. The old GGA-NASA data, on the other hand, represent well the previously accepted "high-capture" measurements. These latter data have been used for most of the calculations presented in this report.

Unresolved resonance parameters were prepared for the new GGA-NASA data with the code PMING (see Appendix B), which searches for the optimum parameters that would minimize the error on the desired infinite dilution cross sections. These unresolved parameters are shown in Table 4.5.

Table 4.6 compares the GCFR broad-group cross sections for the old GGA-NASA data, the latest ENDF/B data (Version II), the new GGA-NASA data (between 1 and 800 keV, otherwise ENDF/B-II), and Moxon's values (between 1 and 100 keV, otherwise ENDF/B-II).

4.1.4. Effect of U-238 Cross-Section Uncertainties on Reactor Performance

The impact of U-238 cross-section uncertainties has been investigated by computing some key reactor parameters for the various U-238 capture data sets shown in Fig. 4.5. The calculations were performed in r-z geometry with ten energy groups. All broad-group cross sections were derived with the B_1 and GAROL-GANDY options of GGC-5 (Section 4.2.1). Table 4.7 gives the results that were obtained for the demonstration plant.

The new GGA-NASA data have the greatest impact on reactor performance. The reactivity exceeds by 0.0149 the value obtained with the ENDF/B data. The breeding ratio drops by 0.07 with a resulting detrimental effect on doubling time and fuel costs.

It is also of interest to consider the influence of these various cross-section sets on the performance of a 1000-MW(e) GCFR plant. The comparison is shown in Table 4.8. The reactor has a thermal output of 2564 MW(t), a core volume of 5272 liters, a specific power of 1.294 MW(t)/kg fissile, and an average core enrichment of 15.8%. The results show the same trend as for the demonstration plant. The breeding ratio drops by 0.08

TABLE 4.5

GANDY OPTION UNRESOLVED RESONANCE PARAMETERS

FOR 1970 GGA U-238 CAPTURE CROSS SECTION DATA

Fine Group No.	Midpoint Energy (keV)	Desired Capture Cross Section (barns)	s-Wave Strength Function ($eV^{-1/2} \times 10^4$)	Partial Capture Cross Sections			Scattering Cross Sections	
				s-Wave (barns)	p-Wave (barns)	d-Wave (barns)	Derived (barns)	ENDF/B Ver. II (barns)
51	76.95	0.2469	0.34596	0.0341	0.1226	0.0902	10.72	11.92
52	59.93	0.3084	0.52108	0.0459	0.1613	0.1011	11.39	12.32
53	46.67	0.3744	0.72861	0.0608	0.2074	0.1062	12.17	12.71
54	36.35	0.4409	0.93039	0.0794	0.2594	0.1021	12.99	13.05
55	28.31	0.4670	0.87581	0.0993	0.2939	0.0737	12.98	13.24
56	22.05	0.5273	0.94624	0.1267	0.3427	0.0580	13.44	13.48
57	17.17	0.5420	0.78350	0.1547	0.3522	0.0346	13.06	13.75
58	13.37	0.6024	0.79257	0.1948	0.3830	0.0246	13.33	13.92
59	10.41	0.6690	0.79870	0.2448	0.4070	0.0172	13.63	14.07
60	8.11	0.6728	0.64851	0.2938	0.3685	0.0097	13.23	14.40
61	6.31	0.7871	0.73542	0.3773	0.4019	0.0076	13.99	14.81
62	4.92	0.7826	0.58553	0.4459	0.3316	0.0042	13.51	15.28
63	3.83	0.9608	0.71886	0.5840	0.3733	0.0035	14.71	15.56
64	2.98	1.1935	0.89426	0.7669	0.4230	0.0030	16.48	14.11
65	2.32	1.5163	1.1659	1.0167	0.4969	0.0027	19.42	17.76
66	1.81	1.5604	0.90078	1.1907	0.3683	0.0014	18.02	22.30
67	1.41	1.5774	0.63507	1.3342	0.2422	0.0007	16.15	16.57

$A = 236.01$

$R = 0.92 \times 10^{-12}$ cm

$\langle \Gamma_\gamma \rangle = 19.1 \times 10^{-3}$ eV

$$\langle D \rangle = \begin{cases} 20.8 \text{ eV} & \text{for } J = 1/2 \\ 11.4 \text{ eV} & \text{for } J = 3/2 \\ 6.9333 \text{ eV} & \text{for } J = 5/2 \end{cases}$$

$$\left.\begin{aligned} S^{\ell=1} &= 2.1667 * S^{\ell=0} \\ S^{\ell=2} &= 5.5555 * S^{\ell=0} \end{aligned}\right\} S^{\ell=0} \equiv \left[\frac{\langle \Gamma_n^0 \rangle}{\langle D \rangle}\right]^{\ell=0}$$

TABLE 4.6

U-238 CAPTURE CROSS SECTION
(barn)

Group	Lower Energy (keV)	Old GGA-NASA	ENDF/B Vers.II	ENDF/B-2 + GGA-NASA (new)	ENDF/B-2 + Moxon
1	3679	0.0117	0.0113	0.0113	0.0113
2	1353	0.0458	0.0534	0.0534	0.0534
3	497.9	0.1349	0.1405	0.1237	0.1405
4	183.2	0.1478	0.1421	0.1197	0.1421
5	67.38	0.2519	0.1980	0.1936	0.1938
6	24.79	0.3831	0.3912	0.3901	0.3530
7	9.119	0.5526	0.6356	0.5603	0.5634
8	3.355	0.8171	0.8818	0.7188	0.7808
9	0.454	1.1487	1.0736	1.0944	1.1449
10	0.414 eV	1.4807	1.3907	1.3906	1.3906

TABLE 4.7

EFFECT OF VARIOUS U-238 CAPTURE DATA

FOR THE DEMONSTRATION PLANT

Data Set	k_{eff}	$\%\Delta k/k$[a]	$\%\Delta M/M$[b]	$\bar{\alpha}$[c]	Breeding Ratio[d]	Doubling Time (yrs)[e]
ENDF/B-II[f]	1.0390	--	--	0.209	1.34	15.9
New GGA-NASA[g]	1.0554	+1.49	-2.3	0.215	1.27	20.0
Moxon[g]	1.0498	+0.99	-1.5	0.214	1.29	18.6
Old GGA-NASA[h]	1.0491	+0.93	-1.4	0.174	1.33	16.9

[a] With respect to ENDF/B-II

[b] Change in critical mass with respect to ENDF/B-II, based on the empirical relationship: 1% fissile mass → 0.66% $\Delta k/k$

[c] Average fissile capture-to-fission ratio

[d] Breeding ratio based on (U-238 + Pu-240)/(Pu-239 + Pu-241)

[e] Linear doubling time = $2.74/S(1+\bar{\alpha})\ (BR-1)\ (1-F)L$, where S = specific power (MW(t)/kg fissile), L = load factor (0.8), F = fertile fraction of total fissions (= 0.161 for the demonstration plant)

[f] With high Pu-239 α and low Pu-240 capture

[g] With ENDF/B-II U-238 data, high Pu-239 α, and low Pu-240 capture

[h] With low Pu-239 α and high Pu-240 capture

TABLE 4.8

EFFECT OF VARIOUS U-238 CAPTURE DATA

FOR THE 1000-MW(e) PLANT

Data Set	k_{eff}	$\%\Delta k/k$[a]	$\%\Delta M/M$[b]	$\bar{\alpha}$[c]	Breeding Ratio[d]	Doubling Time (yr)[e]
ENDF/B-II[f]	0.9850	--	--	0.210	1.50	5.4
New GGA-NASA[g]	1.0024	+1.76	-2.7	0.217	1.42	6.5
Moxon[g]	0.9966	+1.18	-1.8	0.216	1.45	6.0
Old GGA-NASA[h]	1.0010	+1.63	-2.5	0.175	1.50	5.6

[a] With respect to ENDF/B-II

[b] Change in critical mass with respect to ENDF/B-II, based on the empirical relationship: 1% fissile mass → 0.66% $\Delta k/k$

[c] Average fissile capture-to-fission ratio

[d] Breeding ratio based on (U-238 + Pu-240)/(Pu-239 + Pu-241)

[e] Linear doubling time = $2.74/S(1+\bar{\alpha})$ (BR-1) (1-F)L, where S = specific power (MW(t)/kg fissile), L = load factor (0.8), F = fertile fraction of total fissions (= 0.182)

[f] With high Pu-239 α and low Pu-240 capture

[g] With ENDF/B-II U-238 data, high Pu-239 α, and low Pu-240 capture

[h] With low Pu-239 α and high Pu-240 capture

and the doubling time increases by about 20% when the new GGA-NASA set replaces ENDF/B, Version II.

The comparison in reactor performance shown in Table 4.8 refers to the GCFR. As far as performance of the sodium fast reactor is concerned, the low U-238 capture cross sections decrease the breeding ratio by about the same amount, but the percentage drop of the breeding gain (BR-1) is larger because of the smaller breeding ratio ($\sim$1.25). Since the doubling time is inversely proportional to the breeding gain, fuel cycle economics are more affected by the low capture than is the case for the GCFR.

In conclusion, the use of the recent low capture U-238 data adversely affects the economics of the GCFR. On the other hand, as noted in Sections 6.1.3 and 6.6, reactor safety is improved because of the 30% larger Doppler coefficient and more negative steam flooding reactivity effect.

4.2. METHODS FOR SPECTRUM CALCULATIONS

Spectrum calculations for the preparation of few-group cross-section sets are performed with the GAM code, which is the fast section of GGC (GAM-GATHER-COMBO) (Ref. 25). The GAM code has been under active development at Gulf General Atomic over the last ten years, and it has been used extensively for the design of various fast and thermal reactors. Besides the basic cross-section data, the code GGC requires as input a value for the Dancoff factor for the heterogeneous treatment of the resonance region. This Dancoff factor is computed separately by a collision probability method which is described in Section 4.2.2.

4.2.1. The Fast Section of GGC

The GGC program solves the multigroup transport equation in two separate energy regions: the fast region, where only downscattering is allowed, and the thermal region, where upscattering is allowed. Spatial dependence of the flux is represented by a single input buckling which can be positive, negative, or zero.

Usually only the fast section of GGC, labelled GAM, is used in GCFR physics work. The current version of GAM offers a wide choice of options for flux and resonance calculations. Most of these options deal with the treatment of resonances where two levels of complexity are available:

	Resolved Resonances	Unresolved Resonances
Simple treatment	GAMNIT	TUZ
Complex treatment	GAROL	GANDY

All possible combinations of these four basic options may be used in the preparation of broad-group cross sections. The choice depends on the degree of accuracy required by a particular problem.

The current version of GGC (called GGC-5) is a major extension of the older GGC codes, which contained only the simple resonance treatments GAMNIT and TUZ. The methods GAROL (Ref. 41) and GANDY (Ref. 42) were embodied in separate codes that have subsequently been improved and incorporated into GGC, so either combination of treatments is now available.

4.2.1.1. Resolved Resonances. Table 4.9 compares the features of GAMNIT and TUZ, the two methods available for the computation of fine-group cross sections in the resolved resonance range.

GAMNIT considers the contribution to a cross section from each resonance and each material. No overlap is accounted for, either between sequences of resonances for the same nuclide or between resonances of various nuclides. A local spectrum calculation is performed in the vicinity of the resonance under consideration by assuming that the resonant absorber is lumped and surrounded by a moderator. Two other moderators may also be present in the lump (one is normally oxygen and the other the combined heavy metals mixed with the resonant absorber). GAMNIT uses the standard GAM data tapes, which contain all 99-group cross sections, background cross sections, and resonance parameters. GAMNIT broadens each resonance for the desired temperature, applies wing corrections, and computes the contribution of that

TABLE 4.9

COMPARISON BETWEEN GAROL AND GAMIT

RESOLVED RESONANCE TREATMENTS IN GGC-5

	GAMNIT	GAROL
Number of regions	2	2
Energy range	Epithermal	Epithermal
Mesh	Constant lethargy	Constant lethargy or velocity. Mesh may also be arbitrary.
Maximum number of energy points	500 points/resonance	10,000 points in 0.414 to 335 eV
Number of fine groups	99	36
Number of materials	1 in the absorber and 2 in the admixed moderator of region-1. In region-2 no materials are specified, since a 1/E flux is assumed.	A total of 10 nuclides (absorbers or moderators) in both regions
Number of resonance absorbers	1 (no more than 15 absorbers per run)	10
Number of resonances	250/absorber	No limit (uses cross sections instead of resonance parameters)
Resonance treatment	Isolated (each resonance separately)	Continuous with overlap (all resonances combined)
Formulation	Differential transport P_o equation	Differential transport P_o equation
Scattering law	Elastic, isotropic, in the center of mass	Elastic, isotropic, in the center of mass
Source distribution	Spatially flat	Spatially flat
Temperature specification	Each resonance absorber	Each resonance absorber
Flux above the resonance region	1/E	1/E

TABLE 4.9 (continued)

Doppler broadening	Yes	Doppler-broadened cross sections from input tape
Dancoff correction	Yes	Yes
Input determined approximations	NR in the admixed moderator, and NR or NRIM in the resonance absorber	None
Special tables	Escape probabilities	Escape probabilities
Grain structure treatment	No	Yes
Edit	Reaction rates, cross sections	Fluxes, cross sections
Data tapes	Part of GAM-II (fast section) data	GAR format tapes prepared by the GAND program from ENDF/B format data
Memory requirement	32K	40K
Report number	GA-7156	GA-6637
Running time of average problem	4 min	5 min
Geometry	Homogeneous, planar, cylindrical, or spherical	Homogeneous, planar, cylindrical, or spherical

resonance to the corresponding fine-group cross section on the basis of the resonance flux.

On the other hand, GAROL considers simultaneously all the resonances of several admixed absorbers, thereby giving due consideration for resonance overlap and the nonrecovery of the energy flux between resonances. GAROL accepts as input the so-called GAR data tapes. These data tapes contain point-wise cross sections (up to 10,000 points between 0.414 eV and 3.355 keV) representing explicitly all resonances. Doppler broadening is done in the preparation of the data tapes, not in GAROL. If the unresolved range extends below 3.355 keV, pseudo-resonances are generated on the basis of statistical data and written on the GAR tapes. However, the user can ignore these pseudo-resonances by specifying GANDY unresolved resonance parameters for energies below 3.355 keV. GAROL solves the differential transport P_o equation for the mixture of up to 10 absorbers and moderators and then computes fine-group cross sections. Unlike GAMNIT, GAROL does not add any background cross section since the basic GAR data include all phenomena.

4.2.1.2. Unresolved Resonances. In TUZ, statistical computational methods are used to evaluate the resonance integral in the unresolved range. The basic data consist of average resonance parameters read from the same GAM data tape used by GAMNIT. Average-reduced neutron width and average level spacing are used in conjunction with a J function table to obtain fine-group capture cross sections. The averaging process is carried out with a 1/E flux in the narrow-resonance approximation. In comparison with GANDY, the TUZ treatment is somewhat limited because the broadening of fission resonances is ignored, the average unresolved parameters do not depend on angular momenta and energy, and effective cross sections are not computed from a calculated flux.

In GANDY, unresolved resonance parameters depending on energy, angular momentum (up to $\ell = 2$), and spin are read from input cards. These parameters are prepared so that the resulting cross sections match available experimental data. The preparation of these parameters is done with a

code which uses an optimization technique to search for the optimum choice of strength functions and radiation and capture widths. GANDY averages Doppler-broadened, angular momentum, and spin-dependent cross sections over appropriate statistical distributions and fluxes to obtain fission, capture, and scattering cross sections at discrete energies. The point-wise cross sections are then averaged with a constant, 1/E, fission spectrum, or arbitrary input flux to obtain fine-group cross sections in the GAM structure. TUZ and GANDY are described further in Table 4.10.

4.2.1.3. Infinite Medium Spectrum Calculation. After calculation of the fine-group cross sections in the resolved and unresolved resonance ranges, GGC proceeds to a complete fast-flux evaluation down to 0.414 eV in a B_1, B_2, B_3, or P_1 approximation on the basis of 99 fine groups. The calculated flux is then used for the preparation of broad-group cross sections.

In Table 4.11, the main features of the fast section of GGC-5 are compared with those of GAFGAR (Ref. 43). GAFGAR is a fast spectrum code offering a more detailed energy treatment (∿16,000 fine groups) than GGC-5, but without consideration of heterogeneity effects. GAFGAR, which was developed at Gulf General Atomic, has been used in particular for checking the accuracy of the energy treatment in GGC-5. The analysis has confirmed that GGC-5 permits reliable evaluations of all quantities of interest in GCFR physics, especially the Doppler effect. A remaining minor discrepancy between GGC-5 and GAFGAR is in the process of being eliminated by the inclusion in GGC-5 of the computation of self-shielded scattering transfer arrays (Ref. 44). Also listed in Table 4.11 are the features of MC^2 (Ref. 45), a code widely used for fast-reactor analysis.

4.2.2. Dancoff Correction

The fast section of GGC-5 includes the effects of cell heterogeneity by means of a two-region model. In the usual cylindrical geometry, the central region represents the fuel smeared over the actual fuel volume and central-hole volume. In the core, the radius of that fuel region is

TABLE 4.10

COMPARISON BETWEEN GANDY AND TUZ

UNRESOLVED RESONANCE TREATMENTS IN GGC-5

	TUZ	GANDY
Resonance treatment	Isolated narrow resonance	Isolated narrow resonance
Number of regions	1	1
Heterogeneous effects	By means of an escape cross section	By means of an escape cross section
Overlap effects	None	None
Grain structure effects	None	None
Neutron width distribution	Chi-squared with 1 degree of freedom	Chi-squared with 1 degree of freedom
Fission width distribution	None (TUZ may not be used for fissionable nuclides)	Chi-squared with 1, 2, 3, or 4 degrees of freedom
Radiation width distribution	Constant	Constant
Scattering cross-section calculation	None	Yes (treats interference between resonance and potential scatter)
Extent of orbital angular momentum	$\ell = 0$ only	$\ell = 0, 1, 2$
Denominator of effective cross-section expression	1/E flux assumed	Computed from narrow resonance approximation
Variation of average unresolved parameters	None (energy and spin independent)	Energy, spin, and angular momentum dependent
Doppler broadening	Yes	Yes
Evaluation of fine-group cross sections	No pointwise evaluation. Computed directly for the GAM fine-group structure.	Evaluated first at up to 100 discrete energies, then averaged with several flux options into GAM fine groups
Resonance data	Stored on the GAM (fast section) data tape	Read from cards
Equation evaluated numerically	Resonance integral	Effective cross section
Method used for J-function evaluation	Table lookup	Adaptive Simpson's rule integration
Reference	GA-2525	GA-8003

TABLE 4.11

A COMPARISON BETWEEN THE FAST SECTION OF THE GGC-5 CODE AND THE GAFGAR AND MC^2 CODES

	GGC-5 - Fast Section	GAFGAR	MC^2
Neutron flux calculation	P_1, B_1, B_2, or B_3 plus 2 or 6 spatial moment option	B_1	P_0, P_1, or B_1 plus buckling iteration option
Spatial dependence	Single buckling (+, -, or 0)	Broad group dependent buckling (+, -, or 0)	Single buckling (+, -, or 0)
Basic program limits	99 fine groups, 500 energies/resonance in GAMNIT option, 10,000 energies in resonance region in GAROL option, 50 broad groups, 15 resonance nuclides in GAMNIT option, 10 resonance nuclides in GAROL option	1740 fine groups in GAF section, 14,700 energies in resonance region in GAR section, 99 broad groups total, 30 nuclides in GAF, either 30 nuclides and 20 broad groups or 13 nuclides and 40 broad groups in GAR	2100 ultrafine groups, 70 fine groups, 16 energies/ultrafine (or fine) group in evaluation of resonance capture and fission, 49 broad groups, 20 materials, ultrafine group treatment limited to A > 9 nuclides
Typical fine-group (or point structure	Fine group $\Delta u = 0.1$ for E > 111 keV and $\Delta u = 0.25$ down to 0.4 eV, $\Delta v = 85$ m/sec for GAROL option in 0.4 to 3355 eV energy range (can use $\Delta u = 0.0009$ in same range)	Fine group $\Delta u = 0.01$ for E > 1.01 keV and $\Delta u = 0.1$ down to E = 0.4 eV, $\Delta v = 85$ m/sec for GAR section in 0.4 eV to 8 keV energy range	Ultrafine group $\Delta u = 0.0083$ in 0.4 to 10^7 eV energy range, fine group $\Delta u = 0.25$ in. 0.4 to 10^7 eV energy range
Input data	Precomputed library of group constants, transfer arrays, resonance parameters for GAMNIT option and pointwise cross sections for GAROL option	Precomputed library of group constants, transfer arrays and pointwise resonance cross sections	Pointwise cross sections, Legendre coefficients and resonance parameters, necessary group constants and transfer arrays are generated as needed for each MC^2 problem

Table 4.11 (continued)

	GGC-5 - Fast Section	GAFGAR	MC^2
Coupling to ENDF/B format data	Infinite dilution GAM data with GFE version of GAND CAROL tape with regular GAND	The GAND code	The ETOE code (written by APDA)
Resolved resonance calculation	GAMNIT option: single level isolated resonance, equivalence theorem heterogeneity for slab, sphere, or cylinder absorber geometries; GAROL option: single level with overlap, 2-region collision probability heterogeneity in same 3 geometries	Single level with overlap and leakage, homogeneous	Single level with overlap (within each ultrafine or fine group), built-in equivalence theorem heterogeneity for slab and cylinder fuel pin geometries; narrow resonance approximation used, i.e., $\phi \propto 1/\Sigma_t$
Sources from fluxes above the resolved resonance region	P_0 sources from isotropic in C. of M. elastic scattering and 1/E flux	P_0 and P_1 sources obtained from fission and anisotropic elastic transfer and inelastic transfer and actual fluxes	P_0 sources obtained from fission and anisotropic elastic scattering plus actual fluxes
Grain structure	Yes	No	No
Dancoff correction	Yes	No	Yes (computed internally)
Flux in moderator region	GAMNIT option: 1/E GAROL option: from solving P_0 equation	No second region	Probably 1/E
Unresolved resonance calculation	TUZ option: s-wave isolated narrow capture resonance; energy independent data; GANDY option: s-, p-, or d-wave isolated narrow capture or fission resonance; arbitrary data	GAF section: s-, p-, or d-wave isolated narrow capture, scatter or fission resonances, variable Γ_f; GAR section: s-, p-, or d-wave capture, scatter or fission resonances picked by random selection process, variable Γ_f	S- or p-wave narrow capture or fission resonance, overlap with one other sequence treated, no self-overlap, escape cross section for given rod geometry added automatically as in resolved calculation, variable Γ_f and Γ_n

Table 4.11 (continued)

	GGC-5 - Fast Section	GAFGAR	MC^2
Elastic scattering treatment	P_0, P_1, P_2, and P_3 fine-group transfer arrays derived separately from up to P_{20} C. of M. data and infinite dilution scattering cross sections (100 pts/fine group)	GAF section: P_0 and P_1 fine-group transfer arrays derived separately from up to P_{20} C. of M. data and self-shielded scattering cross sections (no data available in resolved resonance range) (40 pts/fine group); GAR section: isotropic in the center of mass at 14000 + Doppler-broadened points so that self-shielding and fine structure in flux are both included	Ultrafine groups: P_0 transfer array derived in code from up to P_{20} C. of M. data and infinite dilution scattering cross sections (2 pts/fine group), P_1 transfer array from P_0 by cosine of lab angle at bottom of incident and exit groups; fine groups: P_0 transfer array from $\bar{\mu}$ from library and infinite dilution scattering cross section
Inelastic and (n, 2n) scattering treatment	P_0 fine-group transfer arrays generated separately from discrete level and evaporation models	GAF section: P_0 fine-group transfer arrays generated separately from discrete level and evaporation models; GAR section: not considered except in slowing down sources	Computed in code on fine group basis for discrete level and evaporation models
Special tables	Escape probabilities, J function	None	Complex probability integral
Typical running time	GAMNIT + TU ≃ 5 min GAMNIT + GANDY ≃ 10 min GAROL + TUZ ≃ 6 min GAROL + GANDY ≃ 11 min (on UNIVAC-1108)	6 to 15 min for 2 to 12 nuclides (GAF ≃ 3 min) (on UNIVAC-1108 with 17 ms access drums	20 min to several hours (on CDC-6600)
Major advantages	Very flexible, fastest of these codes, large amount of data available, best treatment of heterogeneous resonance absorption	Most detailed treatment of homogeneous resonance absorption including self-shielding of scattering cross sections and transfer arrays	Most widely used fast-reactor cross section preparation code, good treatment of oxygen and sodium scattering resonances, good unresolved resonance treatment, much data available

0.3048 cm. From the data of Section 3.3, the average pellet volume fraction (fuel + hole) is 28.86%. This leaves 71.14% for the second region that contains the homogeneous mixture of cladding, coolant, and structural materials. The cell equivalent outer radius is then 0.5674 cm.

Collision probabilities are used in GAMNIT and GAROL to account for heterogeneity effects in the resolved resonance range. (In the unresolved range these effects are approximated by an escape cross section. They are ignored above the resonance range.) Only one energy-dependent collision probability is used, namely, the escape probability P^* that gives the probability for a neutron born uniformly and isotropically in the fuel at a specific energy to suffer its first collision in the non-fuel region. This probability is given by

$$P^* = \frac{P(1-C)}{1 - (1-\bar{\ell}\Sigma P)C} \quad , \tag{4-1}$$

where P is the escape probability from the fuel rod, C is the Dancoff correction factor (that is, the probability of a neutron leaving one fuel rod to enter another rod without suffering a collision in the intervening material), $\bar{\ell}$ is the mean chord length in the rod (which is equal to 4V/S, or the rod diameter), and Σ is the total cross section in the rod at the given energy.

GGC-5 computes P internally as a function of energy on the basis of the rod radius and Σ, and then computes P^* from an energy-independent Dancoff factor supplied by the user.

Sauer (Ref. 46) has shown that the Dancoff factor can be accurately computed from a modified form of the rational approximation,

$$C' = \frac{e^{-\tau\Sigma_2\bar{\ell}_2}}{1 + (1-\tau)\Sigma_2\ell_2} \quad , \tag{4-2}$$

where Σ_2 is the total cross section in the non-rod region (moderator region), $\bar{\ell}_2$ is the mean chord length in the moderator region, and τ is a lattice

parameter given by

$$\tau = \frac{\sqrt{\pi/4\alpha}\ \sqrt{1 + V_2/V_1} - 1}{V_2/V_1} + T \ . \qquad (4\text{-}3)$$

Here $\alpha = 1$ for square lattices and 0.866 for hexagonal lattices, V_i are volumes, and $T = -0.08$ for square lattices and -0.12 for hexagonal lattices.

All quantities entering in the calculation of C' and τ refer to a central cylindrical region V_1 inside the cladding outer radius (that is, including fuel, gap, and cladding) and the moderator region V_2. The desired Dancoff factor C (which refers to the outer fuel radius) is then given by

$$C = \frac{P^{io}\ C'\ P^{oi}}{1 - C'\ P^{oo}} \ , \qquad (4\text{-}4)$$

a formula that includes a cladding correction. In that case, the definition of the cladding actually covers the homogenized gap-cladding cylindrical region. Here P^{io} (P^{oi}, P^{oo}) is the probability that a neutron entering the cladding through the inner (outer, outer) surface will leave through the outer (inner, outer) surface without suffering a collision in the cladding. In this expression, the denominator accounts for multiple tangential crossings of the cladding. The probabilities P^{io}, P^{oi}, and P^{oo} are calculated using analytical expressions derived by Kennedy (Ref. 47).

Compared to Monte-Carlo calculations, Eq. (4-4) yields the Dancoff factor with an accuracy of better than 1.5% in the range of interest in GCFR physics, including the case of steam flooding.

The Dancoff factor in the core of the demonstration plant has been calculated to be 0.8145 at an energy of 2 keV. Since its energy dependence rests only on the relatively small variation of the total cross section in the moderator region in the resonance range, its approximation as an energy-independent quantity is quite good.

4.3. NEUTRON SPECTRA

4.3.1. Core Spectrum

The core spectrum used to average broad-group cross sections is derived on the basis of an average core composition with a core buckling given by $B^2 = 9.05\ 10^{-4}\ cm^{-2}$ (based on core dimensions). This spectrum, as calculated by the GAMNIT-TUZ and GAROL-GANDY options of GGC-5 for the heterogeneous cell, is shown in Fig. 4.6. Above the resonance region, the two options use the same methods and data. Between 10 keV and approximately 100 keV, the two options agree very well, thereby demonstrating the adequacy for GCFR physics calculations of the approximation made in GAMNIT-TUZ for the treatment of the unresolved resonance range. As the neutron energy decreases, GAMNIT-TUZ overestimates the flux above 100 eV and underestimates it below 100 eV, by up to 40%. These discrepancies demonstrate that overlap effects are indeed important in the resolved resonance range. It follows that the simple resonance treatment of GAMNIT-TUZ is adequate for general reactor calculations, but not for core characteristics that depend strongly on the low-energy tail of the spectrum, such as Doppler and steam flooding reactivity effects.

Table 4.12 shows the broad-group cross sections obtained by the above two treatments for U-238 and Pu-239. The differences are due mainly to spectrum differences, since the cross-section data are based on the same infinite dilution values. The differences between the two sets of broad-group cross sections lead to an error of 0.001 in multiplication factor.

The core spectrum of the GCFR demonstration plant is typical of that of an oxide fast reactor. The valleys of the flux correspond to the scattering resonances of oxygen and iron. The median flux energy lies at 176 keV.

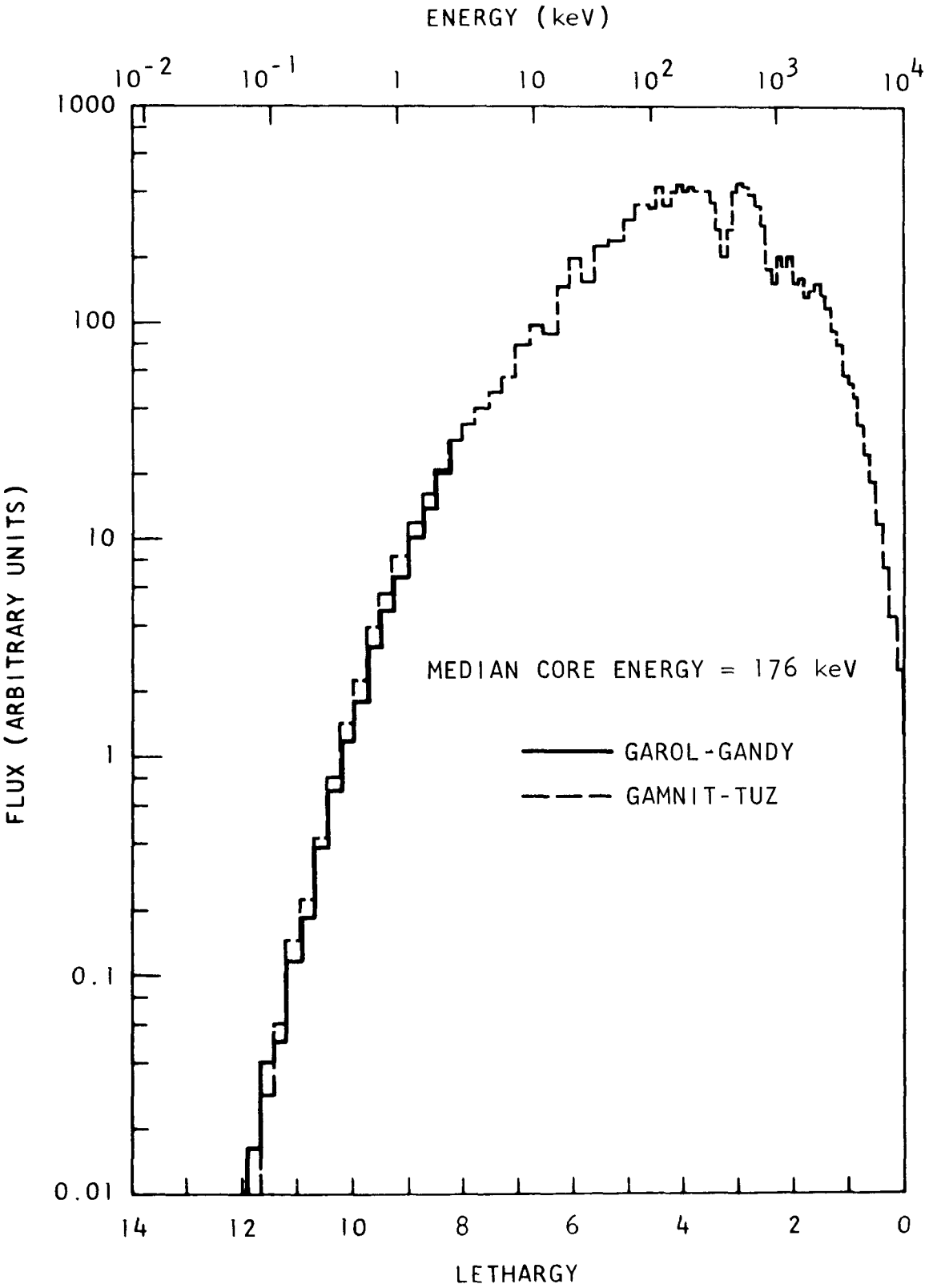

Fig. 4.6. Core spectrum, GAROL-GANDY versus GAMNIT-TUZ

TABLE 4.12

U-238 AND Pu-239 CROSS SECTIONS IN THE CORE
(Heterogeneous Calculation)

Energy Group	Lower Energy (keV)	Lethargy Width[a]	Uranium-238 Capture (barns)		Plutonium-239			
					Capture (barns)		Fission (barns)	
			GAMNIT-TUZ	GAROL-GANDY	GAMNIT-TUZ	GAROL-GANDY	GAMNIT-TUZ	GAROL-GANDY
1	3679	1.4	0.0117	0.0117	0.0066	0.0066	1.914	1.914
2	1353	1.0	0.0458	0.0458	0.0187	0.0187	1.942	1.942
3	497.9	1.0	0.1349	0.1349	0.0791	0.0791	1.641	1.641
4	183.2	1.0	0.1478	0.1478	0.1626	0.1626	1.552	1.552
5	67.38	1.0	0.2555	0.2519	0.2151	0.2151	1.502	1.502
6	24.79	1.0	0.3814	0.3831	0.3749	0.3908	1.473	1.529
7	9.119	1.0	0.5448	0.5526	0.7807	0.7871	1.878	1.881
8	3.355	1.0	0.7783	0.8171	1.2931	1.2906	2.579	2.568
9	0.454	1.0	0.9080	1.1487	2.3408	2.6980	4.009	4.124
10	0.414 eV	7.0	1.3084	1.4807	9.3358	7.9764	10.17	9.172

[a] Zero lethargy at 10,000 keV

4.3.2. Blanket Spectrum

In Fig. 4.7, the blanket spectrum is compared with the core spectrum. The spectrum is much softer in the blanket because of the absence of fissile materials. The median flux energy lies at 38.1 keV, much lower than the 176-keV value in the core.

With the standard 10-energy group set used in GCFR physics work (see Section 4.4), the broad-group cross sections for the blanket are not too different from those in the core. As an example, Table 4.13 compares the capture cross sections of U-238 averaged over the blanket spectrum with those averaged over the core spectrum.

TABLE 4.13

U-238 CAPTURE CROSS SECTION IN CORE AND BLANKET (BARNS)

Group	Blanket	Core
1	0.0116	0.0117
2	0.0456	0.0458
3	0.1347	0.1349
4	0.1502	0.1478
5	0.2599	0.2555
6	0.3822	0.3814
7	0.5365	0.5448
8	0.7130	0.7783
9	0.8014	0.9080
10	1.2836	1.3084

For most calculations, it is thus acceptable to use the same broad-group cross sections in the core and in the blanket. The use of "blanket cross sections" in the blanket instead of "core cross sections" leads to a 0.006 lower multiplication factor.

The blanket spectrum calculation was performed with a negative buckling of $-2.2\ 10^{-3}\ cm^{-2}$, which is a one-group approximation to the inleakage. A

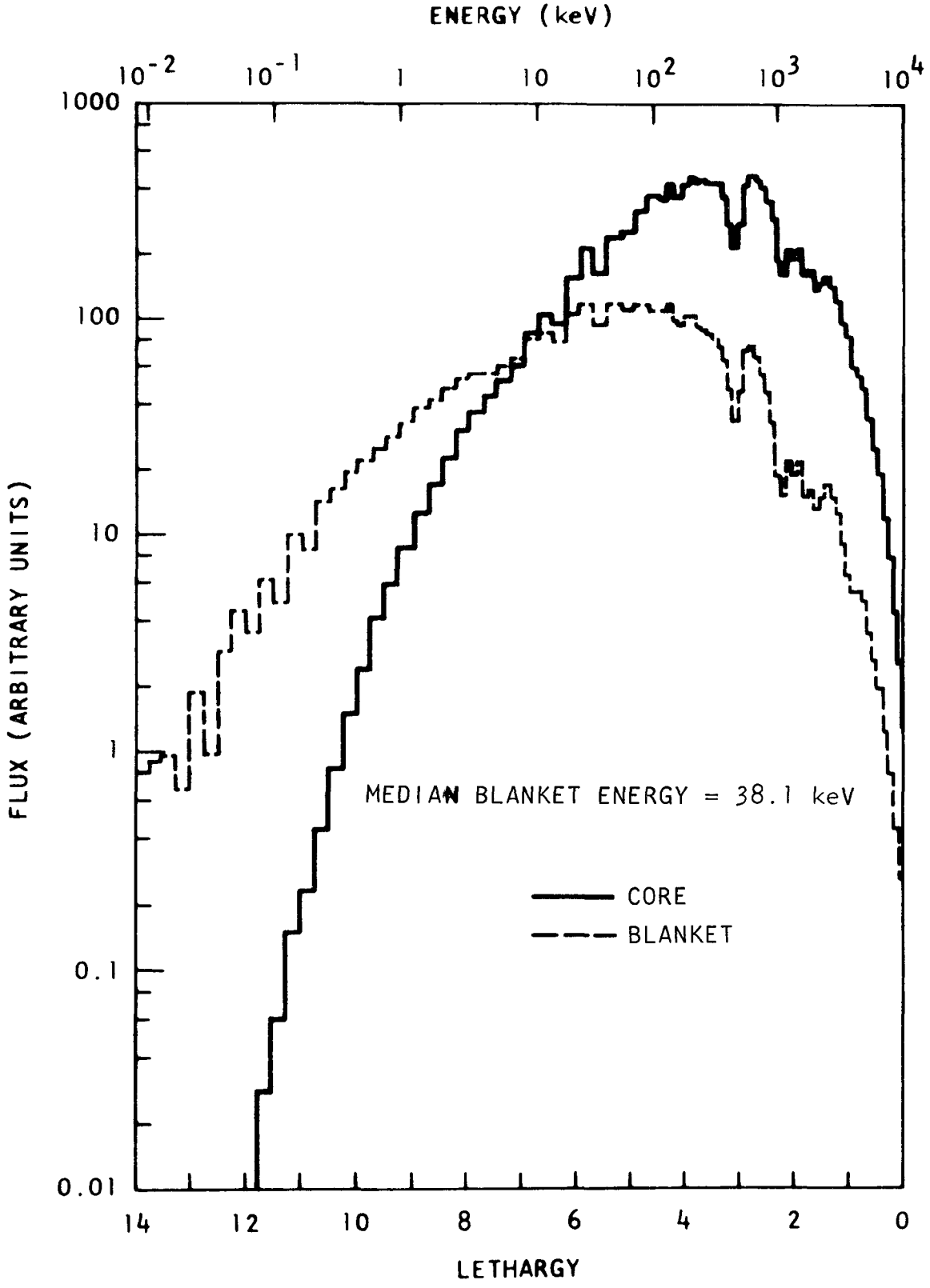

Fig. 4.7. Core and blanket spectrum, GAMNIT-TUZ (negative buckling for blanket)

spectrum calculation with zero buckling was also done. This resulted in a much harder spectrum because of the absence of low-energy leakage sources, but the 10-group cross sections were almost identical to those obtained with the more correct negative buckling.

4.3.3. Heterogeneous Versus Homogeneous Calculations

In GCFR physics work, homogeneous resonance calculations are usually sufficient to represent the most important effects, in particular the energy self-shielding of resonances. Broad-group cross sections derived from a homogeneous calculation are shown in Table 4.14; these can be compared with the heterogeneous GAROL-GANDY values of Table 4.12. Spatial self-shielding is indeed small in all groups, except possibly in the lowest energy group. The homogeneous cross sections overestimate the multiplication factor by 0.0018.

Although homogeneous calculations are adequate for the nominal core composition, a heterogeneous treatment is required for the evaluation of the reactivity coefficient associated with steam flooding because of the greater importance of the resonance flux.

4.4. SELECTION OF BROAD GROUPS

Routine GCFR calculations of power distribution, control rod worths, and reactivity coefficients are performed with 10 broad-energy groups. The group structure, shown in Table 4.12, has sufficient detail in the energy range of importance in GCFR physics. In particular, the lower energy of group 2 corresponds to the U-238 fission threshold. This ensures a proper representation of fertile fast fissions, which account for more than 12% of all fissions in the hard GCFR spectrum. Moreover, the six lower groups cover the important resonance region. Sensitivity analyses (Ref. 1) involving larger numbers of groups have shown that 10 groups are quite sufficient for calculating reactivity coefficients and treating burnup problems without a need for cross-section reaveraging.

In many problems, fewer groups are acceptable. The structure given in Table 4.15 is then adopted. Four groups are usually adequate to yield good power distributions and burnup reactivity changes. Design optimization does not normally require more than four groups.

4.5. FISSION PRODUCT SCHEMES

The list of fission products to be used in burnup calculations is selected by considering all important products from Pu-239 fission (∿69) and by following explicitly only those having a significant poisoning effect in the energy spectrum of the GCFR.

The selection is based on the fission product decay chains given by Meek and Rider (Ref. 48). One nuclide whose half-life is of the order of several years is retained in each possible chain. These nuclides are assumed to be stable during burnup, whereas fission products with shorter half-lives decay immediately after formation. This latter assumption is justified by the long time steps usually chosen in burnup calculations.

The yields y_i are an average of the Pu-239 yields at thermal and fission energies. Nuclides with the largest poisoning product $y_i \cdot \bar{\sigma}_{ci}$ are shown in Table 4.16. There are 14 such nuclides; all others are combined in a nonsaturating aggregate whose cross sections on data tapes are given by $\sum_i y_i \sigma_i$. A second fission product scheme involving explicitly only six nuclides is also shown in Table 4.16. Both schemes lead to nearly identical results in actual burnup calculations for multiplication factors and breeding ratios.

4.6. KINETICS DATA

The fundamental data required for point and multigroup space-dependent kinetics include (1) the total delayed neutron fraction β^j, (2) the relative delayed group abundance β_i^j/β^j, and (3) delayed spectra, where j refers to the various fissionable nuclides and i to the various delayed neutron groups.

TABLE 4.14

HOMOGENEOUS CALCULATIONS OF CORE U-238 AND Pu-239

CROSS SECTIONS PERFORMED WITH GAROL-GANDY

Energy Group	Lower Energy (keV)	U-238 Capture (barns)	Pu-239 Capture (barns)	Pu-239 Fission (barns)
1	3679	0.0117	0.0066	1.914
2	1353	0.0458	0.0187	1.942
3	497.9	0.1349	0.0791	1.641
4	183.2	0.1478	0.1626	1.552
5	67.38	0.2529	0.2151	1.502
6	24.79	0.3836	0.3938	1.534
7	9.119	0.5395	0.7943	1.887
8	3.355	0.7461	1.2983	2.567
9	0.454	1.1711	2.7153	4.149
10	0.000414	1.6735	8.3394	9.493

TABLE 4.15

FEW-GROUP STRUCTURE

Seven-Group Set

Group 1	includes group No. 1,2	in ten-group set
Group 2	includes group No. 3	in ten-group set
Group 3	includes group No. 4	in ten-group set
Group 4	includes group No. 5	in ten-group set
Group 5	includes group No. 6	in ten-group set
Group 6	includes group No. 7	in ten-group set
Group 7	includes group No. 8,9,10	in ten-group set

Four-Group Set

Group 1	includes group No. 1,2	in ten-group set
Group 2	includes group No. 3,4	in ten-group set
Group 3	includes group No. 5,6	in ten-group set
Group 4	includes group No. 7,8,9,10	in ten-group set

Two-Group Set

Group 1	includes group No. 1,2,3,4	in ten-group set
Group 2	includes group No. 5,6,7, 8,9,10	in ten-group set

TABLE 4.16

FISSION PRODUCT SCHEMES

Element	Z	A	Yield y_i
Scheme No. 1			
Mo	42	95	0.0525
Mo	42	97	0.0546
Tc	43	99	0.0589
Ru	44	101	0.0593
Ru	44	102	0.0597
Rh	45	103	0.0573
Pd	46	105	0.0539
Pd	46	107	0.0355
Ag	47	109	0.0142
Cs	55	133	0.0615
Pm	61	147	0.0194
Sm	62	149	0.0135
Sm	62	151	0.00825
Eu	63	153	0.0042
Non-saturating aggregrate	--	---	1.0[(a)]
Scheme No. 2			
Tc	43	99	0.0589
Ru	44	101	0.0593
Rh	45	103	0.0573
Pd	46	105	0.0539
Cs	55	133	0.0615
Pm	61	147	0.0194
Non-saturating aggregate	--	---	1[(a)]

(a) In actual burnup calculations, the yield is set equal to an arbitrary value of 1000, and the few-group cross sections are divided by 1000 in order to avoid depletion of the non-saturating aggregate.

The total delayed neutron fractions (taken from Keepin, Ref. 49) are shown in Table 4.17. For the nuclides U-236, Pu-241, and Pu-242, for which no value is known, use has been made of the empirical expression shown by Keepin (Ref. 50) for the absolute delayed neutron yield per fission:

$$n/F = \exp[0.3721(A-3Z + 1) + 10.663] \ .$$

Here A and Z are the mass and atomic number of a nuclide. (Instead of A-3Z + 1, an often-repeated typographical error in Keepin's book shows the term A-3Z, which is inconsistent with the graph and the data.) On the other hand, the total neutron yield per fission $\bar{\nu}$ may be extrapolated from the value of other nuclides (Ref. 49). On this basis, the following values are obtained:

Nuclide	Absolute Yield, n/F	$\bar{\nu}^j$	$\beta^j = n/F/\bar{\nu}^j$
U-236	0.0220	2.64	0.0083
Pu-241	0.0160	3.5	0.0046
Pu-242	0.0213	3.7	0.0058

The absolute yield of Pu-242 obtained in this manner is consistent with recent measurements (Ref. 51).

The relative delayed group abundances are also shown in Table 4.17. Most of the data come from Keepin (Ref. 52). The data for U-236, Pu-241, and Pu-242 are again obtained by proper interpolation and extrapolation of available data. This appears quite reasonable in view of the smooth and consistent shift in relative abundance when going from U-233 to U-235 and then to U-238; the same holds true for Pu-239 and Pu-240.

The delayed neutron fission spectra also appear in Table 4.17 for the standard 10-energy group set of GCFR physics. These are based on the curves shown by Keepin (Ref. 53). No data are available for delayed groups 5 and 6.

TABLE 4.17

DELAYED NEUTRON DATA[a]

A. Total Neutron Yield per Fission $\bar{\nu}^j$ and Total Delayed Neutron Fraction $\beta^j = \sum_{i=1}^{6} \beta_i^j$

	β^j	$\bar{\nu}^j$
U^{235}	0.00641	2.57
U^{236}	0.00830	2.64
U^{238}	0.01480	2.79
Pu^{239}	0.00204	3.09
Pu^{240}	0.00266	3.3
Pu^{241}	0.00460	3.5
Pu^{242}	0.00580	3.7

B. Relative Delayed Group Abundance β_i^j/β^j

Delayed Group	λ_i (sec^{-1})	U^{235}	U^{236}	U^{238}	Pu^{239}	Pu^{240}	Pu^{241}	Pu^{242}
1	0.0129	0.038	0.033	0.013	0.038	0.028	0.02	0.01
2	0.0311	0.213	0.195	0.137	0.280	0.273	0.26	0.25
3	0.134	0.188	0.180	0.162	0.216	0.192	0.16	0.13
4	0.331	0.407	0.400	0.388	0.328	0.350	0.37	0.39
5	1.26	0.128	0.158	0.225	0.103	0.128	0.16	0.19
6	3.21	0.026	0.034	0.075	0.035	0.029	0.03	0.03

C. Delayed Neutron Fission Spectrum

Energy Group[b]	Prompt Spectrum	Delayed Neutron Group			
		1	2	3	4
1	0.13526	0.0	0.0	0.0	0.0
2	0.4406	0.038	0.069	0.076	0.119
3	0.2933	0.175	0.361	0.336	0.354
4	0.0984	0.348	0.403	0.338	0.330
5	0.0255	0.299	0.113	0.173	0.135
6	0.00601	0.108	0.040	0.059	0.044
7	0.00093	0.028	0.011	0.014	0.015
8	0.0	0.004	0.003	0.004	0.003
9	0.0	0.0	0.0	0.0	0.0
10	0.0	0.0	0.0	0.0	0.0

[a] The index j refers to a nuclide and the index i to a delayed neutron group.

[b] The energy group structure is the same as in Table 4.12.

5. STATIC AND BURNUP CALCULATIONS

Overall reactor performance and critical mass studies are accomplished by static and burnup calculations done with the standard codes in general use at Gulf General Atomic. In this section, some results and comparisons of methods and cross-section data are reviewed.

5.1. TWO-DIMENSIONAL R-Z GEOMETRY

Two-dimensional r-z calculations are normally performed with the code BUG-2 (see Appendix B) in diffusion theory with 10 groups and about 1900 meshpoints (half-reactor). A plot of the radial power distribution is shown in Fig. 5.1, and the axial power distribution is shown in Fig. 5.2. The equivalent one-group extrapolated point lies about 22 cm from the core boundary in both the axial and radial directions.

As stated in Section 3.2, enrichment zoning is determined with the objective of flattening the radial zone power peak. The actual selection of a zoning pattern is performed by hexagonal diffusion calculations, which enable the explicit representation of all fuel elements. It is thus clear that a radial calculation would average out the azimuthal power variation, thereby yielding a lower peak for the outer zones.

5.2. TWO-DIMENSIONAL HEXAGONAL GEOMETRY

Two diffusion theory codes are available at Gulf General Atomic to evaluate power distributions in hexagonal geometry. The one most frequently used, GAUGEF, has a fixed coarse mesh representation that includes two intervals per hexagon, equivalent to seven points per hexagon. The other code, BUGTRI, is more flexible and allows any number of intervals per hexagon; in practice, not more than four are needed.

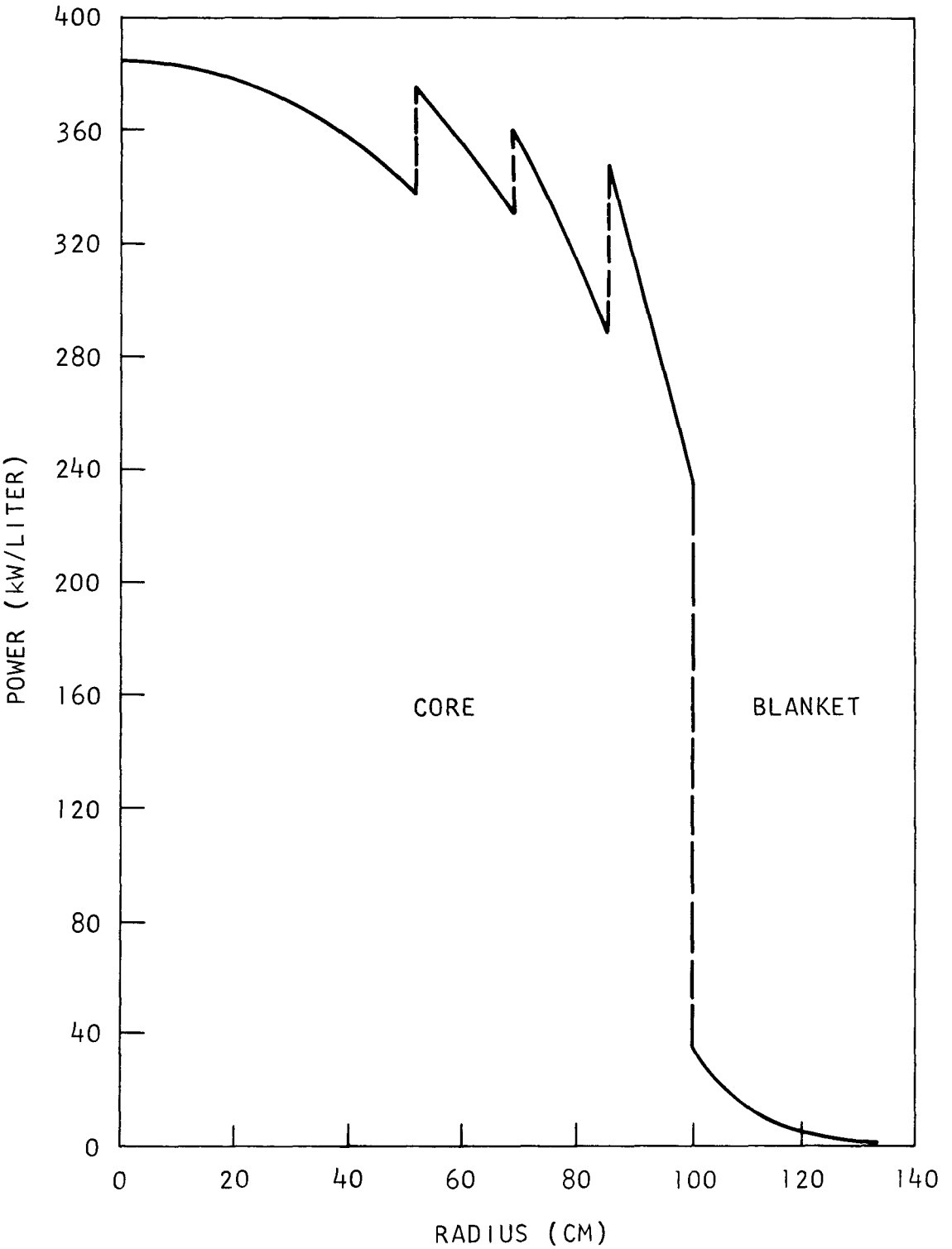

Fig. 5.1. Radial power distribution; fresh core, at midplane

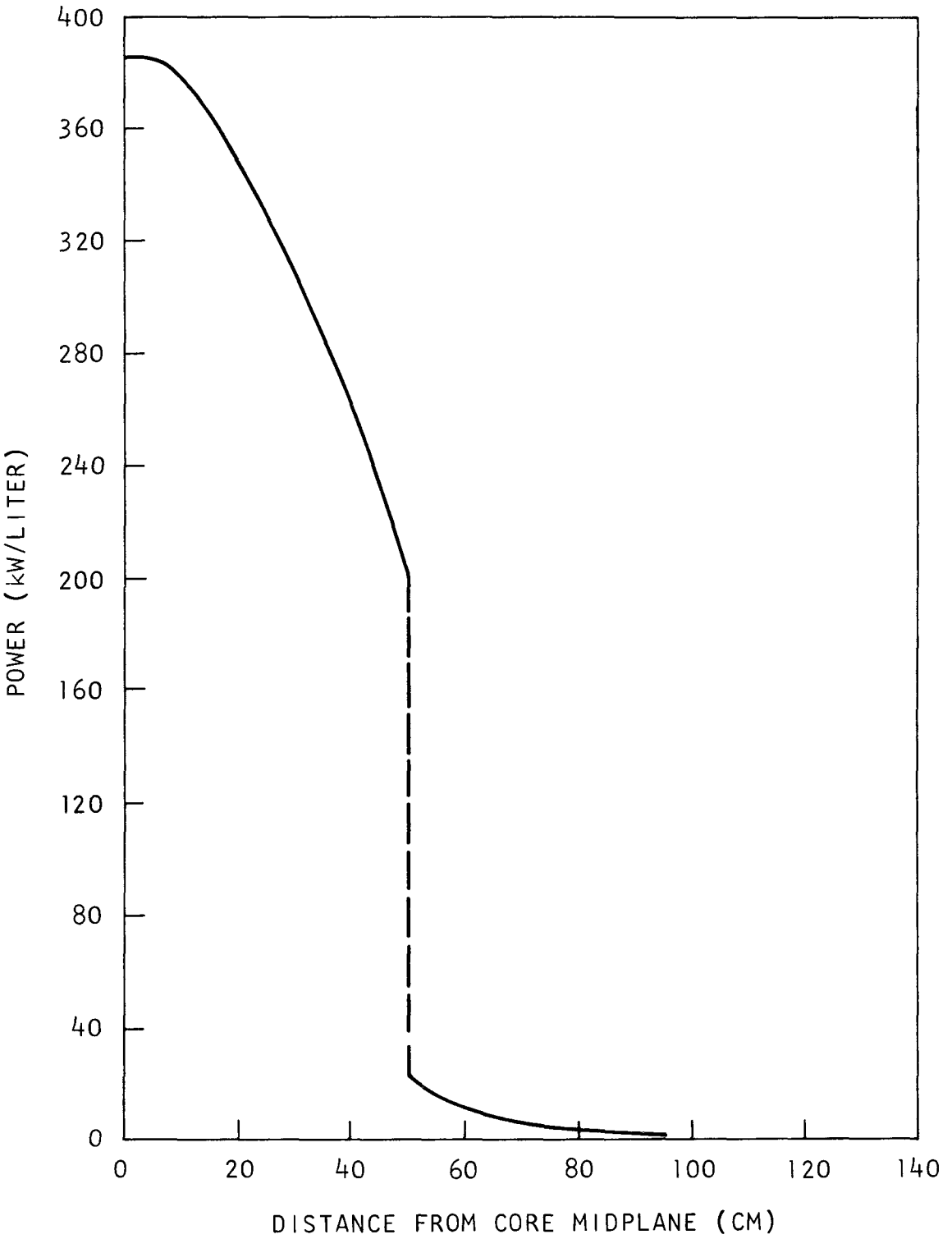

Fig. 5.2. Axial power distribution; fresh core, at midplane

Because of its short running times (seven times less than BUGTRI for the same two-mesh intervals and 28 times less in comparison to BUGTRI four-mesh intervals), GAUGEF is used in most design areas, particularly for power flattening and fuel management. In fact, since GAUGEF is only about three times more time-consuming than a one-dimensional diffusion burnup code, most radial calculations are performed exclusively in hexagonal geometry.

Figure 5.3 shows the power distribution in the core over the three cycles that characterize equilibrium operation, as calculated with GAUGEF in 10 energy groups. Since it is not possible to reload exactly one-third of the elements belonging to an enrichment zone, there is no single equilibrium cycle, but rather three phases in a longer cycle. The reload pattern appears in Fig. 5.3; all elements marked 0 are reloaded at the beginning of the corresponding cycle.

In the equilibrium cycle, the entire range of power distributions in the core can be shown with only six power maps: the beginning-of-cycle and end-of-cycle maps for each of the three cycles. Such a set of maps giving the power in each element for each of the 6 cases is shown in Fig. 5.3. These maps correspond to a core without control rods. The figure has been condensed (because the core has a threefold symmetry) by showing only a 120° segment of each core. Starting at the top left of Fig. 5.3, the beginning-of-cycle case of Cycle 1 shows, for example, a 1-cycle-old fuel element at the core center with an element-to-core average power ratio of 1.027. At the end of this cycle, shown at the top right of Fig. 5.3, the same element is shown as a 2-cycle-old fuel element with a power ratio of 1.026. As the core is reloaded, all the 3-cycle-age fuel is replaced by 0-age fuel, and the new power distribution is shown in the center left map as the beginning of Cycle 2. The cycles of burnup and replacements thus continue; on the six maps shown in Fig. 5.3, the end of Cycle 3 becomes the beginning of Cycle 1 again after reload. Figure 5.3 thus contains the element power ratios for the entire core at all stages of the equilibrium cycle.

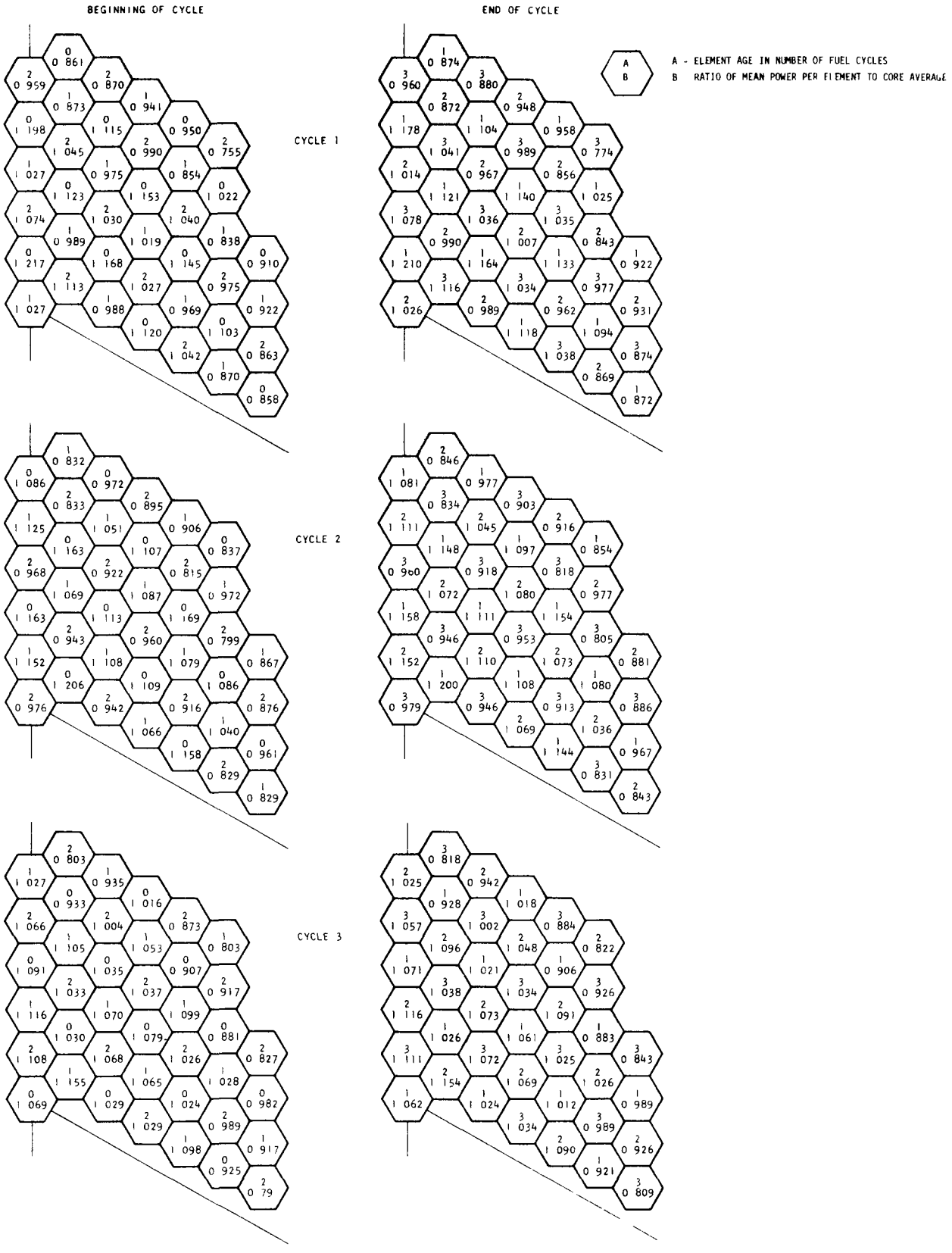

Fig. 5.3. Core reload pattern and power distribution

By following any given location through life, starting with the 0-age case, the entire power history (and coolant orifice settings) can be deduced for any element, since variations between refueling are linear. The results show, in general, that new fuel slowly tends to fall in power if it starts above average and to rise in power if it starts below average. The change in power during a given cycle for any given element tends to be only a few percent at most, showing that the effect of power changes on orifice settings during a given cycle will be quite small. Furthermore, the control-rod program compensates for those power shifts and limits even more the variation in local power level. Over all three equilibrium cycles, the ratio "average element power/core average power" never exceeds the value of 1.22.

With respect to power flattening, it should be recalled that the design objective is to obtain equal power peaks in all zones at midcycle. Conceptually, there would then be at least four fuel pins, one in every zone, operating at the maximum core power density. However, the maximum average element power by zone tends to be smaller in the outer zones because of the larger power tilts.

Over most of the core, the peak element power is close to the average element power; i.e., the power profile in most elements is reasonably flat. However, the elements located near the core-blanket interface (either in the core or in the blanket) exhibit a sizable power tilt owing to the strong gradient of the neutron flux.

Figure 5.4 shows the power distribution by points in the core element with the largest tilt that occurs during the three equilibrium cycles. With respect to the power maps of Fig. 5.3, that power distribution occurs at the beginning of Cycle 1 in the element with an average power of 0.755, located near the outer radial boundary of the core. Since power and coolant flow matching is based on the hot-spot temperature for the whole element, such elements will generally be overcooled.

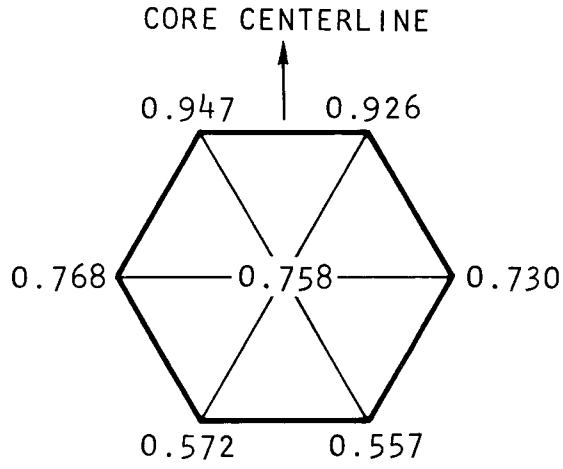

AVERAGE = 0.755
MAX/AVG = 1.254

A. CORE ELEMENT

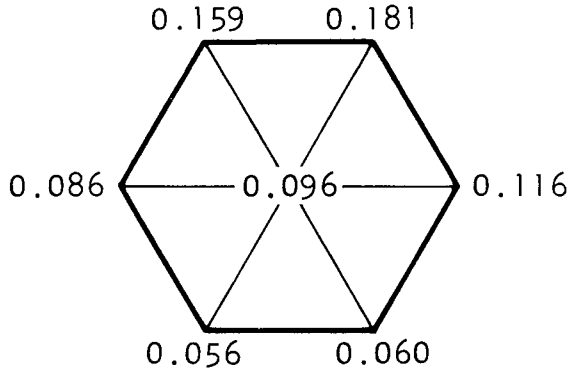

AVERAGE = 0.102
MAX/AVG = 1.78

B. BLANKET ELEMENT

NOTE: RATIO OF POWER TO CORE AVERAGE POWER;
7 VALUES PER HEXAGON

Fig. 5.4. Power distribution in single elements

Also shown in Fig. 5.4 is the power distribution in a typical first-row blanket element. The power tilt is much larger than in the core, but the power level is also much lower.

The maximum radial power peak over the three cycles is 1.30. It occurs at beginning of Cycle 1 in the core element with an average of 1.198 (first column, Fig. 5.3), i.e., not in the element with the largest average power or the element with the largest power tilt.

As stated at the beginning of this section, GAUGEF incorporates a built-in coarse mesh grid that may not always be adequate to handle the strong heterogeneity effects at the core-blanket interface. This possibility was investigated by comparing 4-group GAUGEF calculations to 4-group, fine-mesh (four intervals per hexagon) BUGTRI calculations. The results shown in Table 5.1 indicate that the coarse mesh grid of GAUGEF is adequate for most design purposes. GAUGEF underestimates the average power for the elements near the core-blanket interface by a few percent. The core peak-to-average is underestimated by about 6%. This discrepancy is certainly not negligible in the fuel design stages of the reactor, but it is otherwise acceptable, especially in view of the 28 times shorter running times.

5.3. CONTROL ROD CALCULATIONS

5.3.1. Generalities

As stated in Section 3.8, the reactor is controlled by two sets of control rods that are completely independent of each other. Under normal conditions, the so-called control system is the only one being used. Control rods and shutdown rods have the same outer diameter and they are inserted in identical control fuel elements. It follows that cell calculations for establishing rod worths apply to both the control and shutdown systems. However, the problems related to control rod heating, burnup, and effects on power distribution are relevant only for the control system.

TABLE 5.1

COMPARISON OF GAUGEF COARSE MESH

AND BUGTRI FINE MESH

	GAUGEF	BUGTRI
Running time, sec (one diff. calc.)	20	560
Multiplication factor	1.0173	1.0179
Average power in element		
At center	0.976	0.957
At core edge	0.970	0.985
Blanket	0.046	0.048
Core local leak	1.33	1.41
Core fractional power	0.973	0.972

The control rod system is intended to cover all the reactivity requirements listed in Table 3.8, i.e., $17.00. The number and locations of the control set were chosen according to the following criteria:

1. All control rods should have about the same reactivity worth, which must be less than $1.00.

2. The rods in that set used to cover the burnup allowance must be located so as to maintain a satisfactory power distribution as they are withdrawn throughout the burnup cycle.

3. The rod locations should make it possible to alternate the functions of covering burnup and providing control among all rods of the set to equalize burnup of the absorber material.

4. The control-rod system should be able to cover all reactivity requirements, including the shutdown margin, with one stuck rod.

In accordance with these criteria, the central ring of six rods, the outer ring of 12 rods, and a set of three rods in the middle ring of 12 positions are designated control rods. The requirement of holding $17.00 with one stuck rod leads to a worth of $17/20 = $0.85 per rod. The complete set of 21 rods is then worth $17.85. The control rod layout is shown in Fig. 5.5 and the required boron concentration in Table 5.2.

The shutdown system consists of six rods whose locations are shown in Fig. 5.5. With the operational mode planned for the shutdown rods, there is no necessity for limiting their worth to a value less than $1.00 each. To meet the shutdown requirements (described in Sections 3.7 and 3.8) with one stuck rod requires a reactivity worth of $8/5 = $1.60 each, or a total of $9.60 for the set of six. As shown in Table 5.2, such a worth can be achieved with boron carbide enriched to 37% B-10.

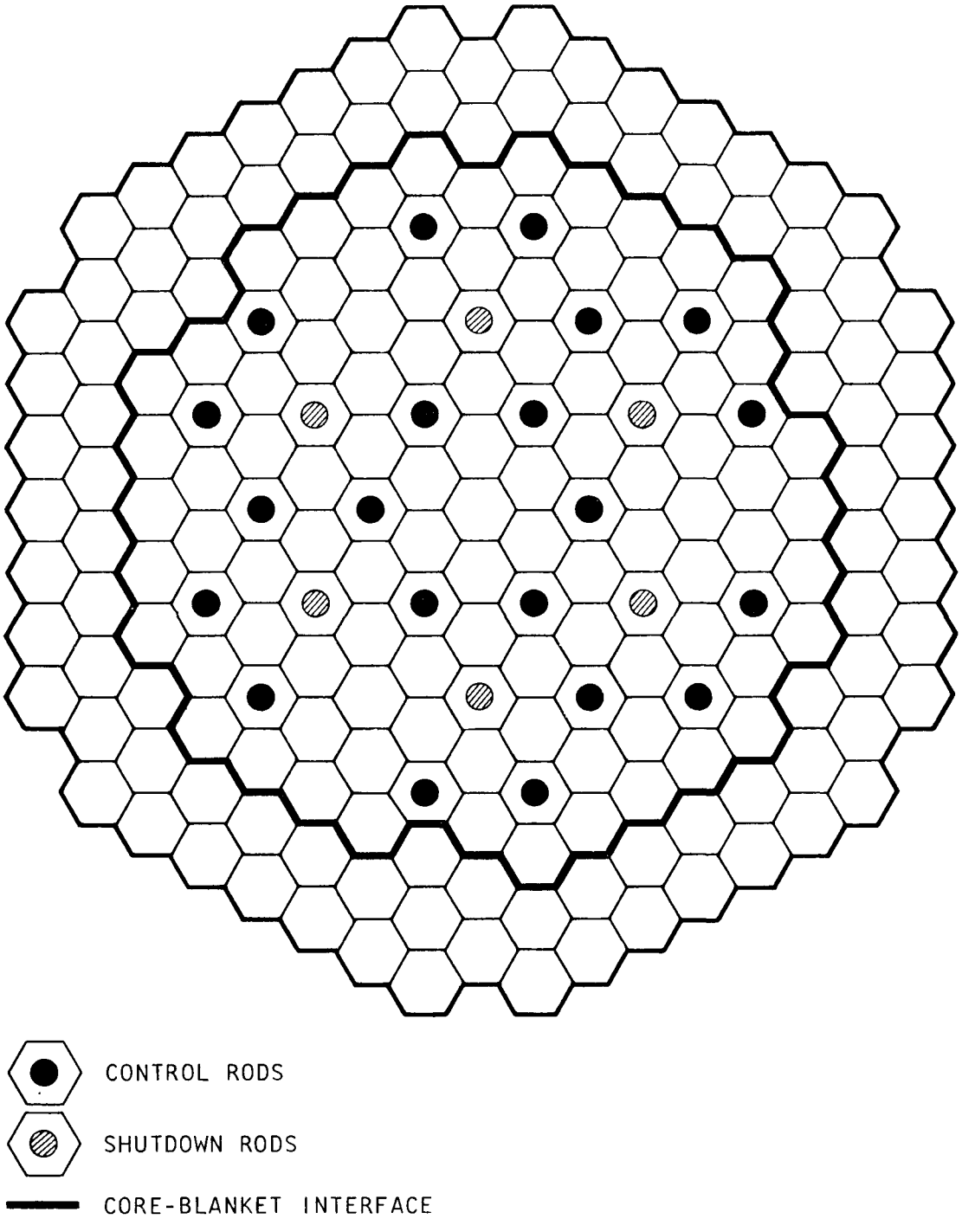

Fig. 5.5. Locations of control rods

TABLE 5.2

CONTROL ROD COMPOSITIONS

Set	Location	Fraction of B_4C	Volume Fraction of Graphite	Enrichment of B^{10}
Control	Center ring	0.75	0.25	Natural (19.78%)
	Middle ring	1.0	0	Natural
	Outer ring	1.0	0	37%
Shutdown	Middle ring	1.0	0	37%

5.3.2. Cell Calculations for Boron and Tantalum

Boron carbide mixed with graphite is the absorbing material usually selected for fast-reactor control. However, the possibility of using tantalum control rods to circumvent the difficulties arising from boron burnup has been suggested. Cell calculations involving tantalum were therefore also performed, but in that case the calculations dealt only with pure natural tantalum.

A series of one-dimensional transport theory cell calculations were done for various compositions to provide shielding factors and estimates of relative worths. The central region of the cell corresponded to the control rod and the surrounding region to the average fresh fuel composition. The cell volume was that of one hexagonal fuel element, a choice that yields shielding factors directly applicable to the two-dimensional hexagonal code GAUGEF, which represents each fuel element explicitly. Such a cell treatment is somewhat approximate since the flux at the boundaries of a control element is certainly not flat, but more refined studies indicate that the accuracy is sufficient for overall calculations.

In the fast spectrum of the GCFR, self-shielding is not very important. For natural boron and tantalum, the changes in shielding factors are second-order effects and the worth is primarily determined by the volume and

density of the absorber. Typical self-shielding factors are shown in Table 5.3 for the boron concentrations actually selected for the various control rod banks (as given in Table 5.2) and for natural tantalum. The group structure is given in Table 4.2.

The desired reactivity worth for each rod group is obtained either by diluting the natural boron carbide with additional graphite or by increasing the inside diameter of the annular absorber pellets in the case of the inner rods or by increasing the enrichment of the B-10 isotope in the case of the outer rods, as shown in Table 5.2. The rod worth calculations established that the worth, for a given boron composition, varies to a good approximation as the square of the flux, as a function of radial position.

Under the present circumstances, the use of tantalum has been rejected because of its smaller worth. For equal volume, the worth of tantalum in the GCFR energy spectrum amounts to 60% of that of natural boron. The choice of tantalum would be detrimental to reactor performance because it would entail larger rods or a greater number of rods. Furthermore, heat generation in the control rod itself is smaller with boron. When the absorption of core-produced gamma rays from fissions, captures, and decay of fission products, the absorption of gamma rays originating from captures in tantalum itself, and the absorption of beta and gamma rays from decay of the capture product Ta-182 are taken into account, the average volumetric heating rate amounts to 140 W/cm^3. In boron, the energy (2.5 MeV) is absorbed in the rod. The resulting average heating for natural boron reaches 60 W/cm^3.

5.3.3. Control Rod Burnup

A preliminary hand calculation of control rod burnup assuming

$$N = N_o e^{-\sigma\phi t}$$

yielded $N/N = 0.82$ for one 250-day burnup period at constant flux. The value of σ included the appropriate shielding factor. A more detailed

TABLE 5.3

SELF-SHIELDING FACTORS

Energy Group	Central Ring of 6	Middle Ring of 9	Outer Ring of 12[a]	5-cm-o.d. Tantalum Rod
1	0.860	0.845	0.841	0.775
2	0.890	0.876	0.870	0.785
3	0.899	0.887	0.803	0.694
4	0.920	0.909	0.862	0.711
5	0.937	0.926	0.912	0.683
6	0.919	0.905	0.808	0.493
7	0.943	0.930	0.692	0.347
8	0.878	0.857	0.591	0.221
9	0.777	0.744	0.445	0.128
10	0.594	0.549	0.243	0.053

[a] Also for the shutdown rods in the central ring

cell calculation was run to refine this estimate. The cell consisted of a hollow natural B_4C rod with steel guide tube surrounded by one-ninth of the core volume. The absorber was divided into three burnup regions to allow for spatial burnup effects. After 250 days of full power burnup, the atom density ratios were N/N_o = 0.865, 0.864, and 0.862 for the three rod regions. From these results it was concluded that hand calculations are sufficient. Both calculations underestimate the burnup slightly since the shielding factors were kept constant.

Since rod worth is roughly proportional to the boron density, a fully inserted rod may lose about 14% of its worth in one burnup period if kept fully inserted. The approximately $9 of excess reactivity burned up in one period would be held by three groups of three rods each. These groups would then have average residence times of 42, 125, and 208 days in the course of one 250-day burnup period. It would be desirable not to have to replace absorbers more often than fuel. If each group of three is swapped with another group of three in the same ring, the exposure per period can be halved. The average residence time for three burnup periods (the life of the fuel element) would then be 62, 187, 312 days. The group with the 312-day exposure would have lost 17% of its worth, the 187-day group 10%, and the 62-day group 4%.

These calculations indicate that the boron rod will preserve its effectiveness for as long a period as the life of the fuel element in which it resides, i.e., about 3 yr. Over this period, the average rod worth will decrease by 10%. The control fuel element and its control rod will thus be replaced at the same time.

5.3.4. Control Rod Programs

Control rod programming schemes are designed to meet operating control requirements while at the same time yielding a time-dependent power distribution compatible with design bases. Furthermore, they should lead to high average fuel burnup and low average control rod burnup.

At the beginning of an equilibrium cycle, $9 of reactivity needs to be controlled at hot-operating conditions. Therefore, approximately nine control rods are fully inserted. Of these, three belong to the inner ring and six to the outer ring; the rod locations are shown in Fig. 5.6. The following order for withdrawing rods is adopted:

1. A symmetrical triplet in the outer ring comes out.

2. The remaining triplet in the outer ring comes out.

3. The triplet in the inner ring comes out.

This procedure maintains an azimuthally symmetric power distribution while minimizing both the number of rods in an intermediate position and distortion of the axial power distribution. The pattern is also well suited to interchanging rod groups in a given ring to equalize azimuthal burnup of fuel elements and control rods.

Power distribution studies show that control rods have some influence, even if small, on the core power distribution. The control rod program described here uses this factor to help maintain a nearly constant power distribution over a burnup cycle. With no control rod effects, the power tends to shift to the core center because of the fissile depletion in the highly enriched outer zone and the fissile buildup in the low-enriched central zone. To compensate for this power shift, the inner set of three rods is the last group to be withdrawn.

5.3.5. Effect on Power Distribution

The effects of the control rod program described in the preceding section on the core power distribution are illustrated in Fig. 5.6. These calculations correspond to a completely fresh core. The azimuthal variations in the power distribution produced by the three different ages of fuel normally present in an equilibrium cycle are thus not represented,

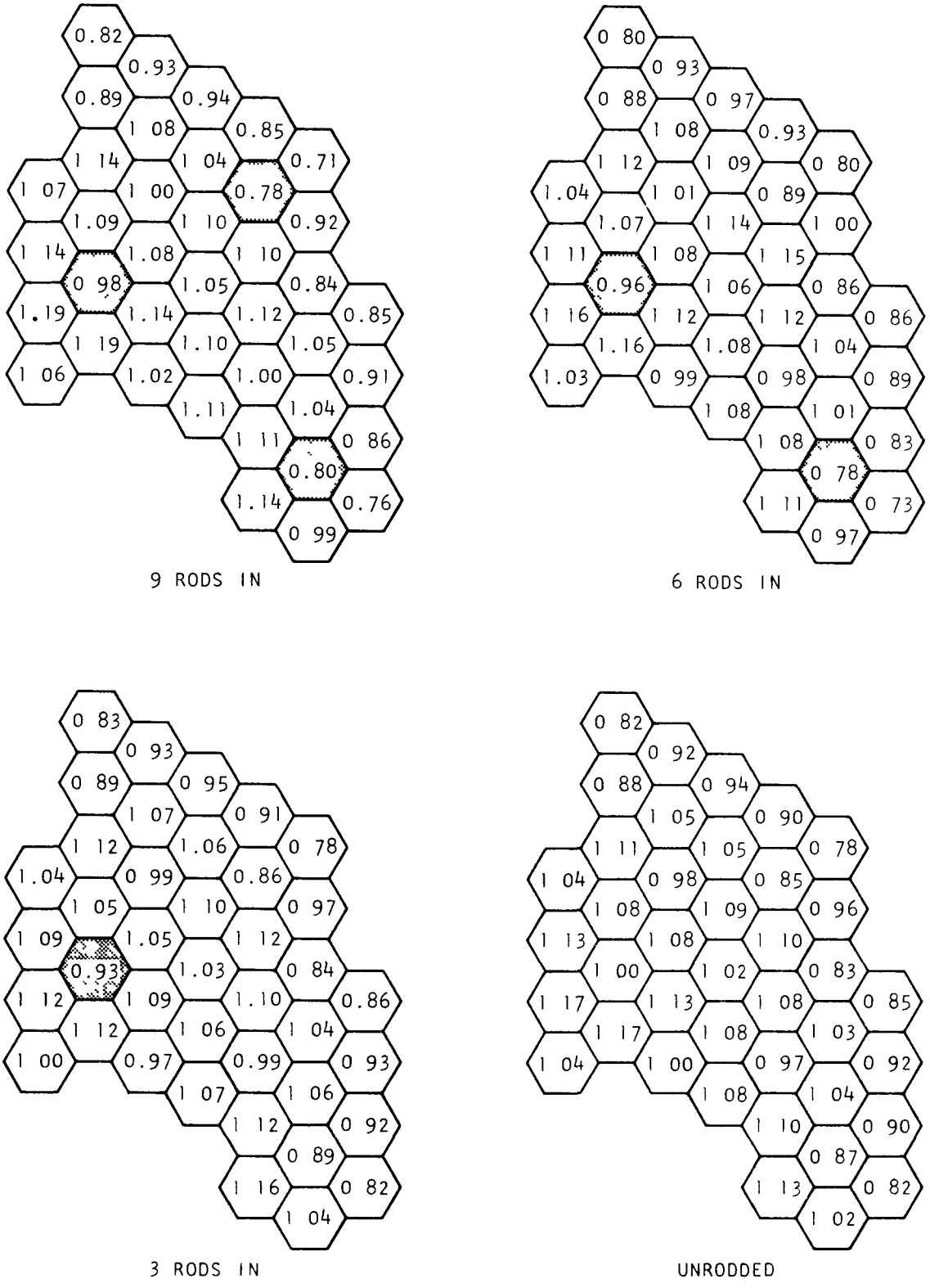

Fig. 5.6. Power distributions in core for various numbers of control rods inserted

but this is a second-order effect. Furthermore, power shifts due to a fuel burnup that would normally accompany control rod withdrawal are not reflected in Fig. 5.6. The time-dependent power distribution with no control rods will be discussed in Section 5.4.

The number given for the power density in each element is the ratio of the average power density in that element to the average core power density. Fuel elements containing a control rod have less fuel than adjacent fuel elements in the same zone. The fuel loadings are reduced by the factor 0.875, corresponding to the volume occupied by the control rod. The relative power densities shown in Fig. 5.6 for control fuel elements should therefore be multiplied by 1.143 (i.e., 1/0.875) to obtain the relative power density for the fuel rods in those elements.

These calculations show that control rods have a small influence on the power distribution. The power level is decreased by less than 10% in the fuel element containing the control rod, and much less in the adjacent elements. The overall power level at the center of the core is depressed by less than 5% when three rods of the inner ring are fully inserted.

5.4. STREAMING EFFECTS

The GCFR fuel arrangement consists of an array of cylindrical rods separated by the helium coolant, which is for most purposes equivalent to a void. In the demonstration plant, about 45% of the core volume is occupied by the coolant; this fraction would be even larger in the core of the commercial GCFR. Beside the coolant void, about 12% of the demonstration plant core accounts for the gaps between fuel element boxes and empty control rod channels. Altogether, 57% of the core is occupied by unobstructed channels parallel to the reactor center line extending from the top to the bottom of the reactor.

In reactor physics calculations, the presence of voids is routinely taken into account by homogenizing all materials over a volume that includes the voids. This procedure is adequate when the characteristic dimensions of the voids are much smaller than the average mean free path in the assembly. For larger void dimensions, the homogenization procedure becomes erroneous even for a random void arrangement and more so for a parallel void arrangement. The presence of voids facilitates neutron diffusion in both the radial and axial core directions. This results in the so-called neutron streaming effects which tend to increase leakage and thereby decrease the multiplication factor.

Because of the large void fraction, neutron streaming effects deserve particular attention in the physics evaluation of a GCFR. However, as will be shown, the long neutron mean free path in a GCFR (about 6 cm compared with a rod pitch of 1 cm) considerably limits the magnitude and importance of neutron streaming effects. In most instances, core analyses based on homogenized cross sections are quite adequate.

5.4.1. Calculational Methods

Neutron streaming is by nature a transport effect and hence cannot be treated by the standard methods of diffusion theory. An exact analysis would require a transport theory calculation involving all the fuel rods in the reactor. Monte Carlo techniques could be used, but the cost would be excessive. In practice, all theoretical analyses of neutron streaming attempt to derive, from transport theory cell calculations, modified diffusion parameters that will account for streaming effects when used in standard homogeneous diffusion calculations.

The most complete study of neutron streaming has been performed by Benoist (Refs. 54, 55). Transport leakages of the voided lattice are matched to the diffusion leakages of the homogenized lattice in the radial and axial core directions:

$$F_k = D_k B_k^2 \quad , \qquad k \equiv r \text{ or } z \quad , \tag{5-1}$$

where F_k is the ratio of the transport leakage in the direction k to the total flux in the cell, D_k is the diffusion coefficient for direction k, and B_k^2 is the buckling for the same direction. On the basis of this enforced equality and an evaluation of the transport leakage in an infinite and regular lattice, Benoist established the following formula:

$$D_k = \frac{1}{3} \frac{\sum_i \sum_j V_i \phi_i \lambda_j P^*_{ij,k}}{\sum_i V_i \phi_i} , \qquad (5\text{-}2)$$

where V_i is the volume of region i in the cell, ϕ_i is the average neutron flux, λ_j is the total mean free path in region j, and $P^*_{ij,k}$ are the directional collision probabilities between regions i and j.

Equation (5-2) was derived for monoenergetic neutrons and can be used in multigroup calculations by separate application to each group. Group correlation is usually negligible and the influence of absorption appears only in a corrective term to Eq. (5-2), as mentioned in Ref. 54. For most applications, especially for fast reactors, Eq. (5-2), which neglects absorption and group correlation, is adequate. Therefore, the directional diffusion coefficients D_k will depend exclusively on the cell geometry and the total macroscopic cross section in the cell regions.

The cell of the GCFR demonstration reactor is described in Table 3.5. The fuel rod considered in the present calculation includes the homogenized central hole, fuel, gap, and cladding. The rod pitch used here (p = 1.006) is larger than the true pitch (0.98 cm) for the purpose of representing interbox voids and control rod channels.

The simplified cell has two regions, the void and the homogenized fuel rod, characterized by a radius a = 0.358 cm, a pitch p = 1.006 cm, and an equivalent Wigner-Seitz radius b = 0.528 cm. By using Benoist's reciprocity and complementary relationships between $P^*_{ij,k}$, Eq. (5-2) can be written:

$$D_k = \frac{1}{3}\lambda \left[1 + \frac{V_c}{V}\left(1 + \frac{\lambda_c}{\lambda} P^*_{cc,k}\right)\right] \quad . \qquad (5\text{-}3)$$

Here λ is the transport mean free path in the rod and V_c/V is the void fractional volume in the cell. On the other hand, $P^*_{cc,k}$ is the directional collision probability from void to void, which is zero. However, the product $\lambda_c P^*_{cc,k}$ remains finite and non-zero as the void mean free path λ_c goes to infinity. In the derivation of Eq. (5-3) from Eq. (5-2), it has also been assumed that average fluxes in fuel and cavity are equal, a valid assumption for the fast energy range.

In order to evaluate D_k, it is thus necessary to calculate the reduced probabilities $p^*_{cc,k}$ which have a finite value for a void:

$$p^*_{cc,k} = \frac{S}{2V_c} \lambda_c P^*_{cc,k} \quad ,$$

with S being the lateral surface of the rod and V_c the cavity volume. The reduced probabilities $p^*_{cc,k}$ are given by the following sum:

$$p^*_{cc,k} = p_{cc,k} + \sum_{\ell=1}^{\infty} p^{(\ell)}_{cc,k} \quad ,$$

where the first term corresponds to a first-flight collision probability and the others to multiple collisions.

If the channels are parallel to the axial direction and scattering is isotropic, then for $k \equiv z$, the contribution of multiple collisions vanishes identically and $p^*_{cc,z} = p_{cc,z}$. For the radial direction, the secondary terms do contribute (positively) to $p^*_{cc,k}$ in the case of small channel dimensions. However, this contribution is negligible for very tight lattices, which is the case for the GCFR cell.

Therefore, only the reduced first-flight directional collision probabilities $p_{cc,z}$ and $p_{cc,r}$ need be evaluated in order to calculate the diffusion coefficients D_z and D_r.

Evaluation of $p_{cc,z}$ and $p_{cc,r}$ - First Approach

The first approach followed for the calculation of the reduced probabilities $p_{cc,z}$ and $p_{cc,r}$ is the one suggested in Appendix VIII of Ref. 54 for tight lattices. In analogy with the physical model of the usual collision probabilities, the following assumptions are made:

1. The escape probability for a neutron born uniformly and isotropically in the cavity is approximately given by the escape probability from a cylinder with the same mean chord length as the cavity.

2. Neutrons entering and leaving the fuel rod do so in an isotropic angular distribution (cosine current).

The collision probability $P_{cc,k}$ will then include the contribution of multiple boundary crossings and will also depend on the blackness of the fuel rod. After going to the limit $\lambda_c \to \infty$, the following formulas are derived for the reduced directional collision probabilities:

$$p_{cc,z} = \frac{2}{\Gamma_z}\left[1 + \frac{1}{3}(1 - \Gamma_z)\right] \quad , \tag{5-4}$$

$$p_{cc,r} = \frac{1}{\Gamma_r}\left[1 + \frac{7}{9}(1 - \Gamma_r)\right] \quad . \tag{5-5}$$

Here Γ_z and Γ_r are the directional blacknesses of the fuel rod and are given by

$$\Gamma_z = \frac{8}{3}\frac{a}{\lambda}\left[1 - \frac{a}{\lambda} T_z \frac{a}{\lambda}\right] \quad , \tag{5-6}$$

$$\Gamma_r = \frac{16}{9}\frac{a}{\lambda}\left[1 - \frac{a}{\lambda} T_r \frac{a}{\lambda}\right] \quad , \tag{5-7}$$

where T_z and T_r are functions of a/λ, given graphically by Benoist (Refs. 54, 55).

The directional diffusion coefficients D_k, with $k \equiv r$ or $k \equiv z$, are then given by

$$D_k = \frac{1}{3} \lambda \left[1 + \frac{V_c}{V} \left(1 + \frac{2 V_c}{S \lambda} p_{cc,k} \right) \right] \quad , \tag{5-8}$$

and Eqs. (5-4) through (5-7).

Benoist states (Ref. 54) that assumption (1) above leads to an underestimation of 15% at most for $p_{cc,k}$. Thus D_k may be somewhat underestimated by Eq. (5-8).

Evaluation of $p_{cc,z}$ and $p_{cc,r}$ - Second Approach

The second approach to the evaluation of the reduced collision probabilities attempts to describe more accurately the different paths that can be followed by neutrons. In analogy with the physical model of usual collision probabilities, this splits the probability $p_{cc,k}$ into its various components:

1. The neutrons born uniformly and isotropically in the cavity that suffer a first collision in the cavity without entering the fuel rod or without escaping the cell through the Wigner-Seitz equivalent radius.

2. The neutrons born uniformly and isotropically in the cavity that suffer a first collision in the cavity after having crossed the fuel rod without collision, and without escaping the cell.

3. The neutrons born uniformly and isotropically in the cavity that leave the cell through the Wigner-Seitz equivalent radius, either directly or after having crossed the fuel rod, and then come back.

Again, it should first be assumed that the cavity mean free path is finite; the limit is taken afterward.

For the third component, it is assumed that the neutrons leaving the cell return isotropically (white boundary condition) and that the returning neutrons, which hit the fuel rod, enter the latter isotropically.

The first and second components of $p_{cc,k}$ have been evaluated by Benoist (they correspond to his Q_k and Q_k' functions). The third term can be evaluated by summing up the contribution of multiple crossings of the cell boundary, on the basis of complementary and reciprocity relationships between collision probabilities and blacknesses. The final expression for $p_{cc,k}$ can be viewed as a special case of Eq. (25) in Ref. 55 (with $\Delta = 0$, since here the outside region returns all neutrons):

$$p_{cc,k} = \frac{a}{a+b}\,(Q_k + Q_k') + \frac{\lambda}{a}\,\frac{\left(1 - \frac{a}{\lambda} W_k\right)^2}{1 - \frac{a}{\lambda} T_k} \quad . \tag{5-9}$$

The functions Q_k, Q_k', W_k, and T_k are given graphically by Benoist (Refs. 54, 55) versus $\eta = a/\lambda$ and $\alpha = a/b$, with $k \equiv r$ or $k \equiv z$. With this expression, the directional diffusion coefficients may then be evaluated by Eq. (5-8).

The second approach should give more accurate results than the first since the physical model is closer to reality. The validity of the approach hinges on the assumption of isotropic boundary crossing, an assumption that is usually quite good for the very tight lattice of the GCFR.

5.4.2. One-Group Evaluation

The methods described in the preceding section will first be used in a one-group, bare reactor calculation of streaming effects. The basic data are as follows:

Homogenized Nuclear Data (over rod and coolant void)

Absorption macroscopic cross section, Σ'_a . . . . . 0.00411 cm^{-1}

Transport macroscopic cross section, Σ'_{tr} . . . . . 0.1575 cm^{-1}

Diffusion coefficient, D' . . . . . 2.117 cm

Homogeneous Nuclear Data (homogenized over rod only)

Absorption macroscopic cross section, Σ_a . . . . . 0.00893 cm^{-1}

Transport macroscopic cross section, Σ_{tr} . . . . . 0.3424 cm^{-1}

Transport mean free path, λ . . . . . 2.921 cm

The results of the calculations are shown in Table 5.4.

TABLE 5.4

DIRECTIONAL DIFFUSION COEFFICIENTS

	Method 1	Method 2
Reduced Collision Probabilities		
p_{cc}, r	8.42	8.82
p_{cc}, z	9.40	9.44
Diffusion Coefficients		
D_r	2.137	2.167
D_z	2.211	2.214
$D = (D_z + 2D_r)/3$	2.161	2.183

These results led to the following conclusions:

1. The two approaches discussed in the preceding section are in good agreement for the evaluation of the reduced probabilities $p_{cc,k}$. As expected, the first approach yields lower values than the second, by 4.5% for $p_{cc,r}$ and by 0.5% for $p_{cc,z}$.

2. The directional diffusion coefficients D_r and D_z are thus also in good agreement. The agreement between both approaches is especially good for the axial direction, which is indeed the direction for

which the calculations are the most straightforward within Benoist's theory. As expected, D_r and D_z are larger than the standard diffusion coefficient D'. The rigorous isotropic diffusion coefficient, given by $D = (D_z + 2\ D_r)/3$, is also larger than D'. On the one hand, D_z is larger than D' because of the easier diffusion in the direction parallel to the void channels. On the other hand, D_r is larger than D' owing to the error introduced by the homogenization for the diffusion across successive layers of material and void; the free ride in the voids is underestimated by the lower atom density of the homogenized mixture.

3. For reasons stated in the discussion of the method, the results of the second approach should be the most accurate. Therefore, they will be used in the evaluation of the effect of neutron streaming on the reactivity of the demonstration plant.

Neutron streaming increases leakage in the axial direction and also, to a lesser extent, in the radial direction. The axial diffusion coefficient D_z was found to be larger than the homogeneous D' by 0.097 and larger than D_r by 0.050. The increased leakage results in a decrease in reactivity. One-group perturbation yields

$$\frac{\Delta k}{k} = - \frac{B_z^2 \cdot \delta D_z + B_r^2 \cdot \delta D_r}{\Sigma_a' + D' B^2} = -0.011 \quad , \tag{5-10}$$

where the extrapolated height is 145 cm, the extrapolated radius is 122 cm, $\Sigma_a' = 0.00411\ cm^{-1}$, and $D' = 2.117$ cm.

5.4.3. Multigroup, Multiregion Evaluation

For a more reliable analysis of streaming effects, it is necessary to take into account energy and spatial distributions. The formalism of Section 5.4.1 (second approach) is applied to the diffusion coefficient in every energy group and every region.

An analysis of the computed energy- and space-dependent D_z and D_r leads to two conclusions:

1. Streaming affects most strongly the low-energy groups. For the fastest group, D_z is 2% larger and D_r is 1% larger than D'_{hom}; for the slowest group, D_z is up to 11% larger and D_r up to 5.5% larger than D'_{hom}. This is simply a reflection of the fact that homogenization is good when the transport mean free path is large in comparison with the cell dimensions.

2. $\delta D_z = D_z - D'_{hom}$ and $\delta D_r = D_r - D'_{hom}$ are nearly independent of the region, because the transport mean free path is roughly the same in all core regions and blanket. More interesting is the fact that δD_z and δD_r are relatively weakly dependent on energy. This results in greater impact of streaming on the lower-energy groups.

Once the directional diffusion coefficients for all regions and groups are known, it is then possible to investigate the effects of streaming upon some characteristic reactor parameters, such as k_{eff}, conversion ratios, average region fluxes, and leakage. The best way to study streaming effects is to work directly in two-dimensional diffusion theory with different diffusion coefficients for the two main directions. With some modifications, the two-dimensional code GAMBLE allows such a direct study of anisotropic diffusion. In the difference scheme of GAMBLE, the diffusion coefficient appears only in the expression of four factors, α_1 to α_4, two of which are applied to differences in one direction and two in the other direction. It is thus possible to insert the directional diffusion coefficients in lieu of the single homogeneous diffusion coefficient in the evaluation of the corresponding α_i. To accomplish this change, the modified GAMBLE program requires as input a pair of diffusion coefficient modifiers (the ratios D_k/D_{hom}) for each material region and energy group.

The results of the ten-group, six-region study of streaming for the GCFR demonstration plant, performed with the modified GAMBLE program, are given in Table 5.5.

TABLE 5.5

DIFFERENCES BETWEEN HOMOGENIZED 10-GROUP, TWO-DIMENSIONAL CALCULATIONS WITH AND WITHOUT STREAMING CORRECTION

Multiplication factor	-0.8%
Core conversion ratio	-0.1%
Breeding ratio	+0.6%
Peak-to-core average power	-0.5%
Axial leakage	+9.0%
Radial leakage	+6.0%

The effect of streaming on reactivity is seen to be somewhat smaller than predicted by the one-group analysis of Section 5.4.2. Since D_k is relatively independent of energy, the one-group perturbation formula should give a good estimate of streaming effects on reactivity. The difference is due to the excessive leakage predicted by the geometric buckling. The core conversion ratio decreases because of spectral hardening; the spectrum is harder due to the higher streaming leakage at low energy. The overall breeding ratio increases because of the increased core leakage, and for the same reason the core peak-to-average ratio decreases.

Streaming effects in a larger GCFR are about the same as in the demonstration plant. As illustrated by Eq. (5-10), the larger δD_k associated with the larger coolant fraction of the commercial GCFR are compensated by the smaller buckling of large cores.

6. REACTIVITY COEFFICIENTS

Reactor stability and safety depend on the existence of negative coefficients of reactivity. The GCFR relies in this respect on the Doppler and expansion coefficients.

Reactivity coefficients can be grouped in two broad categories. The first category includes all the effects that do not presuppose an accident condition, such as Doppler, expansion, and coolant effects. The second category includes coefficients that imply some kind of preliminary accident, such as fuel removal, cladding removal, and steam reactivity effects.

6.1. DOPPLER EFFECT

The Doppler effect represents the most reliable negative feedback mechanism for all fast-reactor types. As demonstrated by various safety studies (Ref. 1), the Doppler effect in the GCFR is large enough to limit adverse consequences of reactor transients.

In a GCFR, there are no changes in material composition during normal or accidental transients that could drastically reduce the Doppler effect. Only the very unlikely melting of all the cladding could somewhat reduce the Doppler effect because of the resulting spectrum hardening. In this respect, it is of interest to note that economic objectives in GCFR design are not hampered by the safety problems of positive reactivity coefficients. Since helium voiding does not lead to a large positive reactivity insertion or to a reduction in Doppler effect, essential reactor characteristics such as shape and fissile enrichment can be selected solely on their economic merit.

6.1.1. Evaluation of Total Doppler Effect

To evaluate the Doppler effect, ten-group cross sections were computed at 300°, 1300°, and 3000°K. The GANDY-GAROL options of GGC-5 were used. The change in reactivity from the normal (1300°K) case to each of the other two conditions was calculated using the two-dimensional perturbation theory code GAPER-2D. Unperturbed flux and adjoint flux values were used in the computation, a procedure justified by Hummel and Okrent (Ref. 56).

The reactivity changes obtained from the perturbation calculations are converted to a Doppler coefficient by assuming a form $C(T/T_o)^{-x}$ for the dependence of that coefficient on temperature. By normalizing temperatures to the operating temperature T_o, the coefficient C becomes the Doppler coefficient at operating temperature. The coefficient C is a useful quantity for comparison of various reactor designs and also the performance of various reactors (more useful than the quantity CT_o^x). For the GCFR demonstration plant, the Doppler coefficient of reactivity is

$$\frac{1}{k}\frac{\delta k}{\delta T} = -\frac{2.6\ 10^{-6}}{(T/T_o)^{1.1}}\ (°K^{-1}) \qquad T_o = 1300°K.$$

The temperature exponent in the expression for the Doppler coefficient depends strongly on the treatment of p-wave resonances and overlap effects. As shown by Hummel and Okrent (Ref. 57), the inclusion of p-wave and overlap effects (as done in the GAROL-GANDY option of GGC-5) leads to an exponent that is up to 30% higher than the value obtained when such factors are neglected (as in the GAMNIT-TUZ option of GGC-5). The value of 1.1 shown here is, incidentally, in good agreement with that obtained from the curve plotted by Hummel and Okrent (Ref. 57) (1.08 for the fertile-to-fissile ratio of the GCFR demonstration plant). The latter curve also shows that for the fissile enrichment of a large GCFR (<15%), the temperature exponent would be equal to approximately 1.05.

For most applications, it is sufficient to assume a simple 1/T dependence of the Doppler coefficient, since the difference with the correct

expression is well within the uncertainty with which the Doppler effect is known (see Fig. 6.1). In that case, the value is

$$\frac{1}{k}\frac{\delta k}{\delta T} = -\frac{2.6\ 10^{-6}}{T/T_o} = -\frac{0.0034}{T}\ (^{\circ}K^{-1}) \quad .$$

The Doppler constant of 0.0034 is typical for breeder demonstration plants; for example, this constant has a value of 0.0039 in the 250 MW(e) Phenix, 0.0038 in the 300 MW(e) German Na2, and 0.002 in the 350 MW(e) BN-350 Russian plant (Ref. 58).

The Doppler effect is strongly dependent on the fissile enrichment. The demonstration plant has an average enrichment of 18%. For a commercial GCFR with partial fuel reloading (every six months or every year), the enrichment would be between 14% and 16%, and for a commercial GCFR with batch reloading (every 3 to 4 yr) about 11%. The Doppler constant of the large GCFR could thus be approximately twice the value of the demonstration plant (Ref. 59).

6.1.2. Local, Space-dependent Doppler Effect

The reactivity worth of a unit change in temperature is larger near the core center than at the edge owing to the difference in neutron importance. The spatial dependence of the Doppler effect is shown in Fig. 6.2 in the form of a local Doppler constant that corresponds to the usual 1/T dependence of the Doppler coefficient. For a small temperature change ΔT in a small volume ΔV at an initial average temperature T_1, the Doppler reactivity coefficient amounts to $\Delta k/k\Delta T = -\alpha\Delta V/T_1$, where α is an average value per unit volume over ΔV of the local Doppler constant. Therefore, for a large temperature change in which the average fuel temperature in ΔV goes from T_1 to T_2, the reactivity change $\Delta k/k$ amounts to $-\alpha\Delta V \ell n(T_2/T_1)$.

The local Doppler constant was evaluated by first-order two-dimensional perturbation theory. The same temperature-dependent cross sections were used throughout the reactor, an assumption which implies that the Doppler

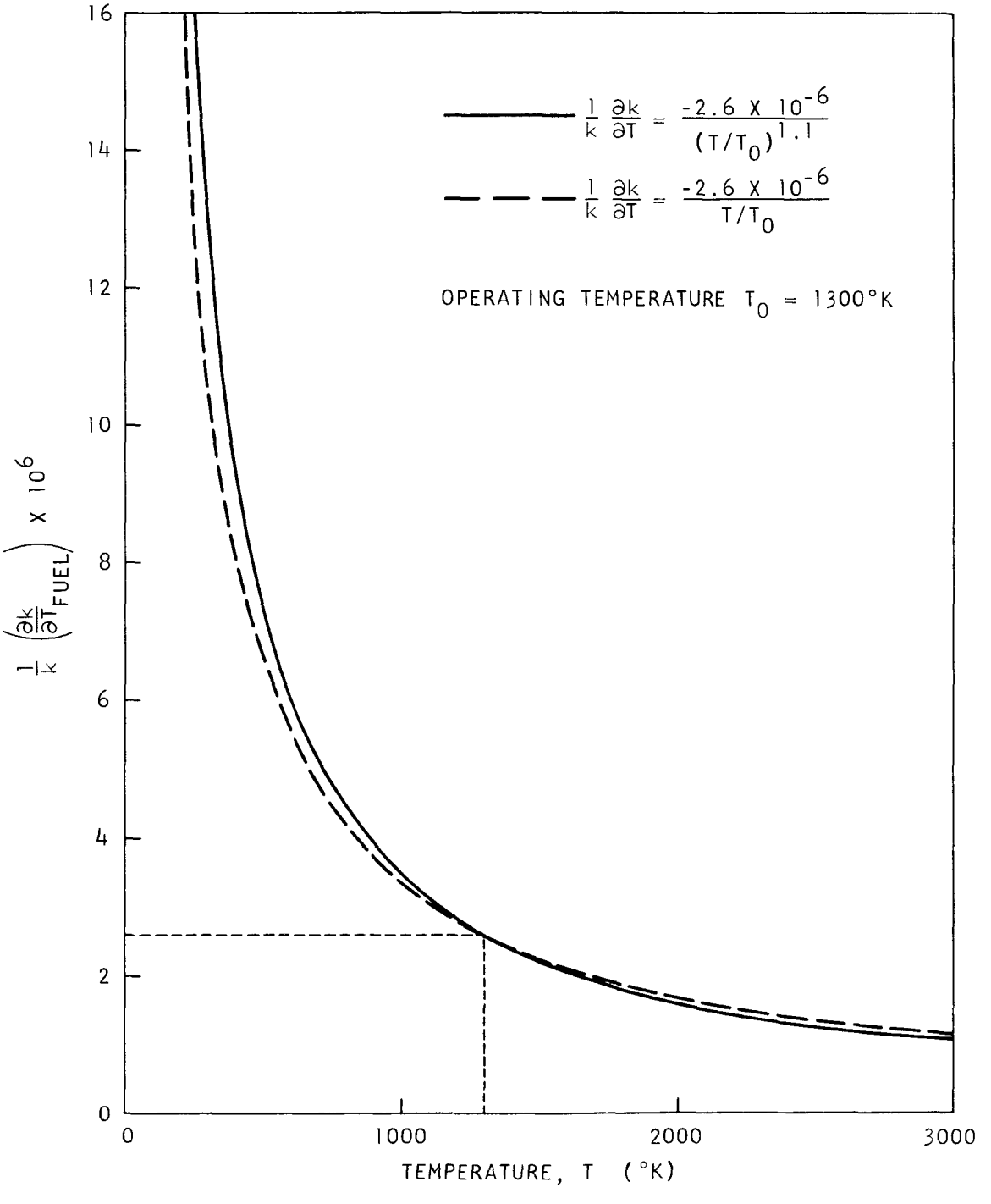

Fig. 6.1. Doppler coefficient

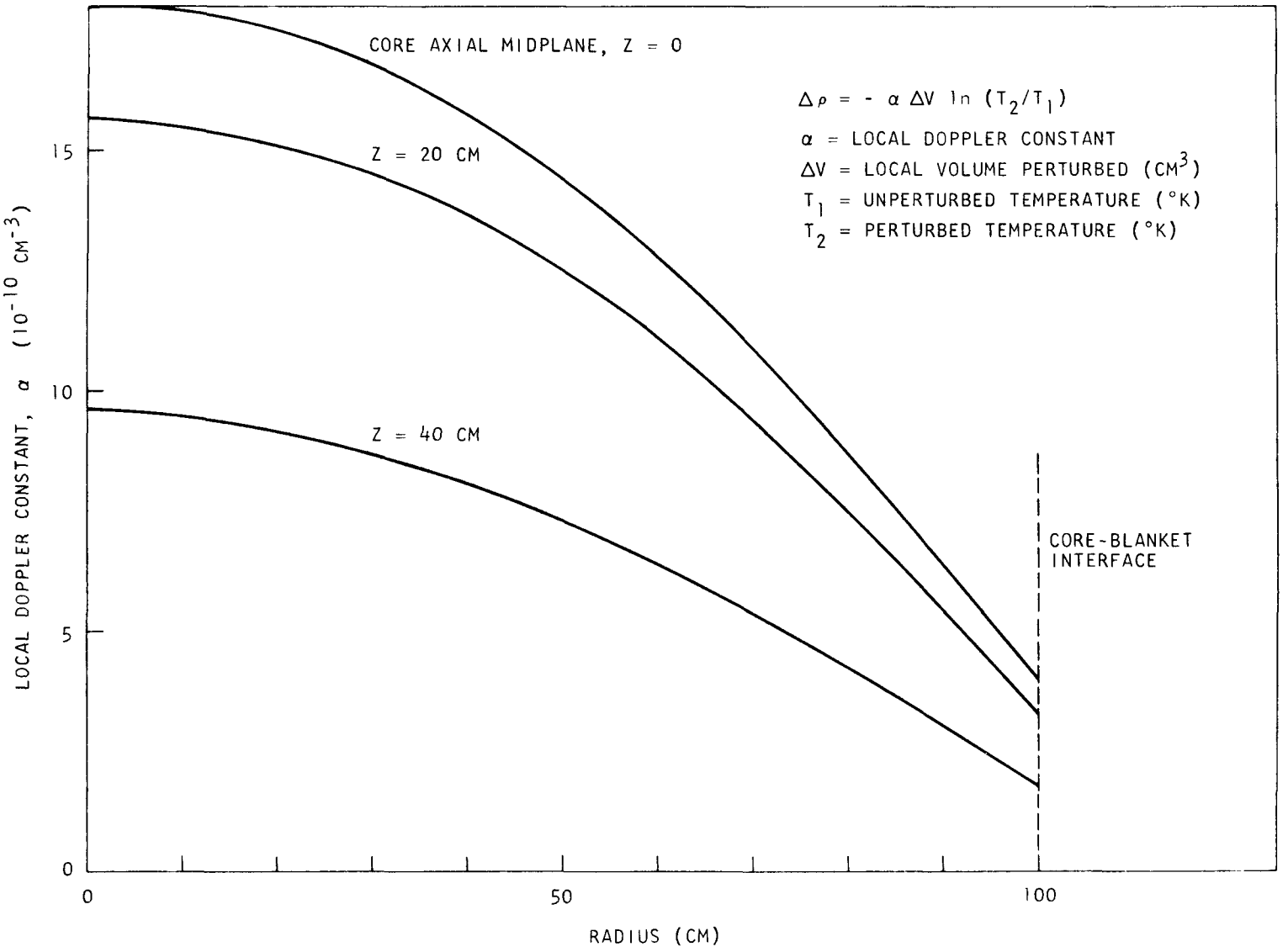

Fig. 6.2. Local Doppler constant α

effect at the average core enrichment applies to the whole reactor. This assumption is acceptable in the core because the spectrum in the various zones is much the same in spite of the different enrichments. In the blanket, however, the Doppler effect is much larger because of the much softer spectrum. In this respect, it is of interest to note that for a uniform temperature change in the whole reactor and the use of core temperature-dependent cross sections in the blanket, the Doppler constant of -0.0034, calculated for the demonstration GCFR, includes a 30% contribution from the blankets. This contribution is underestimated by the use of core temperature-dependent cross sections in the blanket. However, this error is more than compensated by the fact that a power change leading to a one-degree change in core average fuel temperature would result in less than a one-degree change in blanket average fuel temperature.

6.1.3. Influence of Method and Cross-Section Uncertainties

It is generally estimated that the accuracy of current Doppler effect calculations is no better than $\pm$30%. The error stems from two sources: first, the computational methods; and second, the cross-section data.

Although an accurate treatment of the resonance region is important, the methods used for Doppler calculations should above all evaluate correctly the slowing-down sources from above the resonance region. The methods used in GAM, together with the GANDY unresolved resonance treatment, lead to a computationally accurate evaluation of the Doppler effect, as has been ascertained by comparison with the more powerful GAFGAR spectrum code (Section 4.2.1.3).

As mentioned in Section 4.1.3, the unsatisfactory status of U-238 cross sections creates most of the remaining uncertainty in the physics design of fast reactors. This is especially true for the Doppler effect since U-238 is the major contributor. Uncertainties in U-238 capture and inelastic scattering cross sections are most significant for the Doppler effect.

As far as inelastic scattering is concerned, the data uncertainties affect the Doppler effect by less than 5% in a sodium reactor (Ref. 60). The impact should be greater in the GCFR because of the relatively larger moderating importance of U-238 in the absence of sodium.

The effect of U-238 capture cross-section uncertainties has been explicitly investigated by computing the Doppler coefficient with GAM (GANDY-GAROL) for the new low GGA-NASA capture data shown in Fig. 4.5 and discussed in Section 4.1.3. The latter results can thus be compared with those presented in Section 6.1.1 that were with the old high GGA-NASA capture data:

High U-238 Capture (Old GGA-NASA)

$$\frac{1}{k}\frac{\delta k}{\delta T} = \frac{-2.6\ 10^{-6}}{(T/T_o)^{1.1}} \cong \frac{-0.0034}{T}\ (°K^{-1}) \qquad T_o = 1300°K$$

Low U-238 Capture (New GGA-NASA)

$$\frac{1}{k}\frac{\delta k}{\delta T} = \frac{-3.2\ 10^{-6}}{(T/T_o)^{1.08}} \cong \frac{-0.0042}{T}\ (°K^{-1}) \qquad T_o = 1300°K$$

The low U-238 capture data lead to a 20% more negative Doppler constant than the high values. This is a direct consequence of the softer spectrum that results from the lower capture in the 60- to 800-keV range, where most of the GCFR spectrum lies. The Doppler effect is thereby enhanced by the increase in relative capture in the resonance range. As expected, the exponent of the temperature does not change much since it depends essentially on resonance parameters.

The low U-238 capture data above the resonance range affects the magnitude of the Doppler effect by increasing the slowing-down density, but the spectral distribution of the Doppler effect within the resonance range should not change very much. This is indeed apparent in Table 6.1,

TABLE 6.1

SPECTRAL COMPOSITION OF DOPPLER REACTIVITY

FOR HIGH AND LOW U-238 CAPTURE[a]

Group	Low Energy (keV)	High Capture[b] Old GGA-NASA	Low Capture[c] New GGA-NASA
5	67.38	0.7	0.2
6	24.79	4.9	6.2
7	9.12	9.9	13.4
8	3.36	19.2	21.0
9	0.45	56.7	52.1
10	0.0	8.6	7.1
		100.0	100.0
Unresolved	>3.36	34.7	40.8
Resolved	<3.36	65.3	59.2

[a] Reactivity change between 1300° and 3000°K

[b] Together with low Pu-239 α, high Pu-240 capture

[c] Together with high Pu-239 α, low Pu-240 capture

which shows the spectral distribution of the total Doppler reactivity as a percentage of the total negative contribution of the six resonance broad groups for the old data (those used for the Doppler calculations of Section 6.1.1) and the recommended new data. With an arbitrary cutoff point of 3.36 keV, about 60% of the negative contribution originates in the resolved range (this value would exceed 70% in a sodium reactor (Ref. 61)). However, the spectral differences between the old and new data cannot all be attributed to U-238 since the Pu-239 and Pu-240 data were also significantly different.

On the basis of the present analysis, it appears that most of the uncertainty in the Doppler effect is due to the uncertain status of the U-238 capture cross section. Should further measurements confirm the low Karlsruhe-GGA-ORNL values, thereby eliminating most of the capture uncertainty, it would then seem justified to state that the Doppler effect is known within ±10% to 20%, with the remaining error being a compound of cross-section, statistical, and method errors.

When discussing the accuracy of the Doppler coefficient as computed with available physics data and methods, it is well to remember that the average fuel temperature, upon which the Doppler effect is strongly dependent, is not known to the desired accuracy. Heat transfer calculations show that the average fuel temperature is quite sensitive to the magnitude of the conductivity of the gap between fuel and cladding. The manufactured average dimension of the gap (only 0.07 mm) is uncertain, and in any case, fuel relocation and cracking due to irradiation destroy the semblance of a gap. It is therefore difficult to assign a value to the "gap" conductivity, and experimental values may not be generally applicable. At any rate, it is estimated that the uncertainty in average fuel temperature may exceed 100°C. This leads to a reflected uncertainty of about 10% in addition to the 10% to 20% uncertainty in the Doppler coefficient of reactivity.

6.2. EXPANSION COEFFICIENTS

The following volumetric expansion coefficients were computed in two-dimensional diffusion theory:

$$\text{Axial } \frac{\delta k}{k} = -0.21 \frac{\delta H}{H} \quad , \qquad \text{Radial } \frac{\delta k}{k} = -0.66 \frac{\delta R}{R} \quad .$$

The radial volumetric coefficient is used to evaluate the slow reactivity effects of radial core expansion when the reactor is brought from cold to hot operating conditions and distortion due to fuel box swelling (see Table 3.8). There is no significant thermal or radiation mechanism for prompt radial expansion.

The axial volumetric coefficient is also used to evaluate the slow reactivity effect of core distortion shown in Table 3.8. In addition, this coefficient is used to calculate the prompt axial expansion coefficient which is due to the thermal expansion of the cladding carrying the fuel. The cladding is made of type 316 stainless steel, which has a linear thermal expansion coefficient of about 2×10^{-5} $°C^{-1}$ in the temperature range of interest (Ref. 62). If follows that the total prompt expansion coefficient of reactivity is

$$\frac{1}{k} \frac{\delta k}{\delta T} = -4.2\ 10^{-6} \ (°K^{-1})$$

6.3. COOLANT COEFFICIENT

The total coolant worth in the GCFR demonstration plant is 0.0014 δk, or 40¢. Its effect in transients is proportional to the density change, and hence, for all accidents other than depressurization, this component of reactivity is small. Even in depressurization with the severity of the design basis accident ($T_c \sim 40$ sec), reactivity from this source enters very slowly on a neutronic time scale.

The reactivity effect due to helium density changes may be derived from the equation of state of helium during the transient under consideration. At a pressure P and a mean temperature T(°K), the reactivity change $\Delta\rho$ with respect to the nominal pressure P_c and mean temperature T_c is given by

$$\Delta\rho = h\left(1 - \frac{P}{P_c}\,\frac{T_c}{T}\right) ,$$

where T_c = 700°K and P_c = 85 atm.

The reactivity gain h for complete loss of helium is the result of two competing reactivity effects, a positive spectral effect and a negative leakage effect. The spectral component is caused by the decrease in down-scattering, which leads to a harder and therefore more reactive spectrum. The leakage component results from the decrease in transport cross sections, which increases the leakage.

The calculation of h was done in two-dimensional r-z first-order perturbation theory. The results are as follows:

Spectral component:	+0.00228 δk
Leakage component:	-0.00133
Total (h)	+0.00095 = \$0.27

First-order perturbation theory implies the use of unperturbed flux and unperturbed adjoint flux, whereas exact perturbation theory would require the use of perturbed flux and unperturbed adjoint flux. First-order perturbation theory tends to underestimate the helium worth by 10% to 15% (by underestimating the spectral component and by also overestimating the magnitude of the leakage component). Furthermore, the results shown above were derived with the standard 10-group set with a lethargy width of 1.0. This width is probably too large to give a satisfactory representation of the adjoint function, and this in turn may lead to an underestimation of the spectral component by more than 10% (by analogy with the results obtained for sodium voiding (Ref. 63)). Altogether, the value of \$0.40 should be more appropriate.

With this latter value, the helium temperature coefficient at operating average temperature (T_c = 700°K) is

$$\frac{1}{k}\frac{\delta k}{\delta T_{He}} = +2.0 \times 10^{-6} \ (^{\circ}K^{-1}) \quad .$$

The helium worth given above was calculated with low-α Pu-239 cross sections and high U-238 and Pu-240 capture cross sections. The use of Pu-239 Gwin-KFK data; the ENDF/B, Version II, Pu-240 capture cross sections; and the new GGA-NASA U-238 capture cross sections (see Section 4.1) would not appreciably change the helium worth (or the cladding worth, discussed in Section 6.7) because the smaller worth due to the α Pu-239 change would be approximately compensated by the greater worth due to the U-238 and Pu-240 capture changes.

6.4. ISOTHERMAL AND POWER REACTIVITY COEFFICIENTS

Under most circumstances, a reactor transient would involve simultaneous changes in fuel, cladding, and coolant temperatures. The magnitude and timing of the corresponding reactivity feedbacks depend on the transient being considered, i.e., whether it is slow or fast and whether it is initiated by a power change in the fuel or by a change in coolant inlet temperature or flow rate. Any combined reactivity coefficient is thus strictly limited to a particular set of circumstances. The isothermal temperature and steady-state power coefficients represent two such combined reactivity coefficients for simple but well-defined reactor transients.

The isothermal temperature coefficient is defined as the reactivity change caused by a one-degree change in all reactor materials. It is just the unweighted sum of its various components at a given temperature.

Isothermal Temperature Coefficient
(10^{-6} $\Delta k/k/°C$)

	At 20°C[a]	At 312°C[b]
Doppler	-13.4	-6.3
Axial expansion	-4.2	-4.2
Coolant	+11.4[c]	+2.9[c]
Isothermal coeff.	-6.2	-7.6

[a] Zero power, pressurized

[b] Zero power, pressurized, at inlet temperature

[c] Total helium worth, 1.4×10^{-3} Δk

The steady-state power coefficient is defined as the reactivity change caused by a unit increase in power level at constant coolant inlet temperature and flow rate. The change in power is slow enough to permit equilibrium temperatures to be reached everywhere. This coefficient has been evaluated from the asymptotic power level in a series of transients induced by reactivity step insertions. The calculations were performed with a point kinetics code (BLOOST) which incorporates a two-dimensional heat transfer model of the average core pin. The steady-state power coefficient and its components at full power were found to be as follows:

	$\Delta k/k/MW(t)$	$\Delta k/k/\%$ full power
Doppler effect	-2.5×10^{-6}	-2.1×10^{-5}
Axial expansion	-0.9×10^{-6}	-0.7×10^{-5}
He density	$+0.2 \times 10^{-6}$	$+0.2 \times 10^{-5}$
Power coefficient	-3.2×10^{-6}	-2.6×10^{-5}

The same transient calculations showed that for an increase of 1 MW(t), the fuel temperature rises by about 1°C, the cladding temperature by 0.25°C, and the helium temperature by 0.14°C. These weights lead approximately to the correct value for the components of the power coefficient, when multiplied by the Doppler, expansion, and coolant coefficients at operating temperatures.

6.5. OTHER REACTIVITY EFFECTS IN NORMAL OPERATION

The reactivity requirements for the control system, which are given in Table 3.8, include other reactivity effects besides those associated with the fuel, cladding, and coolant temperatures.

Fuel elements of the GCFR demonstration plant are rigidly suspended from a top-mounted grid plate, with no lateral core clamping or bottom grid plate. Grid plate expansion due to changes in coolant inlet temperature and grid plate bending due to the dynamic pressure change core shape and therefore core reactivity. The overall effect amounts to \$1.05 when the temperature rises from 20°C to the operating inlet temperature of 312°C. Most of the effect is due to radial expansion. Assuming linearity, one can define a grid plate coefficient of reactivity of approximately $-1.0\ 10^{-5}\ \Delta k/k/°C$, where the unit temperature change refers to the coolant inlet temperature. However, this reactivity feedback occurs with a considerable delay with respect to core power changes. As shown in Section 6.4, a 1-MW(t) increase in power level (equivalent to a 1°C increase in average fuel temperature) raises the reactor outlet temperature by about 0.28°C. Due to the effect of the heat exchangers, the increase in the inlet temperature is delayed and a much longer time will be required for the helium to transfer the temperature rise to the grid plate. One can therefore define a grid plate coefficient of reactivity which amounts to approximately $-2.8 \times 10^{-6}\ \Delta k/k/°C$, where the unit change refers to the average fuel temperature. Although partially compensated by the positive reactivity introduced by the increase in inlet temperature, this negative effect does increase the power coefficient, especially at lower power levels.

The fuel element boxes located near the core periphery are in a strong temperature gradient caused by the power gradient in the enclosed fuel rods. The inner side (with respect to the core center line) of the box is at a higher temperature than the outer side. The difference in temperatures leads to outward box distortion. As seen in Table 3.8, the worth of this reactivity effect is only 5¢ for the entire cold-to-hot swing.

The other reactivity effects shown in Table 3.8 are long-term effects associated with cladding swelling under irradiation.

6.6. STEAM ENTRY

In the heat exchangers, the helium primary coolant transfers its heat to the water secondary coolant. The failure of a heat exchanger tube would bring steam into the core at a pressure higher than the normal helium pressure. The limiting case would be if no protective actions were taken. In this case the primary system relief valve would open and then maintain a constant pressure (slightly higher than the normal 85 atm) for the mixture of progressively purer steam until complete escape of the helium. The maximum steam density that can be reached in the coolant passages amounts to 0.0545 g/cm^3, or 5.45% of full water density. Figure 6.3 shows the effect of steam entry in the GCFR demonstration plant.

The entrance of steam into the core degrades the flux spectrum by increasing downscattering. This results in a change in the infinite multiplication factor and in neutron leakage. For small steam densities, the multiplication factor decreases as the median neutron energy decreases. For larger steam densities, the multiplication factor may increase or decrease depending on the concentration of absorbers, such as control rods or fission products.

The spectrum calculations for a steam flooded core are performed with the B_1 approximation and the GAROL and GANDY options of GGC-5 (see Section 4.2). Heterogeneity effects gain importance with the introduction of a moderator, but the moderator density is small enough (less than 6% of full water density) to preclude the need for a more detailed space-energy cell calculation than that performed in GGC (two-region probability model) (Ref. 64). In this respect, it is of interest to note that the Dancoff factor (at 2 keV) changes only slightly with steam entry, as shown below:

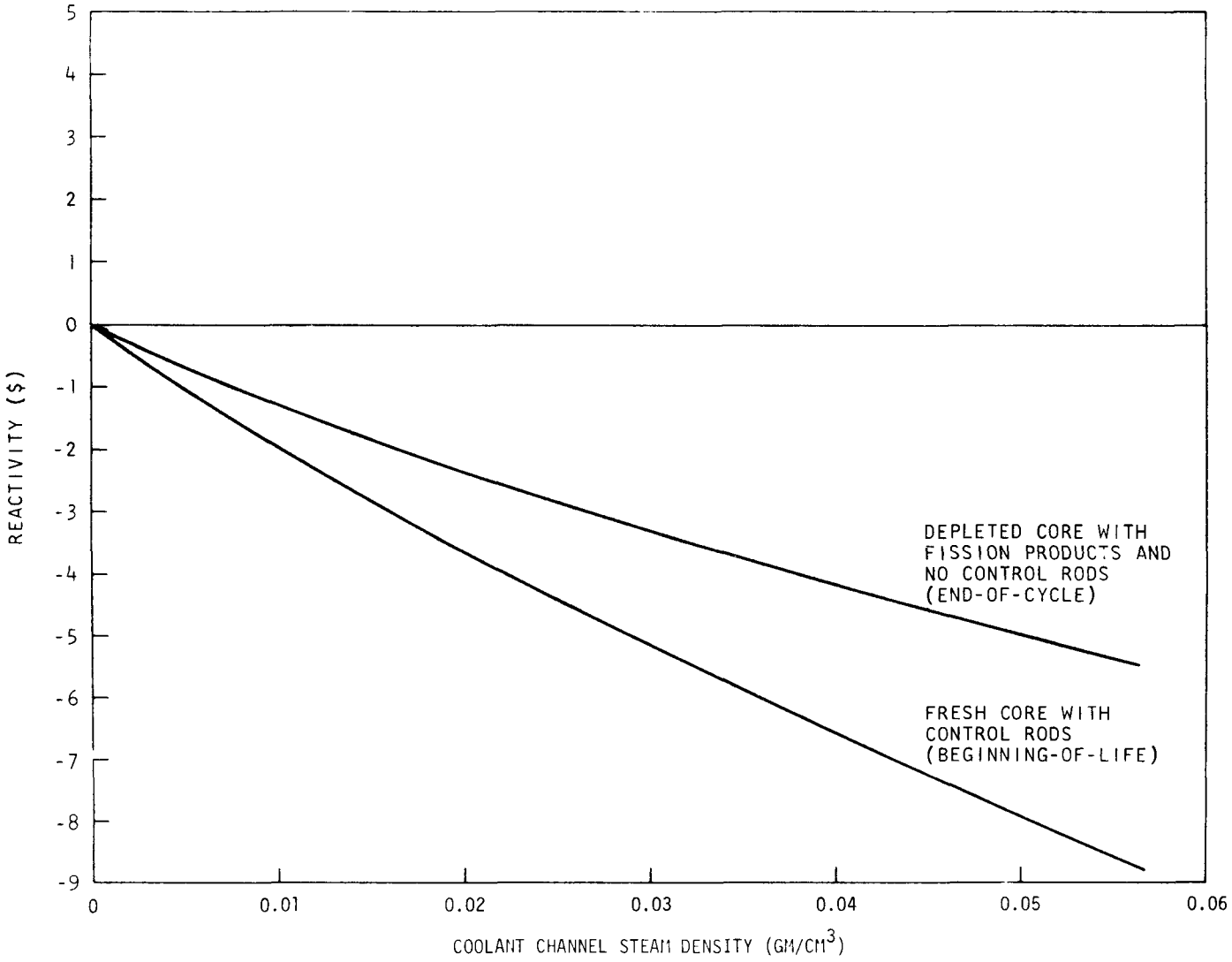

Fig. 6.3. Reactivity effect of steam flooding

Flooding (% of water density)	Dancoff Factor C	1 - C
None	0.8145	0.1855
1	0.8010	0.1990
2	0.7879	0.2121
5	0.7507	0.2493

The energy spectrum calculated with the average core composition ($B^2 = 9.05 \times 10^{-4}$ cm^{-2}) and 5% steam flooding is shown in Fig. 6.4. The spectrum is indeed much softer than for the dry core. To determine the effects of steam entry, the spectrum and broad-group cross sections for all nuclides are reevaluated for each degree of steam entry and then used in explicit two-dimensional r-z diffusion calculations to find k_{eff}. The calculations reported below, which involve control rods or fission products, were performed with broad-group cross sections for boron and fission products averaged over the spectrum of the unpoisoned flooded core. This tends to underestimate their effect.

The steam reactivity effect as a function of steam density is shown in Fig. 6.3 for two core conditions. The lower curve refers to a fresh core maintained critical with about $10 of control rods. The reactivity decreases steadily as steam density increases because there is enough poison material to compensate the increasing fission rate. The upper curve corresponds to the core composition at the end of equilibrium cycle, with fission products but no control rods. The reactivity behavior is much the same as with a rodded fresh core.

The conclusion can therefore be reached that steam entry does not represent a hazard to the operation of the GCFR demonstration plant since the reactivity effect is negative for all operating conditions. Past studies (Ref. 1) of steam flooding in the large GCFR had indicated a possible positive effect and therefore the possible use of resonance poisons such as gadolinium or hafnium. The essential difference lies

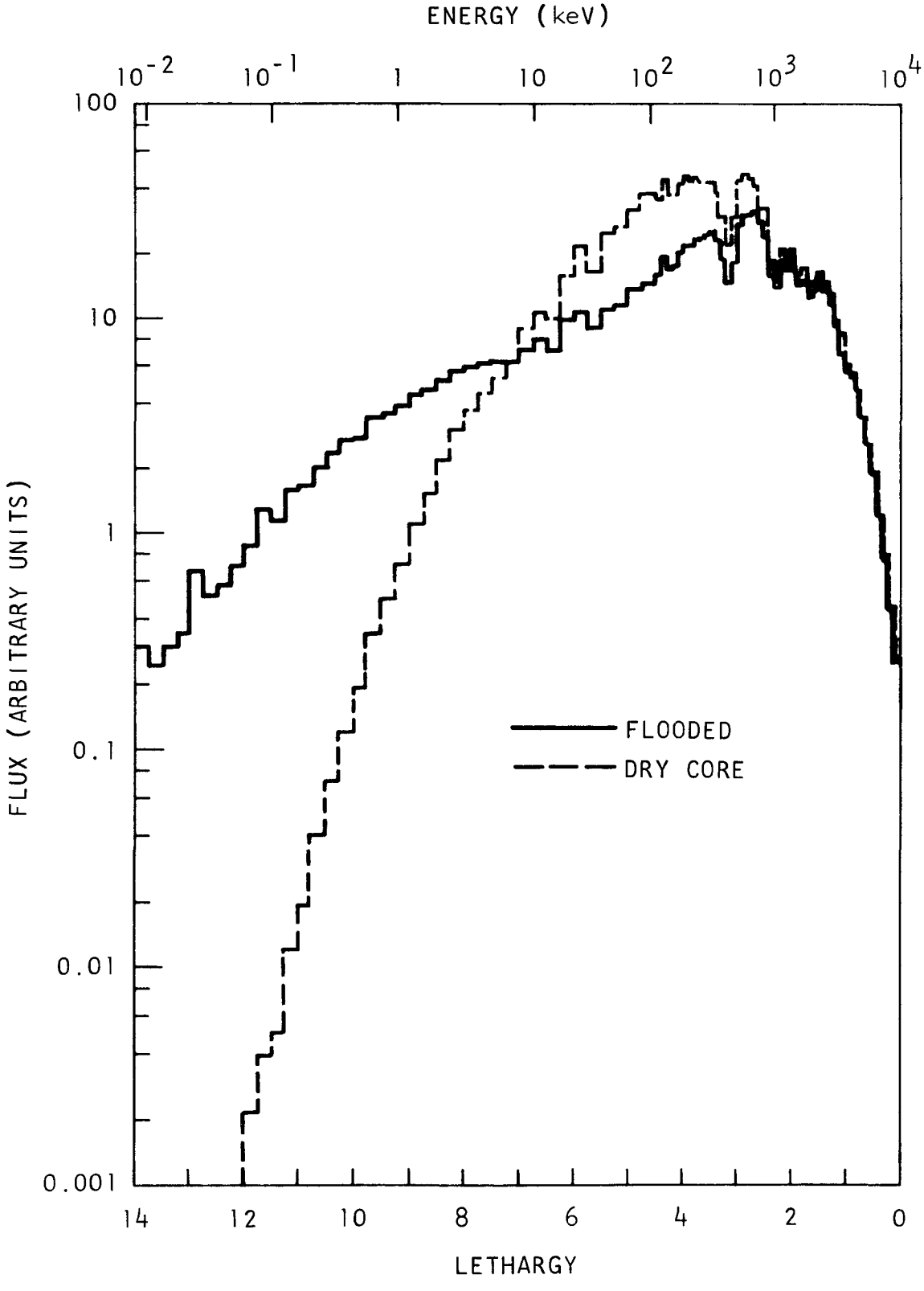

Fig. 6.4. Core spectrum for 5% steam flooding

in the selected mode of fuel management. The designs of the large GCFR plant studied in the past were all based on a batch reloading scheme that took advantage of the near-unity internal conversion achievable in a GCFR and the resulting constant reactivity throughout burnup. A fresh core batch with practically no control rods would indeed have a positive steam effect for maximum steam density (Ref. 65). However, as discussed in Section 3.2, a fuel management scheme based on partial reloading is more desirable for the GCFR demonstration plant. Then, the reactivity decreases with burnup and the initial excess reactivity must be compensated by the insertion of control rods. As a result, partial reloading eliminates the steam flooding reactivity problem by making it negative under all foreseeable conditions.

The concentration of Pu-240 in the plutonium has some influence on the steam reactivity effect. Although this influence is large for nearly full water flooding (Ref. 66), the difference in reactivity is not too significant for the possible range of steam densities and likely spread in Pu-240 concentration. For example, for the curves of Fig. 6.3, the reactivity effect at 5% water flooding decreases by less than $1 when the Pu-240 concentration increases from 15% to 25%.

Of more importance is the impact of cross-section uncertainties. The steam entry reactivity effect has been reevaluated with the revised cross sections of Section 4.1 for the impossible but calculationally simple case of a fresh core with no control rods or fission products. The results were as follows:

Effect of Cross Section Changes

All fresh core - dry to 5% flooding

Old data	+$3.50
New data (Section 4.1)	-$0.30

Therefore, the new cross-section data (i.e., high Pu-239 α, low Pu-240 and U-238 capture) decrease the steam entry reactivity effect. As a

matter of fact, all the indicated cross section changes tend to make the steam reactivity effect more negative. The larger (Gwin's) α values increase capture in the resonance region and the lower U-238 capture of the new GGA-NASA set and the lower Pu-240 capture of ENDF/B, Version II, increase the resonance capture relative to that of the dry core.

6.7. CLADDING REMOVAL REACTIVITY COEFFICIENT

The Doppler and expansion reactivity effects are the dominant feedback mechanism under normal operating conditions and in safety analyses of nondamage accidents. Severe transients of the type typically calculated in hypothetical accident analyses may result in structural damage first to the cladding and then to the fuel. Some tests in the TREAT reactor (Ref. 67) have revealed that under certain circumstances the cladding could melt away, leaving the fuel intact in its cylindrical form, at least initially. The local removal of cladding material leads to a positive reactivity effect in most of the reactor.

Just as in the case of sodium voiding (Ref. 68), the reactivity effect due to cladding removal includes three components: a positive spectral and capture component, and a leakage component. The net effect may be positive or negative depending on the location.

For complete loss of cladding in each of the four enrichment zones and in the whole core, the reactivity effect is as follows:

Case	Reactivity ($)
Cladding loss in zone 1	+2.24
Cladding loss in zone 2	+1.65
Cladding loss in zone 3	+0.43
Cladding loss in zone 4	-1.46
Cladding loss in whole core	+3.22

The positive spectrum component of the cladding effect dominates in all core zones except in the outer zone, where leakage is larger. These values were evaluated from ten-group two-dimensional k_{eff} calculations with the cross sections averaged in an infinite medium with or without cladding.

The local reactivity effect of cladding loss is given in Fig. 6.5. As shown, the core is divided in axial and radial regions in the r-z model. The average reactivity effect in each of these regions has been evaluated by first-order two-dimensional perturbation theory. The number shown in Fig. 6.5 is a volumetric danger coefficient, i.e., the reactivity change due to the complete loss of cladding in 1 cm of core. Again, the effect is positive inside the core and negative near the core-blanket interface.

6.8. FUEL-REMOVAL REACTIVITY COEFFICIENTS

Safety analyses of damage accidents consider the possibility of fuel melting in some subsections of the reactor. Partial fuel melting introduces a negative reactivity feedback that helps in the termination of the accident.

Table 6.2 shows the negative-reactivity-worth distribution of the fuel at various reactor locations. The reactivity perturbation $\Delta k/k$ refers to the removal of all the fuel contained in 1 cm^3 of the assembly (and not to the removal of 1 cm^3 of fuel). These values were computed by two-dimensional perturbation theory.

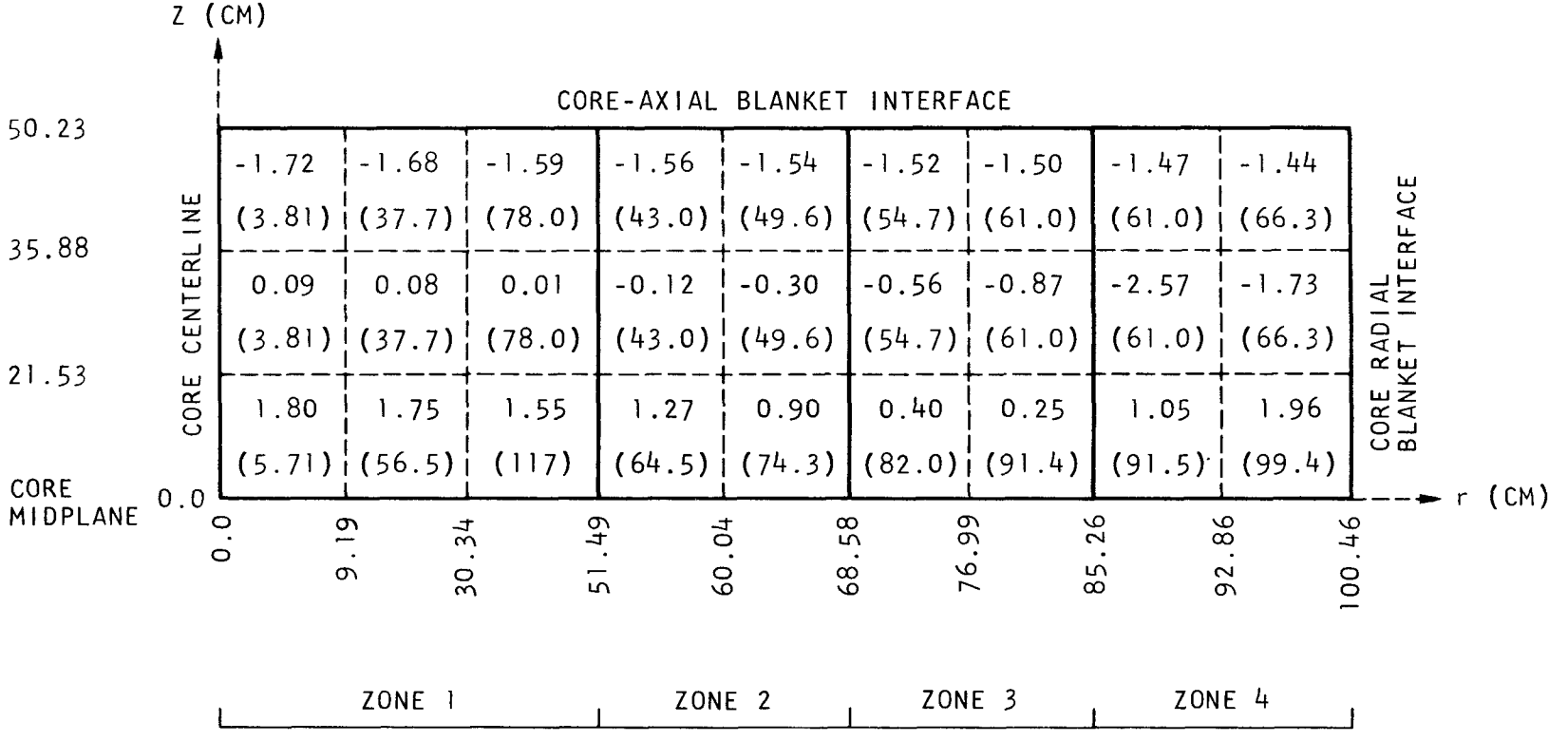

NOTES: THE UPPER NUMBER IN A REGION REPRESENTS THE LOCAL REACTIVITY COEFFICIENT (IN 10^{-8} $\Delta\rho/CM^3$ OF CORE), THE LOWER NUMBER (BETWEEN PARENTHESES) IS THE REGION VOLUME IN LITERS.

THE CORE IS ASSUMED TO BE AXIALLY SYMMETRICAL, BUT THE CLADDING COEFFICIENT REFERS TO CLADDING LOSS ON ONLY ONE SIDE OF THE CORE MIDPLANE.

Fig. 6.5. Local cladding reactivity coefficient

TABLE 6.2

REACTIVITY-WORTH DISTRIBUTION OF THE FUEL MATERIAL WITHIN THE REACTOR

(Units: $10^{-7} \frac{\Delta k}{k}/cm^3$)

Axial Position, z (cm)	Radial position, r													
	0 (cm)	12.5 (cm)	27.5 (cm)	37.5 (cm)	48.25 (cm)	53.25 (cm)	57.5 (cm)	66.79 (cm)	69.29 (cm)	72.5 (cm)	82.63 (cm)	87.63 (cm)	47.73 (cm)	102.73 (cm)
189.4	0	0	0	0	0	0	0	0	0	0	0	0	0	0
187.2	0.093	0.092	0.088	0.083	0.076	0.073	0.069	0.060	0.057	0.054	0.041	0.034	0.020	0.018
177.2	0.103	0.102	0.097	0.092	0.085	0.082	0.079	0.070	0.067	0.064	0.050	0.043	0.027	0.026
167.2	0.133	0.132	0.126	0.120	1.113	0.110	0.107	0.098	0.095	0.091	0.075	0.067	0.047	0.045
157.2	0.200	0.198	0.191	0.185	0.177	0.175	0.173	0.163	0.159	0.155	0.134	0.123	0.094	0.091
147.2	0.338	0.335	0.325	0.316	0.310	0.311	0.311	0.300	0.295	0.291	0.261	0.245	0.198	0.196
142.2	1.511	1.492	1.420	1.347	1.251	1.311	1.274	1.144	1.200	1.145	0.926	0.950	0.664	0.255
137.2	1.594	1.574	1.501	1.425	1.328	1.429	1.393	1.258	1.341	1.285	1.053	1.110	0.805	0.294
127.2	1.735	1.714	1.637	1.559	1.459	1.648	1.612	1.471	1.611	1.551	1.299	1.421	1.079	0.360
117.2	1.853	1.832	1.753	1.673	1.572	1.842	1.807	1.662	1.853	1.790	1.521	1.702	1.328	0.414
107.2	1.938	1.916	1.835	1.754	1.653	1.983	1.949	1.800	2.030	1.964	1.682	1.909	1.510	0.451
94.7	1.976	1.954	1.872	1.791	1.689	2.048	2.014	1.863	2.111	2.044	1.757	2.004	1.594	0.468
82.2	1.938	1.916	1.835	1.754	1.653	1.983	1.949	1.800	2.030	1.964	1.682	1.909	1.510	0.451
72.2	1.853	1.832	1.753	1.673	1.572	1.842	1.807	1.662	1.853	1.790	1.521	1.702	1.328	0.414
62.2	1.735	1.714	1.637	1.559	1.459	1.648	1.612	1.471	1.611	1.551	1.299	1.421	1.079	0.360
52.2	1.594	1.574	1.501	1.425	1.328	1.429	1.393	1.258	1.341	1.285	1.053	1.110	0.805	0.294
47.2	1.511	1.492	1.420	1.347	1.251	1.311	1.274	1.144	1.200	1.145	0.926	0.950	0.664	0.255
42.2	0.338	0.335	0.325	0.316	0.310	0.311	0.311	0.300	0.295	0.291	0.261	0.245	0.198	0.196
32.2	0.200	0.198	0.191	0.185	0.177	0.175	0.173	0.163	0.159	0.155	0.134	0.123	0.094	0.091
22.2	0.133	0.132	0.126	0.120	0.113	0.110	0.107	0.098	0.095	0.091	0.075	0.067	0.047	0.045
12.2	0.103	0.102	0.097	0.092	0.085	0.082	0.079	0.070	0.067	0.064	0.050	0.043	0.027	0.026
2.2	0.093	0.092	0.088	0.083	0.076	0.073	0.069	0.060	0.057	0.054	0.041	0.034	0.020	0.018
0	0	0	0	0	0	0	0	0	0	0	0	0	0	0

7. REACTOR KINETICS

7.1. POINT KINETICS

Point kinetics represent the simplest and most direct approach for the study of reactor transients. Although dimensional kinetics may be desirable or even required for some types of transients, most dynamic problems in fast-reactor physics are amenable to the zero-dimensional, and one-energy-group, treatment of point kinetics. The validity of point kinetics depends in part on an accurate determination of the effective delayed neutron fraction, and to a much smaller extent of the prompt neutron lifetime. These two topics are discussed below.

7.1.1. Prompt Neutron Lifetime

The prompt neutron lifetime, which is defined by Henry (Ref. 69) as

$$\ell = \frac{1}{F} \int_V \int_u \frac{1}{v} \phi(r,u)\ \phi^*(r,u)\ dVdu \quad , \tag{7-1}$$

was calculated by an explicit integration of the two-dimensional r-z direct and adjoint fluxes in ten lethargy groups, according to Eq. (7-1). In this equation, F is a normalization factor that represents the integrated importance of all neutrons born in the reactor, V is the reactor volume, u is the lethargy, v is the associated neutron velocity, r is the position index, and $\phi(r,u)$ is the adjoint flux. The ten-group averaged (1/V) values were obtained from a GGC-5 spectrum calculation for the average reactor composition. The prompt neutron lifetime was found to have a value of 4.3×10^{-7} sec.

7.1.2. Effective Delayed Neutron Fraction

The effective delayed neutron fraction for the delayed group i is given by

$$\bar{\beta}_i = \frac{1}{F} \int_V \int_u \int_{u'} \lambda_o \sum_j \beta_i^j f_i(u) \nu^j(u') \Sigma_f^j(r,u') \phi_o^*(r,u) \phi(r,u') dV du du' , \quad (7\text{-}2)$$

where λ_o is the reactor multiplication factor, β_i^j is the delayed neutron fraction in delayed group i for nuclide j (discussed in Section 4.6), and $f_i(u)$ is the normalized fission spectrum for delayed group i (the same fission spectra, given in Table 4.17, are assumed for all fissionable nuclides j).

The calculations of the β_i's were performed with a two-dimensional r-z perturbation code that allows the explicit integration of Eq. (7-2) on the basis of precomputed direct and adjoint fluxes, in ten-energy groups.

Because of the hard GCFR spectrum, a sizable fraction of all fissions comes from U-238. The average delayed neutron fraction is thereby significantly increased over that for plutonium alone. As shown in Table 7.1, more than 12% of all reactor fissions are indeed produced by U-238 in a fresh core and blanket.

TABLE 7.1

FRACTIONAL REACTOR FISSION RATES

U-235	2.2%	Pu-239.	77.5%
U-238	12.4%	Pu-240.	3.4%
		Pu-241.	4.1%
		Pu-242.	0.4%

The average delayed neutron fraction β_i is simply the sum over the fissionable nuclides of the delayed neutron contribution β_i^j of nuclide j

weighted by the fractional fission rate of that nuclide. The ratio of $\bar{\beta}_i$ to β_i is called the effectiveness and is shown in Table 7.2 for the six delayed neutron groups. Since no fission spectrum is available for groups 5 and 6, the effectiveness for those groups has been computed with the spectrum of group 2 or 4.

TABLE 7.2

DELAYED NEUTRON EFFECTIVENESS

Group i	λ_i
1	0.927
2	0.915
3	0.905
4	0.906
5_2	0.893
5_4	0.901
6_2	0.896
6_4	0.902

These results warrant some comments. Delayed neutrons are not as effective as prompt neutrons because of spectral and spatial effects. The spectral effect is the most important. The softer fission spectrum of delayed neutrons results in an approximately 9% reduction in effectiveness, since these neutrons are less likely to produce fast fissions in U-238. Spatial effects are caused by the presence at different positions in the reactor of nuclides having different contributions in delayed neutrons. While these spatial effects are less important than the spectral effects, the results of Table 7.2 show that they spread over a range of about 4%.

In particular, consider the fact that λ_i decreases when going from group 1 to 4. Yet, as shown in Table 4.17, group 4 has a much harder fission spectrum than group 1 (four times more fissions above the U-238 threshold). Therefore, one would expect to have $\lambda_4 > \lambda_1$. A detailed analysis of spatial fission distributions reveals that 14% of all group

4 delayed neutrons are born in the blanket, as opposed to only 6% in group 1. It follows that group 4 delayed neutrons have a smaller spatial effectiveness because of those neutrons born in the blanket (higher leakage probability, no plutonium present). However, this is more than offset by the larger group 4 spectral effectiveness.

The same kind of explanation holds for the difference between λ_2 and λ_{5_2}, for example. In that case, the spatial effects are isolated since both effectivenesses are based on the group 2 fission spectrum. Eight percent of all group 2 delayed neutrons are born in the blanket, as opposed to 17% for group 5. These 17% have a much lower probability of producing further fissions; therefore, $\lambda_{5_2} < \lambda_2$ in spite of the identical spectrum. Spatial effects also explain some other relationships. For example, $\lambda_{5_2} \cong \lambda_{6_2}$ and $\lambda_{5_4} \cong \lambda_{6_4}$ because $\beta_5^{238}/\beta_5^{239} = \beta_6^{238}/\beta_6^{239}$ with 17% of group 6 delayed neutrons born in the blanket, just as for group 5. Furthermore, λ_{5_4} is not as small in comparison with λ_4, as is λ_{5_2} in comparison with λ_2, because the difference in the fraction born in the blanket is not as large, i.e., 17% versus 14% instead of 17% versus 8%.

On the other hand, the uncertainty arising from the unknown fission spectra of group 5 and 6 is seen to have very little influence on the effectiveness.

Table 7.3 summarizes the results for the average and effective delayed neutron fractions for the GCFR demonstration plant.

For most purposes, a single effectiveness is sufficiently accurate for subsequent kinetics analyses. Almost all the correction is then accounted for by spectral effects. Spatial effects for the different delayed groups compensate each other and do not greatly influence such an average effectiveness.

TABLE 7.3

AVERAGE AND EFFECTIVE DELAYED FRACTIONS

Group	Average Fraction	Effectiveness	Effective Fraction
1	0.096×10^{-3}	0.927	0.089×10^{-3}
2	0.806×10^{-3}	0.915	0.737×10^{-3}
3	0.717×10^{-3}	0.905	0.649×10^{-3}
4	1.406×10^{-3}	0.906	1.273×10^{-3}
5	0.642×10^{-3}	0.893	0.573
6	0.205×10^{-3}	0.896	0.184
Total	3.872×10^{-3}	0.906	3.505×10^{-3}

7.1.3. Point Kinetics Calculations

All point kinetics calculations were performed with the code BLOOST (see Appendix B). This code combines a point kinetics model for the power behavior with a two-dimensional heat transfer model of the average fuel rod, whose temperature changes determine fuel, cladding, and coolant reactivity feedbacks.

An extensive safety analysis of the GCFR demonstration plant has recently been completed. This analysis covers control rod withdrawal accidents, coolant blockage accidents, depressurization accidents, and seismically induced reactivity and power transients. The kinetics part of these calculations have been performed with BLOOST, or simplified versions of this code.

Only slow reactivity insertions will be discussed here. Such insertions are unlikely but possible during reactor operation. They may result, for example, from an uncontrolled movement of control rods. Scram settings must be adequate to prevent fuel melting if such a reactivity insertion should occur.

The reactor is assumed to operate at full power. The maximum fuel temperature is then 2240°C, that is, 540°C below the melting temperature of 2750°C. Ramp rates of $0.4/sec, $1/sec, and $10/sec were investigated, although $0.4/sec is the maximum that can be expected from the limited control rod velocity (25 cm/min). The corresponding times to reach 110% of operating power, 115% of operating power, and the melting temperature near the fuel center line of the hottest rod are shown in Table 7.4.

TABLE 7.4

TIME TO REACH 10% OVERPOWER, 15% OVERPOWER, AND MELTING IN HOTTEST FUEL ROD

Reactivity Insertion ($/sec)	Time (sec)		
	110%	115%	Melting
0.4	29	43	77
1	11	17	33
10	0.9	1.3	5.1

Note: Doppler constant $T\delta k/k\delta T = -0.0042$.

With a 115% scram setting and a scram interval of 0.25 sec, it is seen that there is ample time to prevent fuel melting even for an uncontrolled insertion of a full control rod bank (i.e., a total of $2.4/sec for six rods).

7.2. STABILITY ANALYSIS

The stability of the GCFR demonstration plant was investigated as a function of reactivity temperature coefficients of the fuel, cladding, and coolant. Point kinetics was used and nonlinear effects were neglected.

The method of analysis is based on the point kinetics equations involving the power and six delayed neutron groups. The analysis considers the average core element, which is divided in three axial zones (for the core section of the fuel element only) and three radial zones (fuel, cladding, and coolant). With regard to feedbacks, the Doppler contribution

is weighted axially according to the flux-adjoint flux product, the cladding contribution is uniformly weighted, and the coolant contribution is weighted with coefficients obtained from two-dimensional r-z calculations. Furthermore, the coolant inlet temperature stays constant in time.

The equations of state are linearized and expressed in matrix form. The eigenvalues of the stability matrix as functions of the reactivity coefficients are then determined with the code GASA (see Appendix B).

The results show that the GCFR demonstration plant is stable even if the reactivity coefficients exceed their estimated uncertainty limits. It was found that the boundary between the stable and unstable regions could be represented by a simple equation which is linear in the reactivity coefficients:

$$\alpha_h + 6.09\ \alpha_f + 1.82\ \alpha_c = 0\ . \qquad (7\text{-}3)$$

A negative left-hand side in Eq. (7-3) indicates stability and a positive left-hand indicates instability. In this equation, α_h is the coolant temperature coefficient, α_f is the fuel coefficient, and α_c is the cladding coefficient. From Section 6, at operating conditions these coefficients have the following values:

$$\alpha_h = +2.0 \times 10^{-6} \pm 30\%\ (\Delta k/k/°C)$$
$$\alpha_f = -3.2 \times 10^{-6} \pm 30\%\ (\Delta k/k/°C)$$
$$\alpha_c = -4.2 \times 10^{-6} \pm 20\%\ (\Delta k/k/°C)$$

The stability point corresponding to such values is shown on the stability map in Fig. 7.1. The operating point and its associated uncertainty region lie well within the area of stability. If two of the reactivity coefficients stay within their uncertainty limits, the third coefficient must satisfy the following broad conditions in order to preserve stability; the Doppler coefficient may not be positive, the

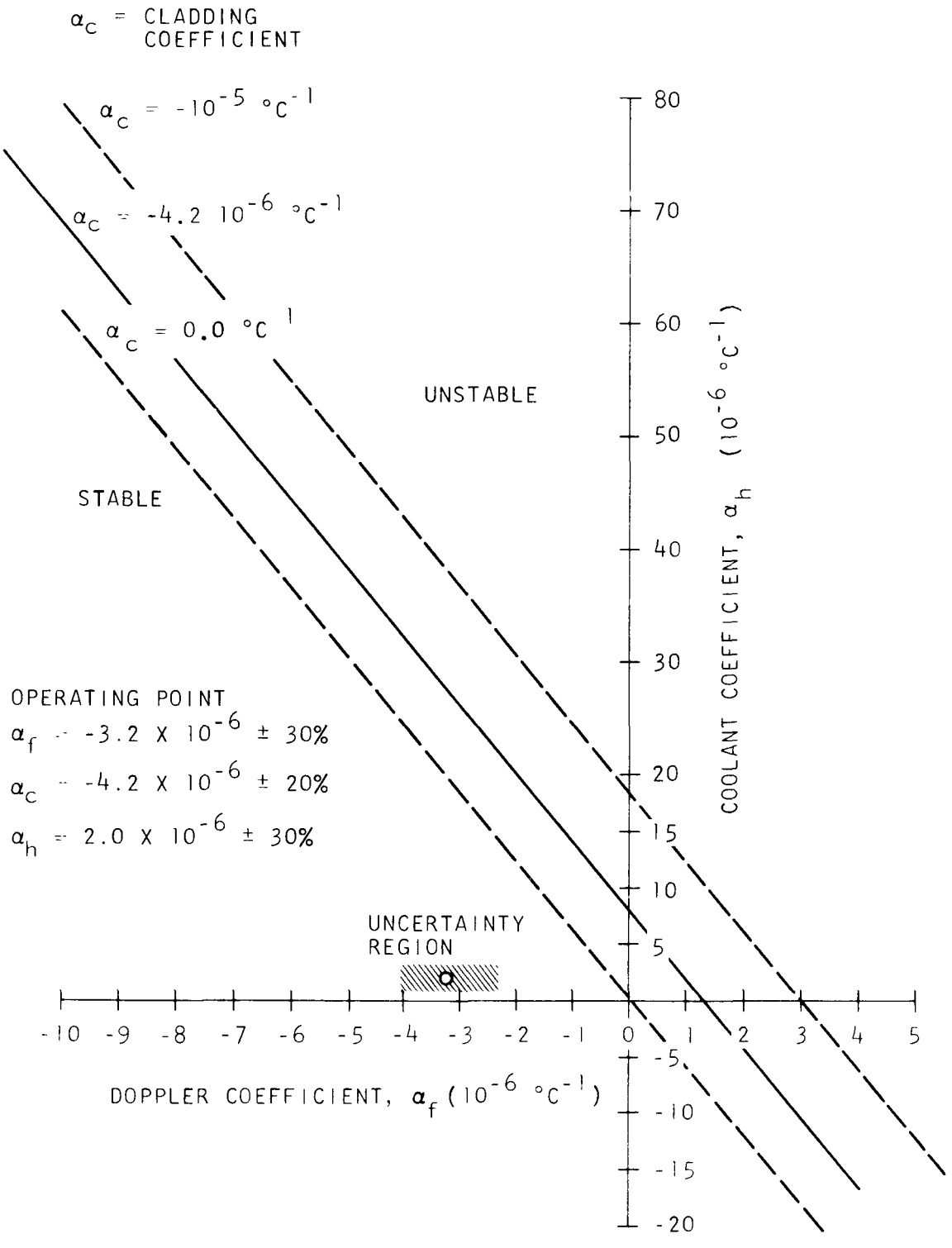

Fig. 7.1. Stability map for the GCFR demonstration plant

cladding coefficient may not be strongly positive, and the coolant coefficient may not be larger than ten times its value at the operating point. These conditions are readily satisfied, and reactor stability in therefore ensured.

7.3. TWO-DIMENSIONAL KINETICS

An exact treatment of the kinetic behavior of a reactor requires a multigroup, dimensional treatment. Until recently (Ref. 70), such an approach was prohibitive with regard to computing time and there were difficulties in obtaining computational stability with time-saving, time-step adjusting schemes. Besides, point kinetics is a reliable tool for predicting transients in a generally well-coupled fast reactor, at least as long as there are no structural changes.

However, as fast-reactor safety analysis becomes more sophisticated, there is a need to treat more accurately the neutronic reactor behavior in severe accidents involving fuel relocation, cladding removal, cooling perturbations, and possibly core slumping.

A one-dimensional, multigroup kinetics code, GAKIT, is in use at Gulf General Atomic. GAKIT (see Appendix B) can handle up to 10 energy groups and six delayed neutron groups. It incorporates a heat transfer model which yields the appropriate temperature feedbacks. GAKIT has been used to investigate one aspect of multigroup kinetics, namely the number of groups that is required to obtain accurate results. Recent publications (Refs. 71, 72) have suggested that the asymptotic periods produced by step insertions of reactivity with no feedback can differ by large amounts in fast-reactor problems, depending on the number of groups used. For example, a fast reactor case with four groups was found to have an asymptotic period 31% greater than that calculated for an otherwise identical 16-group case. Such a discrepancy had been observed in essentially zero-dimensional calculations, which can be compared with conventional point kinetics results.

A pseudo zero-dimensional problem involving a slab with the average material composition of the GCFR demonstration plant was therefore studied. The number of energy groups was varied between two and 10, and reactivity step insertions of $10 and $50 were considered. The principal conclusion reached is that few-group calculations yield excellent agreement with many-group calculations if proper attention is given to the evaluation of group-dependent effective delayed neutron fractions and if input reactivity is the same. Essentially identical results were obtained with 10, four-, and two-group GAKIT calculations and with BLOOST point kinetics calculations.

When a large number of groups is used, the difference in fission spectrum between prompt neutrons and delayed neutrons is properly taken into account by the five-group structure and the multigroup treatment. In that case, the delayed neutron fractions supplied in the input should refer to the average value (column 2 of Table 7.3), without effectiveness correction. At the other extreme, when only one energy group is used, the spectral difference between prompt and delayed neutrons can be accounted for only by means of the effective delayed neutron fractions, which includes a spectral and spatial correction. The same argument holds for material perturbations: with a space-dependent solution in many energy groups, changes in macroscopic capture or fission cross sections can be specified directly according to group and location; with a one-group, zero-dimensional solution, the reactivity equivalent of such perturbations must be computed beforehand.

For an intermediate number of energy groups, it is necessary to use appropriate effective delayed neutron fractions, which depend on the group structure, in order to compensate for the loss of detail in the delayed source spectrum. The importance of delayed neutrons varies significantly depending on whether they are born above or below the U-238 fission threshold. The effectiveness was calculated for each group structure by the standard method of computing the reactivity difference between the reference case and a case in which the fission spectrum is augmented by the amount β

properly distributed in energy. (A direct integration of Eq. (7-2) with a perturbation code, as mentioned in Section 7.1.2, could also have been done. In that case, uncorrected β_i^j should be used, together with the delayed spectrum $f_i(u)$ distributed on the few-group structure.) A different effective delayed neutron fraction was thus obtained for two, four, and 10 groups. The effective β calculated from the 10-group case would be used directly in a point kinetics code such as BLOOST, which has no capability of representing energy-dependent effects. For a two- or four-group GAKIT calculation, the basic delayed fraction is modified by the ratio of the 10-group and few-group effectivenesses. A similar procedure is used to correct, in terms of reactivity, the capture or fission perturbation introduced into the reactor.

ACKNOWLEDGMENTS

The original work on the physics of the Gas-Cooled Fast Breeder Reactor (GCFR) was carried out by Raymond Shanstrom, who established the feasibility of the GCFR concept in association with Peter Fortescue. Later contributors to the field included Alan Baxter, Jeffrey Broido, and John Peak.

This report presents new work and a revision of prior work that reflect the progress accomplished during the last two years. The report incorporates the contributions of several individuals, including, among others, Michael Rothstein, Donald Mathews, Meldon Merrill, William Davison, and Claude Maeder.

The author also wishes to acknowledge the active collaboration of Jeffrey Broido during the final preparation and review.

APPENDIX A

ONE-GROUP REACTOR MODEL

Many fast-reactor parameters can be evaluated from a one-group model, a fact that is particularly true for the GCFR. This appendix presents some simple relationships involving the average core enrichment, conversion ratio, reactivity drop, and zone enrichments.

A.1. DERIVATION OF FORMULAS FOR REACTIVITY DROP

The reactivity drop during burnup is due mainly to the loss of fissile material in the core and gain in the blanket, and accumulation of fission products. In first approximation, these three components are additive and they can be derived from a one-group model.

A.1.1. Reactivity Loss due to Fissile Depletion in the Core

Consider core burnup during a period of T days. With fuel defined as fissile plus fertile materials, one has the following fundamental parameters:

a	kg fissile produced per initial kg of fuel
b	kg fissile destroyed (capture + fission) per initial kg of fuel
C	core conversion ratio, initial
S	fissile specific power [Mw(th)/kg fissile] (core power only)
S'	fuel specific power [Mw(th/kg fuel] (core power only)
e	core initial fissile enrichment (fraction)
β	ratio of final core fissile weight to initial core fissile weight
DIFA	destructions per initial fissile atom $\cong$ kg fissile destroyed per initial kg fissile

These quantities are related by the following formulas:

$S' = Se$ $\qquad C = a/b$ $\qquad DIFA = b/e$

The conservation of fissile material, $\beta e - e = a - b$, leads to

$$\beta \cong 1 - DIFA(1 - C) \ . \qquad \text{(A-1)}$$

On the other hand, the quantity b is given by the expression $b = 24\ TS'/E_9$, where the numerator represents the total energy produced by 1 kg of fuel and the denominator represents the energy produced by the destruction of 1 kg fissile. The quantity E_9 follows from $E_9 = E_f\zeta/(1 + \alpha)$, where E_f is the fission energy yield ($E_f \cong 24{,}000$ MW-hr/kg fissioned); α is the capture-to-fission ratio ($\alpha \cong 0.19$ in the GCFR spectrum); and ζ is the fast fission factor, that is, the total kg fissioned (fertile and fissile) per kg fissile fissioned ($\zeta_{core} \cong 1.17$ in a GCFR spectrum). It then follows that

$$\beta \cong 1 - 0.001\ TS\ (1 - \bar{C}) \ . \qquad \text{(A-2)}$$

The core conversion ratio can be evaluated from a one-group, zero-dimensional expression:

$$C = \frac{N_{238}\,\sigma_{c8} + N_{240}\,\sigma_{co}}{N_{239}\,\sigma_{a9} + N_{241}\,\sigma_{a1}} = \frac{N_{238}\,\sigma_{c8} + \gamma_o N_{pu}\,\sigma_{co}}{\gamma_9\,N_{pu}\sigma_{a9} + \gamma_1 N_{pu}\,\sigma_{a1}} \ ,$$

$$C = \frac{(N_u/N_{pu})\sigma_{c8} + \gamma_o\sigma_{co}}{\gamma_9\sigma_{a9} + \gamma_1\sigma_{a1}} \ .$$

Assuming the standard GCFR isotopic composition for plutonium (i.e., $\gamma_9 = 0.8$, $\gamma_o = 0.155$, and $\gamma_1 = 0.025$) and the demonstration plant one-group cross sections corresponding to the standard, basic data of Section 4 ($\sigma_{c8} = 0.257$ barn, $\sigma_{c8} = 4.68$ barns, $\sigma_{a9} = 2.00$ barns, $\sigma_{a1} = 3.11$ barns), one then has

$$C = 0.1533\ (N_u/N_{pu}) + 0.043 \ .$$

With the enrichment defined as $e = (N_{239}+N_{241})/(N_u+N_{pu})$, one obtains $(N_u/N_{pu}) = (\gamma_9 + \gamma_1)/e-1$ and finally

$$C = \frac{0.1265}{e} - 0.110 \ . \qquad \text{(A-3)}$$

For both demonstration and 1000-MW(e) plants, Eq. (A-3) predicts the conversion ratio with an accuracy better than 2% for C between 0.4 and ∿1.0, as shown in Table A.1.

The reactivity loss due to fissile depletion depends on the fractional loss $(1 - \beta)$ in initial fissile loading. The fractional loss is given by $0.001\ TS(1 - \bar{C})$, from Eq. (A-2), where $\bar{C}$ is now the average of the initial conversion ratio (dependent on e) and the final conversion ratio (dependent on the reduced enrichment βe). Replacing in Eq. (A-3) and then solving for $(1-\beta)$ leads to

$$(1 - \beta) = \frac{1.11\ 10^{-3}\ TS\ (1 - 0.114/e)}{1 + 6.3x10^{-5}\ TS/e} \ . \qquad \text{(A-4)}$$

As seen in Table A.2, this expression predicts the fissile loss with an error smaller than about 10%, except for cores with conversion ratios close to 1.0. This expression is therefore quite accurate for partial reloading schemes.

For cases of practical interest the denominator in Eq. (A-4) varies by only a few percent about the value of 1.05. For the present purpose, Eq. (A-4) can then be simplified to the more convenient linear form:

$$(1 - \beta) \cong 0.001\ TS(1 - 0.114/e) \ . \qquad \text{(A-5)}$$

The reactivity drop corresponding to the fractional fissile loss $(1 - \beta)$ may be evaluated with the help of the influence coefficients derived for the demonstration and 1000-MW(e) plants (Ref. 6, p. 51).

TABLE A.1

CORE CONVERSION RATIOS

Case	Enrichment	Multigroup	Eq.(A-3)
1000 MW(e) - Zone 1	0.122	0.925	0.92
1000 MW(e) - Zone 2	0.136	0.817	0.82
1000 MW(e) - Zone 3	0.161	0.679	0.68
1000 MW(e) - Zone 4	0.230	0.449	0.45
Demonstration plant	0.18	0.595	0.60
Demonstration plant	0.145	---	0.76
1000 MW(e)	0.112	∿1.0	1.02

TABLE A.2

FRACTIONAL LOSS IN CORE FISSILE LOADING

Case	T (days)	S (Mw(th)/kg)	e	Loss	
				Multigroup	Eq.(A-4)
1000 MW(e) (partial reloading)	150	1.15	0.158	0.048	0.050
Demonstration plant	250	0.57	0.180	0.055	0.055
1000 MW(e)	1000	0.76	0.112	0.056	∿0.005
Demonstration plant	300	0.53	0.145	0.031	0.035

A change of 1% in total fissile loading results in a 0.66% change in reactivity. It follows that the reactivity loss corresponding to fissile depletion is given by

$$R_{depletion} = 6.6 \cdot 10^{-4} \text{ TS } \left(1 - \frac{0.114}{e}\right) \qquad (\Delta\rho) \ . \qquad \text{(A-6)}$$

A.1.2. Reactivity Gain due to Fissile Buildup in the Blanket

The buildup of fissile materials in the blanket increases reactivity. Let β' be the ratio of final reactor (core + blanket) fissile weight. With the same kind of simplifying assumptions as before, one has from Eq.(A-2)

$$\beta' = 1 + 0.001 \text{ TS } (BR - 1) \ , \qquad \text{(A-7)}$$

where BR is the reactor breeding ratio.

In units of critical mass, the total fissile gain is $(\beta' - 1)$ and the loss in the core is $(1 - \beta)$ during the burnup interval T. Therefore, the gain in the blanket amounts to $(\beta' - \beta) = 0.001 \text{ TS } (BR - \bar{C})$. In first approximation, the reactivity gain should be proportional to $(\beta' - \beta)$. Calculations on the worth of fuel elements added to the core periphery have shown that adding 1% of the critical mass at the core periphery increases reactivity by about 0.2%. Since much of the blanket plutonium is produced very close to the core, this value should be acceptable for the bred plutonium. Therefore,

$$R_{buildup} = -2 \times 10^{-4} \text{ TS } (BR - \bar{C}) \qquad (\Delta\rho) \ . \qquad \text{(A-8)}$$

Here, BR must be known beforehand, and it is sufficient to evaluate $\bar{C}$ by Eq.(A-3)on the basis of initial enrichment alone.

A.1.3. Reactivity Loss in the Core due to Fission Products

The reactivity loss due to fission product accumulation is in first approximation proportional to the irradiation time T and the core specific power. The proportionality factor is readily derived from the neutron balance of any burnup calculation of the demonstration or 1000-MW(e) plants. On the basis of one-group theory, the reactivity loss due to an absorption fraction f is simply f/k_∞. Then the proportionality constant follows:

$$R_{fp} = 9 \cdot 10^{-5}\ TS \qquad (\Delta\rho) \quad . \qquad \text{(A-9)}$$

A.1.4. Overall Reactivity Drop

Combining Eqs. (A-3), (A-6), (A-8), and (A-9), one obtains the following equation for the total reactivity drop:

$$R = 10^{-4} TS \left(7.3 - 2BR - \frac{0.5}{e} \right) \qquad (\Delta\rho) \quad . \qquad \text{(A-10)}$$

As seen in Table A.3, Eq. (A-10) gives good first-order approximation to the reactivity drop during burnup.

TABLE A.3

REACTIVITY DROP DURING BURNUP

Case	T (days)	S MW(th) (core) / kg fiss(core)	e	BR	Reactivity Loss (Δρ)	
					Multigroup	Eq. (A-10)
1000 MW(e) (partial reload)	150	1.15	0.158	1.50	0.021	0.020
Demonstration	250	0.57	0.180	1.33	0.027	0.027
Demonstration	300	0.53	0.145	1.48	0.012	0.014

It is helpful to relate the reactivity swing to average burnup B and number of cycles n, each of length T full power days, during the life of a fuel element. The average core burnup is given by

$$B = 1000\ nTSe \text{ MWd/Te fuel} .$$

If the total allowable burnup B is specified, then TS = B/(1000 ne) and

$$R = \frac{B}{ne}\left(7.3 - 2BR - \frac{0.5}{e}\ 10^{-7}\right) \quad (\Delta\rho) \quad . \qquad \text{(A-11)}$$

Figure A.1 shows the general dependence of the reactivity loss on the enrichment for various cycle numbers and for values of BR and B typical of a 1000-MW(e) GCFR (i.e., BR = 1.50 and B = 70,000 MWd/Te).

Reactivities are converted to dollars by dividing $R(\Delta\rho)$ by the effective delayed neutron fraction, which is equal to 0.0035 for the GCFR demonstration plant. This same value can also be used for a 1000-MW(e) plant, since the effect of the softer spectrum tends to compensate for the larger fertile concentration.

Furthermore, the elapsed fuel lifetime T_L at load factor L is given by

$$T_L = \frac{B}{1000\ SeL} \text{ days} .$$

Equation (A-11) can also be solved for the enrichment:

$$e = \frac{1.43\ 10^{-5}\ B}{nR'}\left[7.3 - 2BR + \sqrt{(7.3 - 2BR)^2 - 7nR'\ 10^4/B}\right] . \qquad \text{(A-12)}$$

Once reactivity loss per cycle, average burnup, and cycle number have been selected, Eq. (A-12) yields the required average core enrichment e. The mean fissile density p in the fuel material is then given by

$$\rho = \frac{0.040631\ tbc}{(\gamma/e) - 1 + 0.0035454\ (c + 32)} , \qquad \text{(A-13)}$$

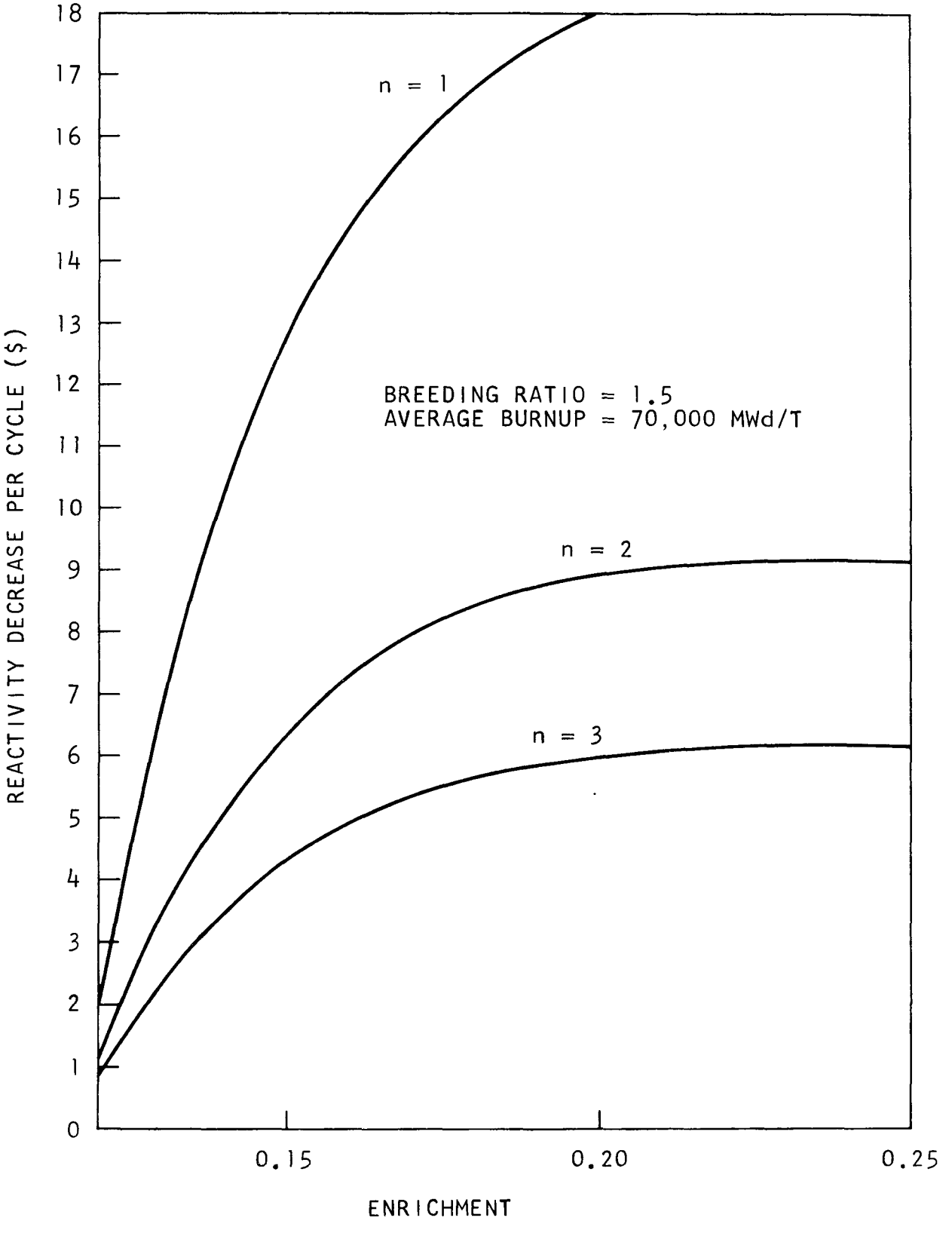

Fig. A.1. Reactivity drop over the cycle, for various cycle numbers, versus core enrichment

where t is the fraction of theoretical density for UO_2 and PuO_2 powder, γ is the fissile isotopic fraction (i.e., $\gamma_{239} + \gamma_{241}$), c is the mean plutonium atomic weight (i.e. $\sum_i i\gamma_i$, i = 239, 240, 241, 242), and b is the fissile weight fraction [i.e., $(239\gamma_{239} + 241\gamma_{241})/c$]. However, the dependence of ρ on the plutonium isotopic composition is weak. Using typical values for the isotopic composition and neglecting the sum of the second and third term in the denominator yields the more convenient expression

$$\rho = 9.72\ te\ ,$$

which is generally better than 2% accurate.

A.2. ZONE FISSILE LOADING

In order to achieve some kind of power flattening, the core is divided in several radial zones having different fissile enrichments. The accepted cirterion stipulates that the peaks of all zones should be equal.

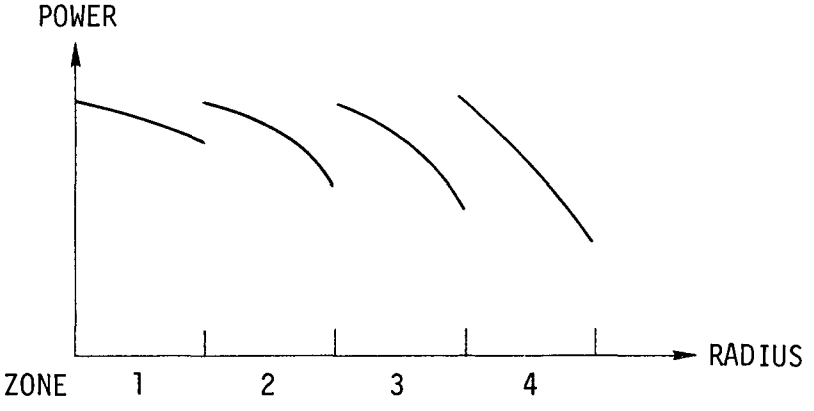

It is therefore necessary to find the relative fissile density $\rho_i/\rho = e_i/e$ for every zone on the basis of zone fractional volumes.

The core is divided into N zones, each zone having a fractional core volume V_i ($\Sigma_i V_i = 1$). A quantity x_i is therefore defined as

$$x_i = \sum_{j=1}^{i-1} v_j \quad , \tag{A-14}$$

with $x_1 = 0$.

Assume a one-group model for the neutral population. The power level at a radial position r is then proportional to the local flux and local enrichment:

$$P(r) \alpha e(r) \cdot \phi(r) \quad . \tag{A-15}$$

If the core had a uniform enrichment, the flux distribution would be $\phi_u(r)$. Equation (A-15) may be rewritten as

$$P(r) \alpha e(r) \frac{\phi(r)}{\phi_u(r)} \cdot \phi_u(r) \quad . \tag{A-16}$$

The analysis of many computer flux diffusion calculations reveals that the following approximation is generally valid:

$$\frac{\phi(r)}{\phi_u(r)} \alpha [e(r)]^{1.5} \quad . \tag{A-17}$$

Equation (A-16) now becomes

$$P(r) \alpha [e(r)]^{2.5} \cdot \phi_u(r) \quad . \tag{A-18}$$

The flux $\phi_u(r)$ is basically a J_o function with a proper extrapolation distance. It turns out that it is quite acceptable to approximate the J_o function by a parabola. Then

$$P(x) \alpha [e(x)]^{2.5} (1 - 0.98\, x) \quad , \tag{A-19}$$

where $x = (r/R_c)^2$ with R_c being the core radius.

The requirement of equal zone peaks then corresponds to

$$P(x_1) = P(x_2) = ... = P(x_N) \quad . \tag{A-20}$$

If the enrichment in the first zone is normalized to 1.0, then

$$e'_i = (1 - 0.98\ x_i)^{-0.4} \quad , \qquad i = 1,N$$

and the average core enrichment is

$$e' = \sum_j^N V_j\ (1 - 0.98\ x_j)^{-0.4} \quad .$$

Therefore, the fractional zone enrichment is given by

$$\frac{e_i}{e} = \frac{(1 - 0.98\ x_i)^{-0.4}}{\sum_j^N V_j\ (1 - 0.98\ x_j)^{-0.4}} \quad , \qquad i = 1,N \quad . \tag{A-21}$$

Table A.4 shows how the fractional enrichments obtained from Eq.(A-21) compare with the multigroup diffusion solution in the case of a 1000-MW(e) GCFR. Table A.5 makes the same comparison for the demonstration plant.

If the fractional zone enrichments of Tables A.4 and A.5 were used in a multigroup dimensional calculation, the peak would be slightly higher in the outer zones than in the inner zones for all fresh fuel. During the equilibrium cycle, the power tends to shift toward the center because of fissile conversion. To a certain extent, Eq.(A-21) therefore includes a systematic bias, which then tends to yield "flat peaks" at mid-cycle.

TABLE A-4

FRACTIONAL ZONE ENRICHMENT FOR 1000-MW(e) PLANT

Zone	V_i	x_i	Fractional Enrichment	
			Multigroup	Approx. Eq. (A-21)
1	0.25	0.0	0.77	0.77
2	0.24	0.25	0.86	0.87
3	0.32	0.49	1.02	1.01
4	0.19	0.81	1.45	1.46

TABLE A-5

FRACTIONAL ZONE ENRICHMENT FOR DEMONSTRATION PLANT

Zone	V_i	x_i	Fractional Enrichment	
			Multigroup	Approx. Eq. (A-21)
1	0.263	0.0	0.80	0.79
2	0.203	0.263	0.94	0.89
3	0.254	0.466	1.03	1.00
4	0.280	0.720	1.20	1.28

APPENDIX B
CODE ABSTRACTS

THIS PAGE IS BLANK

1. NAME OF CODE - BLOOST-7

2. COMPUTER FOR WHICH CODE IS DESIGNED - UNIVAC 1108

3. NATURE OF PHYSICAL PROBLEM SOLVED - BLOOST-7 COMBINES A SPACE-INDEPENDENT REACTOR KINETICS CODE WITH A VERSION OF THE TAC-2D TRANSIENT HEAT TRANSFER CODE. FEEDBACK MODELS ARE PROVIDED FOR BOTH HTGR AND GCFR PROBLEMS BASED ON TEMPERATURE CHANGES IN A SINGLE AVERAGE FUEL ELEMENT. THE CAPABILITY TO STUDY THE TEMPERATURE BEHAVIOR IN NON-AVERAGE ELEMENTS IS ALSO PROVIDED.

4. METHOD OF SOLUTION - A FOURTH ORDER RUNGE-KUTTA INTEGRATION IS USED FOR THE KINETICS EQUATION. A PEACEMAN-RACHFORD ITERATION SCHEME IS EMPLOYED TO SOLVE THE TWO-DIMENSIONAL TIME-DEPENDENT HEAT CONDUCTION EQUATION IN R-Z GEOMETRY.

5. RESTRICTIONS ON THE COMPLEXITY OF THE PROBLEM - TWO DIMENSIONAL HEAT-TRANSFER ROUTINES ARE LIMITED TO RZ GEOMETRY, 36 REGIONS, 15 MATERIALS, 15 RADIAL MESH POINTS, 40 AXIAL MESH POINTS, 6 RADIAL REGION BOUNDARIES, 10 AXIAL REGION BOUNDARIES, AND INNER AND OUTER AXIAL COOLANTS. KINETICS EQUATIONS ALLOW 6 DELAYED GROUPS.

6. TYPICAL RUNNING TIME - BEING A KINETICS CODE THE TYPICAL RUNNING TIME IS DEPENDENT UPON THE TIME THAT THE REACTOR BEHAVIOR IS FOLLOWED. THE AMOUNT OF OUTPUT INFORMATION REQUESTED ALSO HAS AN INFLUENCE. MOST PRACTICAL PROBLEMS ARE RUN IN A FEW MINUTES.

7. UNUSUAL FEATURES OF THE PROGRAM - THE MATERIAL, GAS, AND COOLANT PROPERTIES AND HEAT GENERATION RATES ARE SUPPLIED AS FORTRAN ARITHMETIC STATEMENT FUNCTIONS. THIS SUBROUTINE IS THEREFORE UNIQUE TO A PARTICULAR FUEL ELEMENT DESIGN AND MAY BE CONSIDERED AS PART OF THE INPUT DATA. FOR CASES IN WHICH THE INITIAL TEMPERATURE DISTRIBUTION IS UNKNOWN IT IS POSSIBLE TO RUN THE BLOOST CODE AS A PURE HEAT-TRANSFER CODE OMITTING REACTIVITY INPUT TO THE KINETICS PORTION AND OBTAIN A TEMPERATURE DISTRIBUTION APPROPRIATE TO INITIAL POWER CONDITIONS PUNCHED ON CARDS SUITABLE FOR LATER USE IN KINETICS PROBLEMS.

8. RELATED AND AUXILIARY PROGRAM - TAC-2D, STAND ALONE VERSION OF THE HEAT TRANSFER CODE. REPORTS GA-8868, GA-9262. BLOOST-6, EARILER VERSION WITH SPECIAL ROUTINES TO TREAT FUEL PARTICLE HEAT TRANSFER IN HTGR. REPORT GA-8416.

9. STATUS - PRODUCTION

10. REFERENCES - M. MERRILL, "BLOOST-7, A REACTOR KINETICS-HEAT TRANSFER PROGRAM FOR THE UNIVAC 1108", GA-9832, JAN 20, 1970.

11. MACHINE REQUIREMENTS - 65K MEMORY

12. PROGRAMMING LANGUAGE USED - FORTRAN IV

13. OPERATING SYSTEM - EXEC II

14. OTHER PROGRAM INFORMATION -

15. AUTHOR OF THE ABSTRACT - M. MERRILL

1. NAME OF CODE - BUGTRI

2. COMPUTER FOR WHICH CODE IS DESIGNED - UNIVAC-1108

3. NATURE OF PHYSICAL PROBLEM SOLVED - THE TWO DIMENSIONAL MULTIGROUP NEUTRON DIFFUSION THEORY EQUATIONS FOR TRIANGULAR GEOMETRY ARE SOLVED TO OBTAIN THE MULTIPLICATION FACTOR AND THE SPATIAL FLUX AND POWER DISTRIBUTIONS. COMPLETE REACTOR LIFE HISTORIES WITH PARTIAL REFUELING AT A NUMBER OF RELOAD TIME POINTS CAN BE CALCULATED. THE DEPLETION SCHEME OF ALL BURNABLE NUCLIDES IS SPECIFIED BY THE USER AT EXECUTION TIME. A REGIONWISE DEPLETION SCHEME IS USED. CONCENTRATION DEPENDENT SELF SHIELDING FACTORS MAY BE APPLIED TO ANY NUCLIDE.

4. METHOD OF SOLUTION - OVER A UNIFORM TRIANGULAR MESH GRID, THE SYSTEM OF DIFFERENCE EQUATIONS FOR THE STEADY-STATE SOLUTION IS SOLVED BY AN EXTENSION OF THE POWER METHOD. A FORM OF SUCCESSIVE LINE OVERRELAXATION IS USED IN EACH GROUP. COARSE MESH REBALANCING IS USED TO IMPROVE PREASYMPTOTIC CONVERGENCE BEHAVIOR AND AN EXPONENTIAL EXTRAPOLATION METHOD IS USED TO IMPROVE ASYMPTOTIC CONVERGENCE BEHAVIOR. FOR DEPLETION, THE CODE DECIDES INTERNALLY (FOR EACH TIME STEP AND EVERY NUCLIDE) WHETHER TO USE EITHER A DIFFERENCE APPROXIMATION OR AN ANALYTIC SOLUTION. A FULL TRIANGULAR DEPLETION MATRIX IS ALLOWED.

5. RESTRICTIONS ON COMPLEXITY OF THE PROBLEM -
   MAXIMUM NUMBER OF GROUPS = 10
   MAXIMUM NUMBER OF SPACE MESH POINTS = 20,000
   MAXIMUM NUMBER OF REGIONS = 255
   MAXIMUM NUMBER OF SUBREGIONS = 300
   MAXIMUM NUMBER OF TOTAL NUCLIDES = 40
   MAXIMUM NUMBER OF HEAVY NUCLIDES = 25
   FISSION PRODUCTS AND OTHER BURNABLE NUCLIDES = 25

6. TYPICAL RUNNING TIME - EIGHT TIME STEPS FOR AN X-Y PROBLEM OF 7400 MESH POINTS COULD TAKE 65 MINUTES FOR FOUR GROUPS AND 155 MINUTES FOR 9 GROUPS.

7. UNUSUAL FEATURES OF THE CODE -

8. RELATED AND AUXILIARY PROGRAM - GAMTRI IS USED FOR THE STEADY STATE SOLUTIONS.

9. STATUS - PRODUCTION

10. REFERENCES - GA-8272

11. MACHINE REQUIREMENTS - 65,536 WORDS OF CORE STORAGE, 2 MILLION WORDS OF DRUM STOARGE ON ONE DATA CHANNEL, 3 TAPE UNITS AND A PERIPHERAL PRINTER.

12. PROGRAMMING LANGUAGE USED - FORTRAN IV IS USED ALONG WITH AN ASSEMBLY LANGUAGE PROGRAM FOR BINARY READS OR WRITES OF DRUM OR TAPE.

13. OPERATING SYSTEM - GULF GENERAL ATOMIC VERSION OF THE UNIVAC 1108 OPERATING SYSTEM ENTITLED EXEC-II, GAX23.

14. OTHER PROGRAM INFORMATION -

15. AUTHOR OF THE ABSTRACT - J. DORSEY

1. NAME OR DESIGNATION OF PROGRAM - GAFGAR

2. COMPUTER FOR WHICH PROGRAM IS DESIGNED AND OTHERS UPON WHICH IT IS OPERABLE - UNIVAC-1108

3. NATURE OF PHYSICAL PROBLEM SOLVED - THE PROBLEM IS TO OBTAIN VERY DETAILED NEUTRON FLUX AND CURRENT DISTRIBUTIONS AS FUNCTIONS OF ENERGY CONSIDERING EXPLICITLY THE POSSIBLE OVERLAP EFFECTS BETWEEN RESONANCES OF A RESONANCE ABSORBER AND OF MIXTURES OF RESONANCE ABSORBERS AND TO USE THESE DISTRIBUTIONS TO PREPARE GROUP-AVERAGED CROSS SECTIONS AND TRANSFER ARRAYS FOR USE IN FAST REACTOR ANALYSES.

4. METHOD OF SOLUTION - THE B1 APPROXIMATION TO THE BOLTZMANN EQUATION IS SOLVED FOR THE NEUTRON FLUX AND CURRENT SPECTRA. THE GAF SECTION USES A LARGE NUMBER OF FINE ENERGY GROUPS TO REPRESENT THE CROSS SECTIONS ABOVE THE RESOLVED RESONANCE REGION. THE GAR SECTION USES A VERY LARGE NUMBER OF DISCRETE VELOCITIES IN THE RESONANCE REGION ALONG WITH SLOWING DOWN SOURCES FROM THE GAF SECTION TO TREAT LEAKAGE-DEPENDENT RESONANCE ABSORPTION MORE RIGOROUSLY THAN PREVIOUS CODES.

5. RESTRICTIONS ON THE COMPLEXITY OF THE PROBLEM - THE MAXIMUM OF 1740 FINE GROUPS IN THE GAF SECTION MAY BE SUBDIVIDED INTO 10 OR LESS SETS OF FINE GROUPS HAVING A CONSTANT LETHARGY WIDTH. THE GAR SECTION REQUIRES A UNIFORM SPACING BETWEEN THE MAXIMUM OF 14,700 DISCRETE VELOCITIES. THE MAXIMUM NUMBER OF NUCLIDES IN A PROBLEM IS 20, AND THE MAXIMUM TOTAL NUMBER OF BROAD GROUPS (OUTPUT FOR NUCLEAR DESIGN CALCULATIONS) IS 99 WITH A MAXIMUM OF 20 BROAD GROUPS IN THE GAR SECTION.

6. TYPICAL RUNNING TIME - 4.6 MINUTES (1.1 MINUTES FOR GAF SECTION AND 3.5 MINUTES FOR GAR SECTION) ARE REQUIRED FOR A TEST PROBLEM INVOLVING HYDROGEN, CARBON, OXYGEN, PU239, AND PU240 WITH 731 FINE GROUPS ABOVE 10 KEV IN THE GAF SECTION (DELTAU=0.01), 12,367 VELOCITIES BELOW 10 KEV IN THE GAR SECTION (DELTAV=110 M/SEC), AND 31 BROAD GROUP OUTPUT (11 IN GAF SECTION AND 20 IN GAR SECTION).

7. UNUSUAL FEATURES OF THE PROGRAM - THE GAF SECTION ALLOWS DOWNSCATTER BY ANY PROCESS (ANISOTROPIC ELASTIC SCATTER, INELASTIC SCATTER, (N,2N) PROCESSES, ETC.) FROM ANY FINE GROUP TO ANY LOWER ENERGY FINE GROUP BECAUSE THE FULL P0 AND P1 TRANSFER ARRAYS ARE USED FOR ALL MATERIALS EXCEPT HYDROGEN WHICH IS ASSUMED TO HAVE ONLY ISOTROPIC IN THE CENTER-OF-MASS SYSTEM ELASTIC SCATTER. DATA COMPRESSION TECHNIQUES ARE USED TO REDUCE THE SIZE OF THE TRANSFER ARRAYS. THE GAR SECTION USES A RECURSIVE SCHEME FOR THE CALCULA-

TION OF THE P0 AND P1 SLOWING DOWN SOURCE TERMS WHICH DECREASES THE RUNNING TIME FOR TYPICAL PROBLEMS BY A FACTOR OF 3 TO 4 WHILE STILL ALLOWING ISOTROPIC IN THE CENTER-OF-MASS SYSTEM ELASTIC SCATTER TO ANY LOWER VELOCITY TO BE TREATED RIGOROUSLY. EITHER POSITIVE OR NEGATIVE BUCKLING CAN BE SPECIFIED FOR EACH BROAD GROUP IN EACH SECTION.

8. RELATED AND AUXILIARY PROGRAMS - CROSS SECTION INPUT FOR THE GAFGAR CODE IS PREPARED BY THE GAND CODE FROM ENDF/B FORMAT NUCLEAR DATA FILE TAPES. DATA ON THE GAFGAR CROSS SECTION TAPES MAY BE PRINTED WITH THE P3T CODE. PROCOP IS USED TO COPY SELECTED PROBLEMS FROM 1 OR 2 GAF AND/OR GAR PROBLEM TAPES OR TO LIST THE PROBLEM TAPES. TAPCOP IS USED TO COPY GAFGAR (PACKED RECORD) DATA TAPES. TAPER IS USED TO MERGE GAF/GAR DATA TAPES.

9. STATUS - PRODUCTION

10. REFERENCES - D. R. MATHEWS AND R. J. ARCHIBALD, GAF, A COMPUTER PROGRAM FOR CALCULATION OF NEUTRON SPECTRA AND AVERAGE CROSS SECTIONS IN THE HIGH ENERGY RANGE, GA-7169, JANUARY 20, 1967.
C. A. STEVENS AND R. J. ARCHIBALD, GAR, A COMPUTER PROGRAM FOR EVALUATING LEAKAGE DEPENDENT RESONANCE ABSORPTION, GA-6952, MARCH 16, 1966.
R. J. ARCHIBALD AND D. R. MATHEWS, THE GAF/GAR/GAND FAST REACTOR CROSS SECTION PREPARATION SYSTEM, GAFGAR - A PROGRAM FOR THE CALCULATION OF NEUTRON SPECTRA AND GROUP-AVERAGED CROSS SECTIONS, GA-7542, VOL. I, JANUARY 22, 1968, AND ERRATA, MAY 1968.

11. MACHINE REQUIREMENTS - 52K OF AVAILABLE FAST MEMORY AND 5 MAGNETIC TAPE UNITS PLUS 5 SCRATCH FILES (DRUM FILES ARE USED ON THE UNIVAC1108) TOTALING ABOUT 600K IN CAPACITY

12. PROGRAMMING LANGUAGE USED - FORTRAN IV

13. OPERATING SYSTEM OR MONITOR UNDER WHICH PROGRAM IS EXECUTED - EXEC II, GAX33A.

14. ANY OTHER PROGRAMMING OR OPERATING INFORMATION OR RESTRICTIONS - GAFGAR IS OVERLAYED IN THREE SEGMENTS CONSISTING OF THE GAF SECTION, THE GAR SECTION, AND A COMBINING AND PUNCHING SECTION. THE UNIVAC1107/1108 FORTRAN IV NTRAN I/O ROUTINES ARE USED TO BUFFER THE I/O IN PARALLEL WITH COMPUTING AND TO REDUCE THE NUMBER OF RECORD GAPS ON THE DATA TAPES.

15. AUTHOR OF THE ABSTRACT - R.J. ARCHIBALD, D.R. MATHEWS, R.T. SHANSTROM, C.A. STEVENS, AND M.R. WAGNER

1. NAME OF CODE - GAKIT. A ONE DIMENSIONAL MULTIGROUP KINETICS CODE WITH TEMPERATURE FEEDBACK.

2. COMPUTER FOR WHICH CODE IS DESIGNED - UNIVAC 1108.

3. NATURE OF PHYSICAL PROBLEM SOLVED - THE MULTIGROUP, ONE DIMENSIONAL, TIME-DEPENDENT DIFFUSION-THEORY KINETICS EQUATIONS ARE SOLVED INCLUDING DELAYED-NEUTRON EFFECTS AND TEMPERATURE FEEDBACK BASED ON TWO-DIMENSIONAL HEAT TRANSFER CALCULATIONS. FOR THE ONE-DIMENSIONAL MULTIGROUP KINETICS EQUATIONS, AN ARBITRARY SCATTERING MATRIX AND ARBITRARY FISSION TRANSFER ARE ALLOWED, AND PLANE OR CYLINDRICAL GEOMETRY MAY BE USED. A PIECEWISE LINEAR TIME-DEPENDENT INHOMOGENEOUS SOURCE CAN BE SPECIFIED. FEEDBACK IS AVAILABLE FROM XENON BUILDUP AND TEMPERTURE DEPENDENCE OF CROSS SECTIONS. THE HEAT TRANSFER CALCULATION IS PERFORMED FOR TWO-DIMENSIONAL R-Z FUEL ELEMENT MODELS ASSUMING PREDETERMINED AXIAL-POWER SHAPE FUNCTIONS AND TIME-DEPENDENT POWER AMPLITUDES OBTAINED FROM THE ONE-DIMENSIONAL KINETICS CALCULATIONS. FOR THE FUEL ELEMENTS, AVERAGE FUEL AND MODERATOR TEMPERATURES ARE CALCULATED WHICH DETERMINE, BASED ON TABLES, THE TEMPERATURE-DEPENDENT CROSS SECTIONS. TRANSIENTS MAY BE INTRODUCED BY STEP CHANGES OF CROSS SECTIONS, BY PIECEWISE LINEAR TIME-DEPENDENT CROSS SECTIONS (ROD WITHDRAWAL ACCIDENTS), BY STEP CHANGES OF THE FLOW RATES, OR BY STEP CHANGES OF THE COOLANT INLET TEMPERATURES.

4. METHOD OF SOLUTION - THE MULTIGROUP, ONE-DIMENSIONAL, TIME DEPENDENT DIFFUSION-THEORY KINETICS EQUATIONS ARE SOLVED BY A SEMI-IMPLICIT TIME INTEGRATION METHOD. THE HEAT TRANSFER EQUATIONS ARE SOLVED BY A QUASI TWO-DIMENSIONAL METHOD, ASSUMING THE AXIAL HEAT CONDUCTION IS NEGLIGIBLE COMPARED WITH THE HEAT TRANSPORT DUE TO COOLANT FLOW. FOR THE NUMERICAL SOLUTION OF THE KINETICS EQUATIONS AND ALSO FOR THE SOLUTION OF THE HEAT-TRANSFER EQUATIONS, FINITE DIFFERENCE METHODS IN SPACE AND TIME ARE EMPLOYED. THE MATERIAL PROPERTIES ARE ASSUMED TO BE REGIONWISE CONSTANT. THE CODE IS EQUIPPED WITH AN AUTOMATIC TIME STEP ADJUSTMENT SCHEME.

5. RESTRICTIONS ON THE COMPLEXITY OF THE PROBLEM -
   A) ONE-DIMENSIONAL KINETICS CALCULATION:
      MAXIMUM NUMBER OF PROMPT-NEUTRON ENERGY GROUPS IS 10.
      MAXIMUM NUMBER OF DELAYED-NEUTRON GROUPS IS 6.
      MAXIMUM NUMBER OF HOMOGENEOUS REGIONS (CHANNELS) IS 10.
      MAXIMUM NUMBER OF MESH POINTS IS 100.

B) FUEL ELEMENT GEOMETRY FOR HEAT TRANSFER CALCULATION: IN THE AXIAL DIRECTION, THE FUEL ELEMENT MAY CONSIST OF A BOTTOM REFLECTOR, A CORE SECTION, AND A TOP REFLECTOR. THE BOTTOM AND TOP REFLECTORS MUST HAVE UNIFORM DENSITIES AND UNIFORM THERMAL PROPERTIES, WHILE WITHIN THE CORE SECTION OF THE FUEL ELEMENT UP TO FIVE RADIAL REGIONS MAY BE USED.
MAXIMUM NUMBER OF RADIAL MESH POINTS IS 15.
MAXIMUM NUMBER OF AXIAL MESH POINTS IS 20.
THE FUEL ELEMENTS IN ALL THE CHANNELS MUST HAVE THE SAME GEOMETRY, THE SAME THERMAL PROPERTIES, AND THE SAME INLET TEMPERATURE; BUT THE FUEL ELEMENTS OF DIFFERENT CHANNELS MAY HAVE DIFFERENT COOLANT FLOW RATES AND DIFFERENT AXIAL POWER SHAPES.

6. TYPICAL RUNNING TIME - THE RUNNING TIME IS STRONGLY DEPENDENT UPON THE PROBLEM TYPE AND A CLOSED FORMULA CANNOT BE DERIVED FOR EVEN ONE TIME STEP DUE TO THE USE OF AN ITERATIVE PROCEDURE. IN GENERAL, THE RUNNING TIME WILL INCREASE LINEARLY WITH THE NUMBER OF MESH POINTS AND THE NUMBER OF PROMPT-NEUTRON GROUPS. FOR A TYPICAL ROD WITHDRAWAL ACCIDENT PROBLEM (2 PROMPT-NEUTRON GROUPS, 6 DELAYED-NEUTRON GROUPS, 4 CHANNELS, AND 29 MESH POINTS), THE RUNNING TIME PER TIME STEP ON THE UNIVAC-1108 WAS 0.18 SEC.

7. UNUSUAL FEATURES OF THE CODE -
   A) THE TIME INTEGRATION PROCEDURE IS NUMERICALLY STABLE FOR RELATIVELY LARGE TIME STEPS. THE PROCEDURE IS ASYMPTOTICALLY STABLE FOR TIME STEPS OF ARBITRARY LENGTH.
   B) THE METHOD IS ESPECIALLY SUITED FOR MULTIGROUP CALCULATIONS BECAUSE THE RUNNING TIME INCREASES ROUGHLY LINEARLY WITH THE NUMBER OF ENERGY GROUPS.
   C) THE CODE HAS THE CAPABILITY OF CALCULATING STEADY-STATE CONDITIONS FOR THE COMBINED DIFFUSION AND HEAT TRANSFER EQUATIONS ASSUMING A CERTAIN POWER LEVEL.
   D) THE LIMITS FOR THE NUMBER OF ENERGY GROUPS, MESH POINTS, ETC., CAN EASILY BE CHANGED BY RECOMPILING THE FORTRAN PROGRAM.
   E) THE INPUT OF THE CODE IS FLEXIBLE. FOR EXAMPLE, THE USER CAN SUPPLY HIS TEMPERATURE-DEPENDENT CROSS SECTIONS IN TABLE FORM, OR HE CAN GENERATE TRANSIENTS BY PIECEWISE LINEAR TIME-DEPENDENT CROSS SECTIONS.

8. RELATED AND AUXILIARY PROGRAMS - GAKIN, A ONE-DIMENSIONAL KINETICS CODE WITHOUT TEMPERATURE FEEDBACK.

9. STATUS - THE PROGRAM HAS BEEN IN PRODUCTION USE SINCE SEPTEMBER 1968 AND MAY BE OBTAINED FROM THE ARGONNE CODE CENTER.

10. REFERENCES -

(1) R. FROELICH, S.R. JOHNSON, AND M.H. MERRILL, "GAKIT, A ONE DIMENSIONAL MULTIGROUP KINETICS CODE WITH TEMPERATURE FEEDBACK," GA-8576, GULF GENERAL ATOMIC INCORPORATED (SEPTEMBER 1968).

(2) J.B. ANDREWS AND K.F. HANSEN, NUCLEAR SCI. ENG., 31, 304 (1968).

(3) J.B. ANDREWS, "NUMERICAL SOLUTION OF THE SPACE DEPENDENT REACTOR KINETICS EQUATIONS," PHD THESIS, M.I.T. (MAY 1967).

(4) K.F. HANSEN AND S.R. JOHNSON, "GAKIN, A ONE DIMENSIONAL MULTIGROUP KINETICS CODE," GA-7543, GENERAL DYNAMICS, GENERAL ATOMIC (AUGUST 1967).

11. MACHINE REQUIREMENTS - 65,536 WORDS OF CORE STORAGE AND THE FACILITY FOR SEGMENTING PROGRAMS.

12. PROGRAMMING LANGUAGE USED - FORTRAN IV

13. OPERATING SYSTEM - EXEC-II GAX 23; BUT ANY OTHER SYSTEM WITH SEGMENTING FACILITY CAN BE USED.

14. OTHER PROGRAM INFORMATION -

15. AUTHOR OF THE ABSTRACT - R. FROELICH, S.R. JOHNSON, AND M.H. MERRILL.

1. NAME OR DESIGNATION OF PROGRAM - GAND

2. COMPUTER FOR WHICH PROGRAM IS DESIGNED AND OTHERS UPON WHICH IT IS OPERABLE - UNIVAC-1108

3. NATURE OF PHYSICAL PROBLEM SOLVED - GAND PREPARES THE CROSS SECTIONS NEEDED FOR DETAILED COMPUTATIONS OF NEUTRON ENERGY SPECTRA IN FAST REACTORS FROM A FILE OF BASIC NUCLEAR DATA IN THE ENDF/B FORMAT.

4. METHOD OF SOLUTION - FINE GROUP CROSS SECTIONS AND TRANSFER COEFFICIENT ARRAYS FOR USE IN THE GAF CODE ARE PREPARED USING MODIFIED VERSIONS OF THE ROUTINES USED TO PREPARE GGC4 (ACC ABSTRACT 298) DATA TAPES AS WELL AS THE GANDY CODE (ACC ABSTRACT 341) FOR UNRESOLVED RESONANCE REGION CROSS SECTION GENERATION. POINTWISE CROSS SECTIONS FOR USE IN THE GAR CODE ARE PREPARED USING THE PSEUDO CODE (ACC ABSTRACT 292) TO GENERATE STATISTICAL RESONANCES IN THE UNRESOLVED RESONANCE REGION AND THE FASDOP CODE (ACC ABSTRACT 216) TO GENERATE THE CROSS SECTIONS FROM BOTH THE STATISTICAL RESONANCES AND THE RESOLVED RESONANCE PARAMETERS.

5. RESTRICTIONS ON THE COMPLEXITY OF THE PROBLEM - MAXIMA OF -
   20 ENDF/B MATERIALS PROCESSED IN A SINGLE PROBLEM
   35 RESONANCE LEVELS ON EITHER SIDE OF THE INCIDENT NEUTRON ENERGY

6. TYPICAL RUNNING TIME - 30 MINUTES ARE REQUIRED FOR A TYPICAL PROBLEM.

7. UNUSUAL FEATURES OF THE PROGRAM - THE RESOLVED AND UNRESOLVED RESONANCE CALCULATIONS CAN TREAT PROCESSES INVOLVING NEUTRONS OF ORBITAL ANGULAR MOMENTA ZERO THROUGH THREE (S-, P-, D-, AND F-WAVE INTERACTIONS). THE VERSION OF THE PSEUDO CODE USED IN THIS PROGRAM HAS BEEN MODIFIED TO ALLOW 1, 2, OR 3 DEGREES OF FREEDOM FOR THE DISTRIBUTION OF FISSION WIDTHS.

8. RELATED AND AUXILIARY PROGRAMS - THE BINARY ENDF/B FORMAT NUCLEAR DATA TAPES REQUIRED BY THE GAND CODE ARE PREPARED FROM CARDS OR ENDF/B CARD IMAGE TAPES BY THE ENDFB CODE. THE OUTPUT FROM THE GAND CODE IS INTENDED FOR USE IN THE GAFGAR CODE (ACC ABSTRACT 316). PROCOP COPIES SELECTED PROBLEMS FROM THE GAFGAR PROBLEM TAPES OR LISTS THE TAPE.

9. STATUS - PRODUCTION

10. REFERENCES - R. J. ARCHIBALD AND D. R. MATHEWS, THE GAF/GAR/GAND FAST REACTOR CROSS SECTION PREPARATION SYSTEM, GAFGAR - A PROGRAM FOR THE CALCULATION OF NEUTRON SPECTRA AND GROUP-AVERAGED CROSS SECTIONS, GA-7542, VOL. I, JANUARY 22, 1968, AND ERRATA, MAY 1968.

R. J. ARCHIBALD AND D. R. MATHEWS, THE GAF/GAR/GAND FAST REACTOR CROSS SECTION PREPARATION SYSTEM, GAND - A COMPUTER PROGRAM FOR PREPARING INPUT DATA FOR THE GAFGAR CODE FROM AN ENDF/B FORMAT NUCLEAR DATA FILE, GA-7542, VOL. II, TO BE PUBLISHED.

M. K. DRAKE, C. V. SMITH, AND L. J. TODT, DESCRIPTION OF AUXILIARY CODES USED IN THE PREPARATION OF DATA FOR THE GGC-3 CODE, GA-7158, AUGUST 1967.

S. C. COHEN AND P. K. KOCH, GANDY - A COMPUTER PROGRAM FOR THE EVALUATION OF EFFECTIVE CROSS SECTIONS IN THE UNRESOLVED RESONANCE REGION, GA-8003, MAY 1967.

M. W. DYOS, CONSTRUCTION OF STATISTICAL RESONANCES IN THE UNRESOLVED RESONANCE REGION - THE PSEUDO CODE, GA-7136, MAY 26, 1966.

C. A. STEVENS, FASDOP, A FORTRAN-IV COMPUTER PROGRAM FOR COMPUTING CROSS SECTIONS FROM RESONANCE PARAMETERS, GAMD-6562, AUGUST 9, 1965.

11. MACHINE REQUIREMENTS - 52K MEMORY AND 4 TO 8 MAGNETIC TAPE UNITS PLUS 5 SCRATCH FILES (DRUM FILES ARE USED ON THE UNIVAC1108) TOTALING ABOUT 1310K IN CAPACITY

12. PROGRAMMING LANGUAGE USED - FORTRAN IV

13. OPERATING SYSTEM OR MONITOR UNDER WHICH PROGRAM IS EXECUTED - EXEC II, GAX35.

14. ANY OTHER PROGRAMMING OR OPERATING INFORMATION OR RESTRICTIONS -

15. AUTHOR OF THE ABSTRACT - R.J. ARCHIBALD AND D.R. MATHEWS

1. NAME OR DESIGNATION OF PROGRAM - GANDY

2. COMPUTER FOR WHICH PROGRAM IS DESIGNED AND OTHERS UPON WHICH IT IS OPERABLE - UNIVAC 1108

3. NATURE OF PHYSICAL PROBLEM SOLVED - THE GANDY CODE EVALUATES TEMPERATURE-DEPENDENT EFFECTIVE NEUTRON CAPTURE, FISSION, AND SCATTERING CROSS SECTIONS IN THE UNRESOLVED RESONANCE REGION FROM AVERAGE RESONANCE PARAMETERS.

4. METHOD OF SOLUTION - EFFECTIVE CROSS SECTIONS ARE EVALUATED AT SPECIFIED ENERGIES AND TEMPERATURES USING THE NARROW RESONANCE APPROXIMATION AND ASSUMING ISOLATED RESONANCES. RESONANCE CROSS SECTIONS ARE TREATED ON A STATISTICAL BASIS, USING CHI-SQUARED DISTRIBUTIONS FOR THE PARTIAL WIDTHS. THE LINE SHAPE FUNCTIONS, PSI AND CHI, ARE EVALUATED IN A SUBROUTINE WRITTEN BY NALIBOFF WHICH IS BASED UPON A METHOD DEVELOPED BY ADLER AND NALIBOFF (SEE REFERENCE 2). THE STATISTICAL AVERAGING IS CARRIED OUT USING A QUADRATURE SCHEME INTRODUCED IN THE RAPTURE CODE (ACC ABSTRACT 176).

5. RESTRICTIONS ON THE COMPLEXITY OF THE PROBLEM - GANDY WILL HANDLE AS MANY TEMPERATURES AS DESIRED FOR A MAXIMUM OF 100 ENERGY POINTS. CONSIDERATION IS TAKEN OF NEUTRON ORBITAL ANGULAR MOMENTUM THROUGH D-WAVE (L=2).

6. TYPICAL RUNNING TIME - THE RUNNING TIME IS VERY SENSITIVE TO THE INPUT OPTIONS CHOSEN. FOR A FISSILE NUCLIDE WITH TWO SPIN STATES AND L=0, THE STATISTICAL AVERAGING PERFORMED, THE DENOMINATOR EVALUATED, AND INTERFERENCE SCATTERING NEGLECTED, THE APPROXIMATE RUNNING TIME IS 7 SECONDS ON THE UNIVAC-1108 FOR ONE ENERGY POINT. NON-FISSILE NUCLIDES, WHICH REQUIRE STATISTICAL AVERAGING ONLY FOR THE NEUTRON WIDTH DISTRIBUTION, ARE AN ORDER OF MAGNITUDE FASTER FOR THE SAME DEGREE OF APPROXIMATION. FOR REACTOR DESIGN CALCULATIONS IN WHICH UNRESOLVED RESONANCE CROSS SECTIONS ARE EVALUATED AT ONE-QUARTER LETHARGY INTERVALS, THE EFFECTIVE CROSS SECTIONS IN THE UNRESOLVED RESONANCE REGION FOR U-238 ARE EVALUATED BY GANDY IN APPROXIMATELY 10 SECONDS.

7. UNUSUAL FEATURES OF THE PROGRAM - GANDY INCORPORATES THE FOLLOWING FEATURES WHICH DISTINGUISH THE PRESENT TREATMENT FROM EARLIER UNRESOLVED RESONANCE CALCULATIONS -
   (A) COMPUTATION OF THE UNRESOLVED RESONANCE SCATTERING CROSS SECTION AS WELL AS THE CAPTURE AND FISSION CROSS SECTIONS.
   (B) CONSIDERATION OF S-, P-, AND D-WAVE (L=0, 1, AND 2) NEUTRON ORBITAL ANGULAR MOMENTA.

(C) CONSIDERATION OF ARBITRARY HALF-INTEGER VALUES OF THE TARGET SPIN IN ADDITION TO I=0.
(D) CALCULATION OF THE FISSILE CROSS SECTIONS FOR CHI-SQUARED FISSION WIDTH DISTRIBUTIONS WITH ONE, TWO, THREE, OR FOUR DEGREES OF FREEDOM.
(E) CONSIDERATION OF INTERFERENCE SCATTERING.
(F) INCLUSION OF THE DENOMINATOR IN THE CALCULATION OF THE EFFECTIVE CROSS SECTION.

8. RELATED AND AUXILIARY PROGRAMS - GANDY IS A FORTRAN IV EXTENSION OF THE RAPTURE CODE AND THE UNRESOLVED RESONANCE TREATMENT INCORPORATED IN THE MC**2 PROGRAM. GANDY IS INCORPORATED IN THE GAND PORTION OF THE GULF GENERAL ATOMIC FAST CROSS SECTION PACKAGE, GAF/GAR/GAND (ACC ABSTRACTS 316, 345).

9. STATUS - PRODUCTION

10. REFERENCES - S. C. COHEN AND P. K. KOCH, GANDY, A COMPUTER PROGRAM FOR THE EVALUATION OF EFFECTIVE CROSS SECTIONS IN THE UNRESOLVED RESONANCE REGION, GA-8003, MAY 1967.

F. T. ADLER AND Y. D. NALIBOFF, A DIRECT METHOD FOR THE EVALUATION OF THE RESONANCE LINE SHAPE FUNCTIONS, JOURNAL OF NUCLEAR ENERGY, PARTS A/B, VOL. 14, PP. 209-211, 1961.

J. H. FERZIGER, P. GREEBLER, M. D. KELLEY, AND J. W. WALTON, RESONANCE INTEGRAL CALCULATIONS FOR EVALUATION OF DOPPLER COEFFICIENTS, THE RAPTURE CODE, GEAP-3923, JULY 1962.

B. J. TOPPEL, A. L. RAGO, AND D. M. OSHEA, MC**2, A CODE TO CALCULATE MULTIGROUP CROSS SECTIONS, ANL-7318, JUNE 1967.

R. J. ARCHIBALD AND D. R. MATHEWS, THE GAF/GAR/GAND FAST REACTOR CROSS SECTION PREPARATION SYSTEM, GAND - A COMPUTER PROGRAM FOR PREPARING INPUT DATA FOR THE GAFGAR CODES FROM AN ENDF/B FORMAT NUCLEAR DATA FILE, GA-7542, VOL. II, TO BE PUBLISHED.

11. MACHINE REQUIREMENTS - GANDY REQUIRES 11,300 STORAGE LOCATIONS AND THE DATA STORAGE REQUIREMENT IS APPROXIMATELY 15,800 LOCATIONS. TWO I/O DEVICES ARE REQUIRED FOR READING AND PRINTING AND ONE ADDITIONAL I/O DEVICE IS NECESSARY IF THE PROGRAM IS LOADED FROM TAPE.

12. PROGRAMMING LANGUAGE USED - FORTRAN IV

13. OPERATING SYSTEM OR MONITOR UNDER WHICH PROGRAM IS EXECUTED - EXEC II, GAX33 DATED DECEMBER 19, 1967.

14. ANY OTHER PROGRAMMING OR OPERATING INFORMATION OR RESTRICTIONS - ADAPTION OF THE GANDY CODE TO A SMALLER MACHINE WITH A FORTRAN IV COMPILER CAN BE MADE BY CHANGING ARRAY DIMENSIONS WHICH WILL ALLOW FOR CALCULATIONS AT FEWER ENERGY POINTS.

15. AUTHOR OF THE ABSTRACT - P.K. KOCH AND S.C. COHEN

1. NAME OR DESIGNATION OF PROGRAM - GAROL

2. COMPUTER FOR WHICH CODE IS DESIGNED - UNIVAC-1108

3. NATURE OF PHYSICAL PROBLEM SOLVED - GAROL COMPUTES EFFECTIVE GROUP CROSS SECTIONS FOR THE RESOLVED RESONANCES OF A MIXTURE OF ISOTOPES IN A TWO-REGION CELL. BASIC CROSS SECTIONS INCLUDE TEMPERATURE DEPENDENCE. THE PROGRAM ALLOWS A CHOICE OF GEOMETRIES AND CAN ACCEPT AN ARBITRARY TABLE OF ESCAPE PROBABILITIES. A DANCOFF CORRECTION MAY BE USED TO ACCOUNT FOR SHADOWING EFFECTS IN A TIGHT LATTICE, AND CROSS SECTIONS MAY BE 1/V, CONSTANT, COMPUTED FROM BREIT-WIGNER RESONANCE PARAMETERS, OR GIVEN IN TABULAR FORM. THE MESH MAY BE CHOSEN AT EQUAL ENERGY OR LETHARGY INTERVALS, PROPORTIONAL TO THE NEUTRON VELOCITY, OR AS AN ARBITRARY TABLE OF VALUES.

4. METHOD OF SOLUTION - THE COLLISION PROBABILITY METHOD YIELDS TWO COUPLED INTEGRAL EQUATIONS WHICH ARISE FROM A NEUTRON BALANCE IN EACH REGION. THESE ARE SOLVED NUMERICALLY TO OBTAIN THE FLUX SPECTRUM IN EACH REGION, AS WELL AS GROUP CROSS SECTIONS FOR EACH REGION AND FOR THE CELL.

5. RESTRICTIONS ON THE COMPLEXITY OF THE PROBLEM -
   NUMBER OF NUCLIDES EQUAL TO OR LESS THAN 10.
   NUMBER OF RESONANCES PER ISOTOPE EQUAL TO OR LESS THAN 500.
   TOTAL NUMBER OF RESONANCES FOR ALL ISOTOPES EQUAL TO OR LESS THAN 600.
   NUMBER OF REGIONS EQUAL TO OR LESS THAN 2.

6. TYPICAL RUNNING TIME - VARIES CONSIDERABLY FROM PROBLEM TO PROBLEM. WITH 2 ISOTOPES, U235 AND H, AND 6600 ENERGY POINTS COVERING THE ENERGY RANGE, 0.5 EV TO 950 EV, THE RUNNING TIME WAS 3 MINUTES.

7. UNUSUAL FEATURES OF THE PROGRAM - OVERLAP OF RESONANCES OF AN INDIVIDUAL RESONANCE ABSORBER AND OF MIXTURES OF DIFFERENT RESONANCE ABSORBERS IS TREATED EXACTLY. SLOWING DOWN IN ALL ISOTOPES IS COMPUTED EXACTLY, SO THAT THE NR APPROXIMATION NEED NOT BE MADE FOR A HEAVY MODERATOR. GRAIN SELF-SHIELDING EFFECTS MAY BE TREATED ACCORDING TO A METHOD DEVELOPED BY DYOS AND POMRANING.

8. RELATED AND AUXILIARY PROGRAMS -
   (1) THE GAR PROGRAM (GA-6952 AND GA-7542) IS A HOMOGENEOUS VERSION OF GAROL EXTENDED TO CONSIDER LEAKAGE IN THE B1 APPROXIMATION.

(2) THE NEUTRON SPECTRUM AND GROUP CONSTANT CALCULATION SECTION OF THE GAROL PROGRAM IS INCLUDED IN THE GGC5 PROGRAM.

9. STATUS - PRODUCTION

10. REFERENCES -

(1) C.A. STEVENS AND C.V. SMITH, "GAROL, A COMPUTER PROGRAM FOR EVALUATING RESONANCE ABSORPTION INCLUDING RESONANCE OVERLAP," GA-6637, AUGUST 24, 1965.
(2) M.W. DYOS AND G.C. POMRANING, "EFFECTIVE THERMAL NEUTRON CROSS SECTIONS FOR MATERIALS WITH GRAIN STRUCTURES," NUCL. SCI. ENG. 25, 8(1966).
(3) M.W. DYOS, "THE CALCULATION OF RESONANCE ABSORPTION IN DOUBLY HETEROGENEOUS MEDIA," GA-7077, APRIL 7, 1966.
(4) J. ADIR, ET AL, "GGC5, A COMPUTER PROGRAM FOR CALCULATING NEUTRON SPECTRA AND GROUP CONSTANTS," GA-8871, MARCH 1970.

11. MACHINE REQUIREMENTS - 45K OF AVAILABLE FAST MEMORY, ONE MAGNETIC TAPE UNIT (ADDITIONAL TAPE UNITS OR DRUM FILES ARE REQUIRED ONLY IF INPUT CROSS SECTIONS ARE READ FROM CARDS).

12. PROGRAMMING LANGUAGE USED - UNIVAC, FORTRAN V EXCEPT FOR ONE SUBROUTINE USED FOR THE CONVERSION OF NUCLIDE IDENTIFICATION NUMBERS WHICH IS WRITTEN IN UNIVAC 1108 ASSEMBLY LANGUAGE.

13. OPERATING SYSTEM - UNIVAC EXEC II

14. OTHER PROGRAMMING INFORMATION - THE PROGRAM IS DIVIDED INTO A DATA TAPE PREPARATION SECTION AND A NEUTRON SPECTRUM AND GROUP CONSTANT CALCULATION SECTION. THE TWO SECTIONS MAY BE RUN SEPARATELY OR CONCURRENTLY, E.G. DATA TAPES MAY BE SAVED FOR LATER USE.

15. AUTHOR OF THE ABSTRACT - D. MATHEWS.

1. NAME OF CODE - GASA

2. COMPUTER FOR WHICH CODE IS DESIGNED - UNIVAC #108

3. NATURE OF PHYSICAL PROBLEM SOLVED - GASA EVALUATES THE STABILITY OF MOTION OF A SYSTEM AGAINST SMALL PERTURBATIONS ABOUT SOME EQUILIBRIUM STATE BY CALCULATING THE ROOTS OF THE COEFFICIENT MATRIX OF THE LINEARIZED EQUATIONS OF THE STATE VARIABLES OF THE SYSTEM.

4. METHOD OF SOLUTION - $\dot{X} = AX(T) + Q(T)$
EVALUATE THE ROOTS OF THE (NXN) CONSTANT MATRIX A (X IS A VECTOR OF LENGTH N OF THE STATE VARIABLES OF THE SYSTEM. Q(T) IS A VECTOR OF SOME EXTERNAL PERTURBATION) BY THE QR TRANSFORM METHOD. CALCULATE THE TRANSFER FUNCTION BETWEEN ANY TWO STATE VARIABLES, OR BETWEEN A STATE VARIABLE AND THE PERTURBATION, AND PLOT THE RESULTS.

5. RESTRICTIONS ON COMPLEXITY OF THE PROBLEM -
LIMITED TO A SET OF 25 EQUATIONS
ROOTS OF A EVALUATED TO WITHIN +/- 10-8

6. TYPICAL RUNNING TIME - ABOUT 5 SECONDS FOR A (8X8) MATRIX, I.E. A SET OF 8 EQUATIONS

7. UNUSUAL FEATURES OF THE CODE - A SPECIAL, FAST METHOD IS EMPLOYED TO INVERT THE MATRIX A.

8. RELATED AND AUXILIARY PROGRAM - NONE

9. STATUS - PRODUCTION

10. REFERENCES - GAMD-7282, "GASA - A GENERAL LINEAR STABILITY ANALYSIS CODE",A. BAXTER, JULY 15, 1966.

11. MACHINE REQUIREMENTS -

12. PROGRAMMING LANGUAGE USED - FORTRAN IV

13. OPERATING SYSTEM - EXEC II

14. OTHER PROGRAM INFORMATION -

15. AUTHOR OF THE ABSTRACT - A. BAXTER

1. NAME OR DESIGNATION OF PROGRAM - GAUGE-F

2. COMPUTER FOR WHICH PROGRAM IS DESIGNED AND OTHERS UPON WHICH IT IS OPERABLE - UNIVAC 1107/1108, ALSO OPERABLE WITH MINOR MODIFICATION ON IBM 360/65.

3. NATURE OF PHYSICAL PROBLEM SOLVED - THE TWO-DIMENSIONAL MULTIGROUP NEUTRON DIFFUSION THEORY EQUATIONS FOR A UNIFORM TRIANGULAR MESH ARE SOLVED TO OBTAIN THE MULTIPLICATION FACTOR AND THE SPATIAL FLUX AND POWER DISTRIBUTION OF FAST REACTORS WITH HEXAGONAL CORE CONFIGURATION. THE CODE IS EQUIPPED WITH A BURNUP SECTION TO ALLOW CALCULATION OF COMPLETE REACTOR LIFE HISTORIES WITH PARTIAL REFUELING AT A NUMBER OF RELOAD TIME POINTS. AT EACH DISCRETE TIME POINT, A CONTROL ROD SEARCH MAY BE PERFORMED TO MAINTAIN CRITICALITY AT ALL TIMES. THREE MODES OF OPERATION ARE POSSIBLE: 1) STRAIGHT BURNUP CALCULATION; 2) DEPLETION CALCULATION WITH CONTROL ROD CRITICALITY SEARCH, ALLOWING THE ADJUSTMENT OF A NUMBER OF CONTROL ROD BANKS ACCORDING TO A PRESCRIBED ROD SEQUENCING SCHEME; AND 3) A SERIES OF STATIC CALCULATIONS WITH INSERTION OF RODS INTO FIXED PRESCRIBED POSITIONS. AN OUTPUT CONTROL OPTION ALLOWS CONSIDERABLE FLEXIBILITY IN THE AMOUNT OF EDIT GIVEN FOR EACH TIME POINT.

4. METHOD OF SOLUTION - A SEVEN-POINT DIFFERENCE EXPRESSION FOR A UNIFORM 60-DEGREE TRIANGULAR MESH IS USED, ASSUMING THAT THE SMALLEST HOMOGENEOUS REGION HAS THE FORM OF AN EQUILATERAL HEXAGON WHICH MAY REPRESENT AN INDIVIDUAL FUEL OR BLANKET ELEMENT. A COARSE MESH IS IMPOSED ON THE FINE CALCULATIONAL MESH WHICH SUBDIVIDES THE TOTAL REACTOR VOLUME INTO A NUMBER OF PATCHES. A PATCH CONSISTS OF A CLUSTER OF SEVEN HEXAGONAL ELEMENTS. THE BLOCK INVERSION METHOD IS APPLIED TO SOLVE DIRECTLY FOR ALL INNER POINTS OF A PATCH FOR GIVEN VALUES AT THE PATCH BOUNDARIES. DURING THE INNER ITERATION AN ALTERNATING SCHEME IS USED TO IMPROVE PATCH BOUNDARY FLUX VALUES OR INNER FLUX VALUES. THE FISSION SOURCE IS UPDATED AFTER EACH PAIR OF INNER ITERATIONS. A COARSE MESH REBALANCING PROCEDURE IS APPLIED AFTER EACH FISSION SOURCE ITERATION. IN ADDITION, AN ASYMPTOTIC FISSION SOURCE EXTRAPOLATION IS USED PERIODICALLY TO ELIMINATE THE NEXT-TO-LOWEST EIGENFUNCTION. THE CODE AUTOMATICALLY RECOGNIZES THE EXISTENCE OF 60, 120 OR 180-DEGREE ROTATIONAL SYMMETRIES IN THE PROBLEM CON-

FIGURATION AND EXPLOITS IT TO REDUCE COMPUTER TIME AND PRINTOUT.
THE DEPLETION SCHEME OF ALL BURNABLE NUCLIDES IS SPECIFIED BY THE USER AT EXECUTION TIME. A GENERAL AND FLEXIBLE BURNUP ROUTINE SYSTEM ALLOWS AN OPTIMAL CHOICE OF EITHER A DIFFERENCE APPROXIMATION OR AN ANALYTICAL SOLUTION OF THE DEPLETION EQUATIONS. THE CODE DECIDES INTERNALLY, FOR EACH TIME STEP AND EVERY NUCLIDE, WHICH APPROXIMATION IS USED.

5. RESTRICTIONS ON THE COMPLEXITY OF THE PROBLEM -
A BASIC RESTRICTION OF THIS CODE VERSION IS THE FACT THAT UPSCATTERING IS NOT ALLOWED. HOWEVER, SCATTERING MAY OCCUR FROM ANY NEUTRON ENERGY GROUP INTO EVERY LOWER ENERGY GROUP. THE FLUX IS ASSUMED TO BE ZERO AT THE OUTER REACTOR BOUNDARY.

10 NEUTRON ENERGY GROUPS
1363 MESH POINTS (INCLUDING OUTER REACTOR BOUNDARY)
327 HEXAGONAL ELEMENTS
125 BURNUP REGIONS
40 NUCLIDES
80 MICROSCOPIC CROSS SECTION BLOCKS
5 VARIABLE SELF-SHIELDING FACTOR TABLES
55 CONTROL RODS IN 15 BANKS
NO RESTRICTION IN THE NUMBER OF BURNUP TIME STEPS

6. TYPICAL RUNNING TIME -
A) A 10-GROUP PROBLEM WITH 37 PATCHES, 823 MESH POINTS, 120-DEGREE SYMMETRY, 32 NUCLIDES, 87 BURNUP REGIONS AND NO CRITICALITY SEARCH REQUIRES 1 MIN. PER LONG TIME STEP (UNIVAC 1108).
B) A FULL-SIZE PROBLEM WITH NO SYMMETRY AND WITH CRITICALITY SEARCH TAKES ABOUT 5 MIN. PER TIME STEP.

7. UNUSUAL FEATURES OF THE PROGRAM - GAUGE-F, LIKE GAUGE, MAKES USE OF THE DIRECT BLOCK INVERSION METHOD, WHICH LEADS TO AN IMPROVED CONVERGENCE RATE OF THE INNER SPATIAL ITERATION.

8. RELATED AND AUXILIARY PROGRAM -

9. STATUS - READY FOR PRODUCTION USE.

10. REFERENCES - M.R. WAGNER, "GAUGE, A TWO-DIMENSIONAL FEW GROUP NEUTRON DIFFUSION-DEPLETION PROGRAM FOR A UNIFORM TRIANGULAR MESH", GA-8307, GULF GENERAL ATOMIC INCORPORATED (1968).

11. MACHINE REQUIREMENTS - 65,536 WORDS OF CORE STORAGE.

15,548 WORDS OF DRUM STORAGE, 3 TAPE UNITS AND A PERIPHERAL PRINTER.

12. PROGRAMMING LANGUAGES USED - FORTRAN V. FOR BINARY READING AND WRITING ON DRUM THE ROUTINE NTRAN, AN ASSEMBLY LANGUAGE (UNIVAC 1108) PROGRAM, IS USED.

13. OPERATING SYSTEM OR MONITOR UNDER WHICH PROGRAM IS EXECUTED - GULF GENERAL ATOMIC VERSION OF THE UNIVAC 1108 OPERATING SYSTEM EXEC-VIII.

14. ANY OTHER PROGRAMMING OR OPERATING INFORMATION OR RESTRICTIONS -

15. AUTHOR OF THE ABSTRACT-

G. ABAI AND M.R. WAGNER
GULF GENERAL ATOMIC EUROPE
8006 ZURICH, SWITZERLAND
109 WEINBERGSTRASSE

1. NAME OF PROGRAM - GFE2

2. COMPUTER FOR WHICH PROGRAM IS DESIGNED - UNIVAC 1108

3. NATURE OF PHYSICAL PROBLEM SOLVED - GFE2 PREPARES 1/E FLUX WEIGHTED, ZERO TEMPERATURE, INFINITE DILUTION GROUP AVERAGED CROSS SECTIONS AND SCATTERING TRANSFER ARRAYS FOR USE IN THE FAST SECTIONS OF THE GGC-4 AND GGC-5 CODES FROM A FILE OF BASIC NUCLEAR DATA IN THE ENDF/B VERSION II FORMAT (THE ENDF/B VERSION I FORMAT CAPABILITY OF THE ORIGINAL GFE CODE IS ALSO RETAINED).

4. METHOD OF SOLUTION - GFE2 IS AN EXTENDED SPECIAL PURPOSE VERSION OF THE GAF CROSS SECTION PREPARATION SECTION OF THE GAND2 CODE. THE EXTENSIONS INCLUDE THE COMPUTATION OF P_3 INSTEAD OF P_1 SCATTERING TRANSFER ARRAYS AND A HIGH SPEED, ZERO TEMPERATURE, INFINITE DILUTION RESOLVED RESONANCE CALCULATION VIA THE INDER CODE (GA-7158).

5. RESTRICTIONS ON THE COMPLEXITY OF THE PROBLEM - MAXIMA OF -

   (A) 20 ENDF/B MATERIALS PER PROBLEM

   (B) 375 RESOLVED RESONANCES PER ℓ-STATE (ANGULAR MOMENTUM STATE) PER ISOTOPE

   (C) 375 ENERGIES PER ℓ-STATE PER ISOTOPE FOR ENERGY-DEPENDENT UNRESOLVED PARAMETERS (LRU=2, LRF=1 OR 2)

   (D) 99 GROUPS (LIMITED BY INDER)

   (E) LF=1 OR 5 SECONDARY ENERGY DISTRIBUTION LAWS IN FILE 5 CANNOT BE PROCESSED IN THE PRESENT VERSION

   (F) INELASTIC SCATTERING IS ASSUMED TO BE ISOTROPIC IN THE LABORATORY SYSTEM

6. TYPICAL RUNNING TIME - 5 MINUTES

7. UNUSUAL FEATURES OF THE PRQGRAM - THE RESOLVED AND UNRESOLVED RESONANCE CALCULATIONS CAN TREAT PROCESSES INVOLVING NEUTRONS OF ORBITAL ANGULAR MOMENTA ZERO THROUGH THREE (S-, P-, D-, AND F-WAVE INTERACTIONS). A VIRTUALLY UNLIMITED (OVER 2 MILLION) NUMBER OF TABULAR ENERGIES MAY BE USED IN THE ENDF/B FORMAT FILE 3 DATA. THIS IS ACHIEVED BY BREAKING THE ENDF/B FILE 3 DATA UP INTO 2000 WORD BLOCKS. A SIMILAR SCHEME IS USED TO PROCESS THE ANGULAR DISTRIBUTION DATA FROM AN ENDF/B FORMAT FILE 4 WITHOUT SIGNIFICANT RESTRICTIONS ON THE AMOUNT OF INPUT DATA.

8. RELATED AND AUXILIARY PROGRAMS - THE GFE2 CODE IS CLOSELY RELATED TO THE GAND2 CODE. THE BINARY ENDF/B FORMAT NUCLEAR DATA TAPES REQUIRED BY THE GFE2 CODE ARE PREPARED FROM CARDS OR ENDF/B CARD IMAGE TAPES BY THE ENDFB2 CODE (THE ENDFB2 CODE IS SIMILAR TO THE DAMMET CODE DISTRIBUTED THROUGH THE CSEWG). THE OUTPUT OF THE GFE2 CODE IS INTENDED FOR USE AS INPUT TO THE MAKE CODE (GA-7158) WHICH PREPARES DATA TAPES FOR USE IN THE FAST SECTIONS OF THE GGC-4 AND GGC-5 CODES.

9. STATUS - PRODUCTION

10. REFERENCES -

(1) R. J. ARCHIBALD AND D. R. MATHEWS, "THE GAF/GAR/GAND FAST REACTOR CROSS SECTION PREPARATION SYSTEM, GAND - A COMPUTER PROGRAM FOR PREPARING INPUT DATA FOR THE GAFGAR CODE FROM AN ENDF/B FORMAT NUCLEAR DATA FILE," GA-7542, VOL. II, TO BE PUBLISHED.

(2) M. K. DRAKE, C. V. SMITH, AND L. J. TODT, "DESCRIPTION OF AUXILIARY CODES USED IN THE PREPARATION OF DATA FOR THE GGC-3 CODE," GA-7158, AUGUST 1967.

(3) J. ADIR AND K. D. LATHROP, "THEORY OF METHODS USED IN THE GGC-4 MULTIGROUP CROSS SECTION CODE," GA-9021, OCTOBER 1968.

(4) D. MATHEWS, ET AL., "GGC-5, A COMPUTER PROGRAM FOR CALCULATION OF NEUTRON SPECTRA AND GROUP CONSTANTS," GA-8871, IN PREPARATION.

11. MACHINE REQUIREMENTS - 65K WORD AVAILABLE FAST MEMORY AND 2 MAGNETIC TAPE UNITS PLUS 7 SCRATCH FILES (DRUM FILES ARE USED ON THE UNIVAC 1108) TOTALING ABOUT 1310K WORDS IN CAPACITY

12. PROGRAMMING LANGUAGE USED - UNIVAC FORTRAN-V

13. OPERATING SYSTEM OR MONITOR UNDER WHICH PROGRAM IS EXECUTED - EXEC-8

14. ANY OTHER PROGRAMMING OR OPERATING INFORMATION OR RESTRICTIONS - USED UNIVAC NTRAN I/O ROUTINES

15. AUTHOR OF THE ABSTRACT - D. R. MATHEWS

1. NAME OF CODE - GGC5

2. COMPUTER FOR WHICH CODE IS DESIGNED - UNIVAC 1108

3. NATURE OF PHYSICAL PROBLEM SOLVED - SAME AS GGC4 WITH THE FOLLOWING ADDITIONS:

   (1) A GAMNIT OR GAROL RESOLVED RESONANCE CALCULATION.
   (2) A TUZ OR GANDY UNRESOLVED RESONANCE CALCULATION
   (3) BUCKLING MAY BE POSITIVE, NEGATIVE, OR ZERO.

4. METHOD OF SOLUTION - SAME AS GGC4 EXCEPT FOR RESONANCE CALCULATIONS USING GAROL OR GANDY.

5. RESTRICTIONS ON THE COMPLEXITY OF THE PROBLEM - SAME AS GGC4 EXCEPT FOR POSITIVE BUCKLING REQUIREMENT AND EXCEPT FOR THE FOLLOWING ADDITIONS: MAXIMA OF --

   500 HYPERFINE ENERGY POINTS/RESONANCE IN GAMNIT
   10,000 TOTAL NUMBER OF HYPERFINE ENERGY POINTS IN GAROL
   15 RESONANCE NUCLIDES IN GAMNIT AND TUZ
   10 NUCLIDES IN GAROL
   20 RESONANCE NUCLIDES IN GANDY

6. TYPICAL RUNNING TIME - SAME AS GGC4 IF USING GAMNIT AND TUZ RESONANCE CALCULATIONS.

7. UNUSUAL FEATURES OF THE CODE - SAME AS GGC4

8. RELATED AND AUXILIARY PROGRAMS - SAME AS GGC4

9. STATUS - PRODUCTION

10. REFERENCES -

(1) ADIR, J., "RESONANCE CROSS SECTIONS IN THE MULTIGROUP CROSS SECTION CODE GGC-5, GA-8871, AUGUST 1969.
(2) COHEN, S.C. AND P.K. KOCH, "GANDY - A COMPUTER PROGRAM FOR THE EVALUTION OF EFFECTIVE CROSS SECTIONS IN THE UNRESOLVED RESONANCE REGION," GA-8003, MAY 1967.
(3) STEVENS, C.A. AND C.V. SMITH, "GAROL - A COMPUTER PROGRAM FOR EVALUTING RESONANCE ABSORPTION INCLUDING RESONANCE OVERLAP," GA-6637, AUGUST 1965.
(4) ADIR, J. AND K.D. LATHROP, "THEORY OF METHODS USED IN THE GGC-3 MULTIGROUP CROSS SECTION CODE, GA-7156, JULY 1967.
(5) ADIR, J., S.S. CLARK, R. FROEHLICH, AND L.J. TODT, "USERS

AND PROGRAMMERS MANUAL FOR GGC-3 MULTIGROUP CROSS SECTION CODE, PARTS 1 AND 2," GA-7157, JULY 1967.

(6) DRAKE, M.K., "DESCRIPTION OF AUXILIARY CODE USED IN THE PREPARATION OF DATA FOR THE GGC3 CODE," GA-7158, AUGUST 1967.

11. MACHINE REQUIREMENTS - 64K MEMORY; ONE I/O DEVICE; 14 TAPE UNITS (SOME OF WHICH MAY BE DRUM AREAS).

12. PROGRAMMING LANGUAGE USED - FORTRAN V

13. OPERATING SYSTEM - UNIVAC EXEC II, GAX36F

14. OTHER PROGRAMMING INFORMATION - SAME AS GGC4; GGC5 IS CHAINED AND SEGMENTED.

15. AUTHOR OF THE ABSTRACT - PAM KOCH

1. NAME OF CODE - PMING

2. COMPUTER FOR WHICH CODE IS DESIGNED - UNIVAC 1108

3. NATURE OF PHYSICAL PROBLEM SOLVED - DETERMINATION OF UNRESOLVED RESONANCE PARAMETERS FOR USE IN THE GANDY CODE THAT WILL YIELD SPECIFIED CROSS SECTIONS.

4. METHOD OF SOLUTION - THE UNCONSTRAINED MINIMIZATION CODE PMIN IS USED TO SEARCH FOR VALUES OF GANDY INPUT PARAMETERS WHICH WILL MINIMIZE THE SQUARE ERROR BETWEEN THE CROSS SECTIONS CALCULATED BY GANDY CODE AND DESIRED VALUES READ AS INPUT.

5. RESTRICTIONS ON COMPLEXITY OF THE PROBLEM - THE PRESENT VERSION ON PCF TAPE NO. 2319 USES THREE INDEPENDENT VARIABLES:
   1) THE S-WAVE STRENGTH FUNCTION
   2) THE S-WAVE AVERAGE RADIATION WIDTH
   3) THE S-WAVE J=1 AVERAGE FISSION WIDTH (FOR FISSIONABLE NUCLEI ONLY).

6. TYPICAL RUNNING TIME - ABOUT 5 SECONDS PER OPTIMIZATION FOR NONFISSIONABLE NUCLIDES AND 60 SECONDS FOR FISSIONABLE NUCLIDES. ALL IN THE INFINITE DILUTION, ZERO TEMPERATURE APPROXIMATION (SIGMPO = 1.0E+15, T = 1.0E-6)

7. UNUSUAL FEATURES OF THE CODE - PMING CAN HANDLE UP TO 100 INDEPENDENT VARIABLES SO THAT ADDITIONAL GANDY INPUT VARIABLES CAN BE OPTIMIZED IF NECESSARY.

8. RELATED AND AUXILIARY PROGRAM - PMIN AND GANDY.

9. STATUS - PRODUCTION

10. REFERENCES - PMIN ABSTRACT, GANDY=GA-8003

11. MACHINE REQUIREMENTS -

12. PROGRAMMING LANGUAGE USED - FORTRAN V

13. OPERATING SYSTEM - EXEC-II

14. OTHER PROGRAM INFORMATION -

15. AUTHOR OF THE ABSTRACT - D. MATHEWS

REFERENCES

1. "A Study of a Gas-Cooled Fast Breeder Reactor. Initial Study: Core Design Analysis and System Development Program," USAEC Report GA-5537, General Dynamics, General Atomic Division, 1964.

2. Fortescue, P., et al., "Safety Characteristics of Large Gas-Cooled Fast Power Reactors," USAEC Report GA-6732, General Dynamics, General Atomic Division, 1965.

3. Broido, J., A. Baxter, and R. Shanstrom, "1000 MW(e) Gas-Cooled Fast Reactor - Interim Study of Neutronics," USAEC Report GA-7007, General Dynamics, General Atomic Division, 1966.

4. "Design Study of a 1000-MW(e) Gas-Cooled Fast Reactor Plant. Volume I, Conceptual Design," General Dynamics, General Atomic Division, unpublished data.

5. "Physics and Safety Analyses, Turbine Drive Penetration and Circulator Feasibility Studies for a 1000-MW(e) Gas-Cooled Fast Breeder Reactor," General Dynamics, General Atomic Division, unpublished data.

6. "Gas-Cooled Fast Breeder Reactor Demonstration on Plant-Nuclear Steam Supply System," Gulf General Atomic, unpublished data.

7. Maeder, C., "Optimization of Gas-Cooled Fast Reactor Blankets," Nucl. Sci. Eng. 42, 89 (1970).

8. "Liquid Metal Fast Breeder Reactor (LMFBR) Program Plan, Volume 9, Physics," USAEC Report WASH-1109, Argonne National Laboratory, 1968.

9. Gwin, R., et al., "Measurements of the Neutron Fission and Absorption Cross Section of Pu-239 over the Energy Region 0.02 eV to 30 keV," Nucl. Sci. Eng. 40, 306 (1970).

10. Lottin, A., et al., "Ratio of Capture to Fission in Pu-239 at keV Neutron Energies," in "Proceedings of the International Conference on Fast Critical Experiments and Their Analysis," USAEC Document ANL-7320, p. 22. Argonne National Laboratory, 1966.

11. Czirr, J. B., and J. S. Lindsey, "A Measurement of the Capture-to-Fission Ratio for Pu-239," USAEC Report UCRL-72080, Lawrence Radiation Laboratory, 1969.

12. Hitchcock, J. T., and B. A. Hutchins, "Pu-239 Unresolved Resonance Data for ENDF/B, Version II," USAEC Report GEAP-134591, General Electric Company, 1970.

13. Schomberg, M. G., et al., in Proceedings of the Symposium on Fast Reactor Physics, and Related Safety Problems, Karlsruhe, 1967, International Atomic Energy Agency, Vienna, 1968.

14. Patrick, B. H., et al., European-American Nuclear Data Committee Report EANDC(UK)-96 "AL", 1968.

15. James, G. D., and B. H. Patrick, "Evaluation of the Pu-239 Fission Cross Section in the Energy Range 1 keV to 100 keV," Atomic Energy Research Establishment Report AERE-M-2065, 1968.

16. Richardson, A., and J. Blons, in European-American Nuclear Data Committee Report EANDC(E)-89U, 1968, p. 179.

17. Langner, I., J. J. Schmidt, and D. Wall, "Tables of Evaluated Neutron Cross Sections for Fast Reactor Materials," Kernforschungszentrum, Karlsruhe, Report KFK-750, 1968.

18. Smith, R. K., R. L. Henkel, and R. A. Nobles, "Neutron-Induced Fission Cross Section for U-233, U-235, U-238, and Pu-239 from 2 to 10 MeV," Bull. Am. Phys. Soc. 2, 196 (1957).

19. Smirenkin, G. N., V. G. Nesterov, and I. I. Bondarenko, "U-233, U-235, and Pu-239 Cross Sections for 0.3-2.5 MeV Neutrons," At. Energ. 13, 366 (1962); translated in Soviet J. At. Energy 13, 974 (1963).

20. White, P. H., et al., "Measurements of the ^{235}U Neutron Fission Cross Section in the Energy Range 0.04-14 NeV," Proceedings of the Symposium on the Physics and Chemistry of Fission, Salzburg, 1965, International Atomic Energy Agency, Vienna, 1966; also J. Nucl. Energy, Pts A/B Reactor Sci. Tech. 19, 325 (1965).

21. Perkin, J. L., et al., "The Fission Cross Sections of U-233, U-234, U-235, U-236, Np-237, Pu-239, Pu-240, and Pu-241 for 24-keV Neutrons," J. Nucl. Energy, Pts A/B 19, 423 (1965); also Atomic Energy Research Establishment Report EANDC (UK)-50"S", 1965.

22. Coté, R. E., et al., "Neutron Cross-Section Measurements on Plutonium," Bull. Am. Phys. Soc. 1, 187 (1957) (also in BNL-325).

23. Hopkins, J. C., and B. C. Diven, "Neutron Capture to Fission Ratios in U-233, U-235, and Pu-239," Nucl. Sci. Eng. 12, 169 (1962).

24. Sampson, J. B., and E. A. Luebke, "Plutonium Fast Power Breeder with Oxide Fuel and Blanket Elements," Nucl. Sci. Eng. 4, 745 (1958).

25. Adir, J., and K. D. Lathrop, "Theory of Methods Used in the GGC-4 Multigroup Cross Section Code," Gulf General Atomic Report GA-9021, 1968.

26. Shunk, E. R., et al., USAEC Reports LADC-7620 and LA-3586, Los Alamos Scientific Laboratory, 1968.

27. James, G. D., and B. H. Patrick, "Evaluation of the Pu-239 Fission Cross Section in the Energy Range 1 keV to 100 keV," Atomic Energy Research Establishment Report AERE-M-2065 (Amended), 1968.

28. Drake, M. K., and M. W. Dyos, "A Compilation and Evaluation of the Nuclear Data Available for the Major Plutonium Isotopes," USAEC Report GA-6576, General Dynamics Corporation, General Atomic Division, 1965.

29. Yiftah, S., et al., in Proceedings of the Symposium on Fast Reactor Physics and Related Safety Problems, Karlsruhe, 1967, International Atomic Energy Agency, Vienna, 1968.

30. Strutinsky, V. M., "Shell Effects in Nuclear Masses and Deformation Energies," Nucl. Phys. A95, 420 (1967).

31. Schmidt, J. J., "Present Status of Physical Knowledge of the Main Reactor Core Data," Kernforschungszentrum, Karlsruhe, Report KFK-966, 1969 (also EURFNR-679).

32. Pitterle, T. A., and M. Yamamoto, "Evaluated Neutron Cross Section of Pu-240 for the ENDF/B File," USAEC Report APDA-218, Atomic Power Development Associates, 1968 (ENDF-122).

33. Friesenhahn, S. J., et al., "Neutron Capture Cross Sections of Molybdenum, Tantalum and U^{238}," NASA Report NASA-CR-72745, Gulf General Atomic, 1970.

34. Fricke, M. P., et al., "Measurements of Cross Sections for the Radiative Capture of 1 keV to 1 MeV Neutrons by Mo, Rh, Gd, Ta, W, Re, Au and ^{238}U," in Proceedings of the Second International Conference on Nuclear Data for Reactors, Helsinki, Finland, June 15-19, 1970, International Atomic Energy Agency, Vienna, 1970.

35. Private communication to M. P. Fricke, Gulf General Atomic, 1970.

36. Menlove, H. O., and W. P. Poenitz, "Absolute Radiative Capture Cross Section for Fast Neutrons in U-238," Nucl. Sci. Eng. 33, 24 (1968).

37. Moxon, M. C., "The Neutron Capture Cross Section of ^{238}U in the Energy Region 0.5 to 100 keV," Atomic Energy Research Establishment (Harwell) Report AERE-R-6074, 1969.

38. Davey, W. G., "An Analysis of the Neutron Capture Cross Section of ^{238}U Between 1 keV and 15 MeV," Nucl. Sci, Eng. 39, 337 (1970).

39. Barry, J. F., J. Bunce, and P. H. White, "Cross Section for the Reaction U-238 (n,γ) U-239 in the Energy Range 0.12-7.6 Mev," J. Nucl. Energy, A/B, 18, 481 (1964).

40. Joanou, G. D., and C. A. Stevens, "Neutron Cross Sections for U^{238}," NASA Report NASA-CR-54290, General Dynamics, General Atomic Division, 1965.

41. Stevens, C. A., and C. V. Smith, "GAROL, A Computer Program for Evaluating Resonance Absorption Including Resonance Overlap," NASA Report NASA-CR-71162, General Dynamics, General Atomic Division, 1965.

42. Cohen, S. C., and P. K. Koch, "GANDY, A Computer Program for the Evaluation of Effective Cross Sections in the Unresolved Resonance Region," USAEC Report GA-8003, General Dynamics, General Atomic Division, 1966.

43. Archibald, R. J., and D. R. Mathews, "GAFGAR, A Program for the Calculation of Neutron Spectra and Group-Averaged Cross Sections," USAEC Report GA-7542 (Vol. I), Gulf General Atomic, 1968.

44. Mathews, D. C., "Self-shielded Scattering Transfer Array Effects," Trans. Am. Nucl. Soc. 13, 324 (1970).

45. Toppel, B. J., et al., "MC^2, A Code to Calculate Multigroup Cross Sections," USAEC Report ANL-7318, Argonne National Laboratory, 1967.

46. Sauer, A., "Approximate Escape Probabilities," Nucl. Sci. Eng. 16, 329 (1963).

47. Maerkl, H., and A. G. Fowler, "A Generalized Method of Calculating the Fast Fission Effect in Coaxial Cylindrical Lattice Cells," Nucleonik 6, 39 (1964).

48. Meek, M. E., and B. F. Rider, "Summary of Fission Product Yields for U-235, U-238, Pu-239 and Pu-241, at Thermal, Fission Spectrum and 14 MeV Neutron Energies," General Electric Company, Nucleonics Laboratory Report APED-5398-A, 1968.

49. Keepin, G. R., Physics of Nuclear Kinetics, Addison-Wesley Publishing Company, Reading, 1965, p. 102.

50. Ibid., p. 101.

51. Keepin, G. R., "Physics of Delayed Neutron-Experimental," Trans. Am. Nucl. Soc. 13, 2, 709 (1970).

52. Ibid., p. 87.

53. Ibid., p. 94.

54. Benoist, P., "Theory of the Diffusion Coefficient of Neutrons in a Lattice Containing Cavities," Commissariat a l'Energie Atomique Report CEA-R-2278, 1964 (translation CEA-TR-R-2278, Stanford University, 1967).

55. Benoist, P., "Streaming Effects and Collision Probabilities in Lattices," Nucl. Sci. Eng. 34, 285 (1968).

56. Hummel, H. H., and David Okrent, Reactivity Coefficients in Large Fast Power Reactors, American Nuclear Society, Hinsdale, 1970, p. 136.

57. Ibid., p. 144.

58. "Liquid Metal Fast Breeder Reactor Program Plan," Volume 6, "Core Design," USAEC Report WASH-1106, Argonne National Laboratory, 1968.

59. Nicholson, R. B., and E. A. Fischer, "The Doppler Effect in Fast Reactors," in Advances in Nuclear Science and Technology, Vol. 4, Academic Press, New York, 1968, p. 110.

60. Hummel and Okrent, ibid., p. 152.

61. Ibid., p. 140.

62. Ibid., p. 164.

63. Ibid., p. 114.

64. Ibid., p. 355.

65. Ibid., p. 373.

66. Ibid., p. 361.

67. Stewart, R. R., et al., "Studies of Fast Reactor Fuel Element Behavior under Transient Heating to Failure," USAEC Report ANL-7522, Argonne National Laboratory, 1969.

68. Hummel and Okrent, ibid., p. 82.

69. Henry, A. F., "Computation of Parameters Appearing in the Reactor Kinetics Equations," USAEC Report WAPP-142, Westinghouse Electric Corporation, Bettis Plant, 1955.

70. Ott, K. O., "Accuracy of the Quasistatic Treatment of Spatial Reactor Kinetics," Nucl. Sci. Eng. 36, 402 (1969).

71. Hitchcock, J. T., K. F. Hansen, and A. F. Henry, "Spectral Effects in Multigroup Kinetics," Trans. ANS 12, 291 (1969).

72. Merrill, M., Gulf General Atomic, "GCFR Space-Dependent Kinetic Studies: Initial Results on the Effect of Group Structure in Fast Reactor Problems," unpublished data, 1970.